

NUMERICAL MODELING OF SHORT TERM MORPHOLOGICAL CHANGES
AROUND COASTAL STRUCTURES AND AT THE RIVER MOUTHS

A THESIS SUBMITTED TO
THE GRADUATE SCHOOL OF NATURAL AND APPLIED SCIENCES
OF
MIDDLE EAST TECHNICAL UNIVERSITY

BY

EBRU DEMİRCİ

IN PARTIAL FULFILLMENT OF THE REQUIREMENTS
FOR
THE DEGREE OF MASTER OF SCIENCE
IN
CIVIL ENGINEERING

SEPTEMBER 2016

Approval of the thesis:

**NUMERICAL MODELING OF SHORT TERM MORPHOLOGICAL
CHANGES AROUND COASTAL STRUCTURES AND AT THE RIVER
MOUTHS**

submitted by **EBRU DEMİRCİ** in partial fulfillment of the requirements for the degree of **Master of Science in Civil Engineering Department, Middle East Technical University** by,

Prof. Dr. Gülbin Dural Ünver
Dean, Graduate School of **Natural and Applied Sciences** _____

Prof. Dr. İsmail Özgür Yaman
Head of Department, **Civil Engineering** _____

Asst. Prof. Dr. Cüneyt Baykal
Supervisor, **Civil Engineering Department, METU** _____

Dr. Işıkhan Güler
Co-Supervisor, **Civil Engineering Department, METU** _____

Examining Committee Members:

Prof. Dr. Ahmet Cevdet Yalçiner
Civil Eng. Dept., METU _____

Asst. Prof. Dr. Cüneyt Baykal
Civil Eng. Dept., METU _____

Prof. Dr. A. Melih Yanmaz
Civil Eng. Dept., METU _____

Asst. Prof. Dr. Gülizar Özyurt Tarakcıođlu
Civil Eng. Dept., METU _____

Asst. Prof. Dr. Melih Çalamak
Civil Eng. Dept., TED University _____

Date: 05.09.2016

I hereby declare that all information in this document has been obtained and presented in accordance with academic rules and ethical conduct. I also declare that, as required by these rules and conduct, I have fully cited and referenced all material and results that are not original to this work.

Name, Last name : Ebru Demirci

Signature :

ABSTRACT

NUMERICAL MODELING OF SHORT TERM MORPHOLOGICAL CHANGES AROUND COASTAL STRUCTURES AND AT THE RIVER MOUTHS

Demirci, Ebru

M.S., Department of Civil Engineering

Supervisor: Asst. Prof. Dr. Cüneyt Baykal

Co-Supervisor: Dr. Işıkhan Güler

September 2016, 157 pages

In this study, XBeach, a two dimensional depth averaged numerical model developed mainly for simulating nearshore hydro- and morphodynamics is applied to two case studies; i) laboratory experiments on short-term morphological changes around a detached breakwater and a T-groin and ii) a fluvial dominated coastal flooding event at the Manavgat river mouth between dates, 4th and 15th December, 1998. In the first part of study, the numerical model is calibrated for the wave, current and bottom evolution conditions using the base experiment in which there are no structures. Later, the model is applied to the detached breakwater and T-groin experiments. It is observed that the numerical model results are in agreement with the measured wave heights and current velocities in the vicinity of structures, however the morphological changes are slightly underestimated. To investigate the scale dependency of numerical model, the laboratory data is scaled up using undistorted Froude scaling and the numerical model is applied to the scaled-up experiments. The

results of latter simulations show that the morphological changes are represented better. In the second part of the study, a preliminary numerical modeling is carried out to investigate the capabilities of the numerical model in combined fluvial-coastal flood events. The numerical model is applied to a twelve day fluvial dominated coastal flooding event, in which the initial and final shorelines measured are compared with the model results. The river mouth has widened at the end of the simulation, as observed, and the eroded material is accreted in front of the river mouth forming a submerged sand bar. The final shoreline between the river mouth and the east jetty shows well agreement with the measured, whereas the wave induced erosion at the seaward edge of west side of the river mouth is underestimated.

Keywords: coastal sediment transport, numerical modeling, XBeach, scale dependency, river mouth morphology

ÖZ

KIYI YAPILARI VE NEHİR AĞIZLARI ÇEVRESİNDE KISA DÖNEMLİ MORFOLOJİK DEĞİŞİMLERİN SAYISAL MODELLENMESİ

Demirci, Ebru

Yüksek Lisans, İnşaat Mühendisliği Bölümü

Tez Yöneticisi: Yrd. Doç. Dr. Cüneyt Baykal

Ortak Tez Yöneticisi: Dr. Işıkhan Güler

Eylül 2016, 157 sayfa

Bu çalışmada, iki boyutlu derinlik ortalamalı bir sayısal model olan yakın kıyıdaکی hidro- ve morfodinamik davranışların benzetimi için geliştirilmiş XBeach sayısal modeli iki farklı veri setine uygulanmıştır; i) ayrık dalgakıran ve T-mahmuz yapılarının varlığında laboratuvar deneylerinin kısa dönemli morfolojik değişimlerin modellenmesi ve ii) Manavgat nehir ağzı çevresinde akarsu hareketlerinin hakim olduğu 4-15 Aralık, 1998 tarihleri arasındaki taşkın olayının modellenmesi. Çalışmanın ilk kısmında, sayısal model, yapı bulunmayan bir deneye ait dalga, akım ve taban değişimlerine göre kalibre edilmiştir. Daha sonra, model ayrık dalgakıran ve T-mahmuz yapılarının varlığındaki iki farklı deney veri setine uygulanmıştır. Sayısal model sonuçlarının ölçülen dalga yüksekliği ve akım hızları ile uyum gösterdiği, ancak morfolojik değişimlerin ölçümlere göre daha az tahmin edildiği gözlenmiştir. Sayısal modelin, ölçek bağımlılığını araştırmak amacıyla, deney verileri geometrik oran korunarak Froude ölçek kurallarına göre prototip ölçülerine getirilmiş ve sayısal model tekrar bu ölçülerde uygulanmıştır. Ölçekli simülasyonların sonuçlarına göre morfolojik değişimlerin ölçümlerle daha uyumlu temsil tahmin edildiği görülmüştür.

Çalışmanın ikinci kısmında, sayısal modelin birleşik akarsu-deniz taşkın olaylarının modellenmesi ile ilgili başlangıç niteliğinde bir uygulaması yapılmıştır. Sayısal model, akarsu hareketinin hakim olduğu ve başlangıç ve bitiş tarihlerinde kıyı çizgisi ölçümü bulunan on iki günlük bir kıyısız taşkın olayında uygulanmıştır. Nehir ağzı, ölçümlerde görüldüğü gibi, simülasyon sonucunda genişlemiş ve aşınan materyal nehir ağzı önünde batık bir kum sedde oluşturmuştur. Model sonucunda nehir ağzı ve doğu mahmuzu arasında kalan kıyı çizgisi ile ölçülen kıyı çizgisi büyük ölçüde uyum göstermiş, ancak, nehir ağzının batı kısmında kalan ve deniz tarafındaki kıyı çizgisindeki aşınma oranı ölçülen değerlere göre daha az tahmin edilmiştir.

Keywords: kıyısız sediman taşınımı, sayısal modelleme, XBeach, ölçek duyarlılığı, nehir ağzı morfolojisi

To my beloved family and
To the beloved ones who make me feel like family

ACKNOWLEDGEMENTS

First of all, I would like to thank my first professors on my coastal engineering path, Prof. Dr. Ayşen Ergin and Prof. Dr. Ahmet Cevdet Yalçiner, who led me to the right way in my graduate studies as well as in my life. Their wisdom and knowledge always inspired me and expanded my horizon.

My special thanks go to Dr. Işıkhan Güler, who have always supported me, enlightened me, show me the right way in any issue not only in my thesis writing period but also in my life. My first thoughts on coastal engineering shaped with his patient explanations and progressed with his suggestive solutions. He was always there to share my joyful times as well as the obstacles that I face both in my studies and in my life. He was always standing by me in any situation. He is not only a great professor but also a great politician with his great point of views. I feel very lucky to know him and be a student of him and I know that our communication will last in the future.

My deepest gratitudes are for my supervisor, Asst. Prof. Dr. Cüneyt Baykal, for his endless patience during my thesis period. He always explained whatever or whenever I ask for something that I do not understand or I need to clarify. He is always the one who is helping me from least to most important issues that I am not sure about. I can not forget his invaluable helps, his great patience as well as his exemplary personality and I believe I could not succeed without his endless supports during my graduate studies. I hope, someday, I would reach his knowledge and judgment capability.

I would also thank Asst. Prof. Gülizar Özyurt Tarakcıoğlu for her great encouragement for the thesis works. She always helped me and answered my questions in any issue during my graduate studies.

I would like to express my gratitudes to Çađıl Kirezci, the love of my life, my source of inspiration, my better half and many other things that the words can not express. Whenever I am happy, sad, crying, laughing, shocked, curious, tired, super-energetic or any emotion that we have, he is the hand that I hold and I am sure I will be holding forever. I would not be wherever I am, without his presence in my life.

I feel lucky to meet and know Hazal Ak, Sena Acar, Duha Metin, Gzde Gney Dođan, Naeimeh Sharghivand and all coastal engineering family. Those overloaded and tiring times would not be such blissful without them.

Finally, I am also grateful to my family, especially my mother, Seval Demirci, for her great effort on me and for her unconditional love. She was always the one who is listening and supporting me any time and anywhere in my life. I owe her most of the things that I have. I also would like to thank my cousin, Pınar Akpınar zkartal, for her great encouragement in this period and in my whole life. She is always meant more than a cousin or even a sister to me.

TABLE OF CONTENTS

	ABSTRACT	V
	ÖZ.....	VII
	ACKNOWLEDGEMENTS.....	X
	TABLE OF CONTENTS	XII
	LIST OF TABLES.....	XV
1	INTRODUCTION.....	1
2	LITERATURE REVIEW	7
2.1	Coastal Sediment Transport Processes	7
2.1.1	Alongshore Sediment Transport.....	7
2.1.2	Cross-shore Sediment Transport	10
2.1.3	Sediment Transport at the River Mouths.....	11
2.2	Numerical Modeling of Coastal Sedimentation	13
3	XBEACH NUMERICAL MODEL DESCRIPTION.....	19
3.1	Model Definition	19
3.2	Wave Transformation Model.....	20
3.2.1	Short Wave Action Balance	21
3.2.2	Wave Breaking	22
3.2.2.1	Wave Breaking for Baldock et al. (1998).....	23
3.2.3	Bottom Friction.....	23
3.2.4	Radiation Stresses.....	24
3.2.5	Wave Shape	25
3.3	Surface Rollers.....	26
3.3.1	Roller Energy Balance.....	27
3.4	Non-Linear Shallow Water Equations.....	28
3.4.1	Horizontal Viscosity	29
3.4.2	Bed Shear Stress	30

3.5	Sediment Transport and Morphology Update	30
3.5.1	Parameters	30
3.5.2	Formulations	32
3.5.2.1	Formulation of Soulsby - Van Rijn (Van Rijn, 1984; Soulsby, 1997)	33
3.5.2.2	Formulation of Van Thiel - Van Rijn (Van Rijn, 2007; Van Thiel de Vries, 2009)	34
3.5.3	Wave Non-linearity	35
3.5.4	Bed Update and Morphology	36
3.6	Boundary Conditions	37
3.6.1	Waves	37
3.6.2	Shallow Water Equations	38
3.6.2.1	Offshore Boundary Conditions	38
3.6.2.2	Lateral Boundary Conditions	38
3.6.2.3	Water Level Boundary Condition	39
3.6.2.4	River and Point Discharge Boundary Condition	39
3.6.3	Sediment Transport	39
4	COMPARISON OF LABORATORY DATA TO XBEACH NUMERICAL MODEL OUTPUT	41
4.1	Large-Scale Sediment Transport Facility (LSTF) Data	41
4.2	Model Setup	45
4.3	Model Calibration	47
4.3.1	Hydrodynamic Parameters	48
4.3.2	Morphology Parameters	52
4.4	Scale Dependency	57
4.5	Comparison of Results	64
4.5.1	Non-scaled LSTF Data	66
4.5.1.1	Experiment Base Case 1 (BC1)	66
4.5.1.2	Experiment Test-1 Case-1 (T1C1)	71
4.5.1.3	Experiment Test-3 Case-1 (T3C1)	77

4.5.2	Scaled LSTF Data ($n_d=25$)	83
4.5.2.1	Experiment Base Case-1 (BC1) (<i>Rescaled</i>)	84
4.5.2.2	Experiment Test-1 Case-1 (T1C1) (<i>Rescaled</i>)	87
4.5.2.3	Experiment Test-3 Case-1 (T3C1) (<i>Rescaled</i>)	93
5	A CASE STUDY: MODELING MANAVGAT RIVER MOUTH WITH XBEACH	101
5.1	Study Area	101
5.2	Model Setup	108
5.3	Determination of the Model Parameters	112
5.3.1	Hydrodynamic Parameters	113
5.3.2	Morphology Parameters	117
5.4	Results and Discussions	119
6	CONCLUSION	141
	REFERENCES	147

LIST OF TABLES

Table 4.1 Average values of offshore wave parameters measured at the offshore boundary (x_{12} , x_{13} and x_{14}) for BC1, T1C1 and T3C1.	43
Table 4.2 Hydrodynamic parameters applied in the model for BC1, T1C1 and T3C1	48
Table 4.3 Morphology parameters applied in the model for BC1, T1C1 and T3C1.	53
Table 4.4 Scaled hydrodynamic parameters applied in the model for BC1, T1C1 and T3C1 ($n_d=25$)	59
Table 4.5 Scaled morphology parameters applied in the model for BC1, T1C1 and T3C1 ($n_d=25$)	60
Table 5.1 Discharge data between 4 th and 15 th December, 1998	106
Table 5.2 Wave Climate Properties for the given duration (4 th -15 th December 1998)	111
Table 5.3 Hydrodynamic parameters applied in model for Manavgat river mouth	113
Table 5.4 Morphology Parameters applied in model for Manavgat river mouth....	117

LIST OF FIGURES

Figure 1.1 Terms describing a typical beach profile (SPM, 1984).	2
Figure 3.1 XBeach model structure flowchart	20
Figure 4.1 The plan view of the LSTF and alongshore locations of measurements of Base Case (BC1 in this study) (Wang et al., 2002a; Gravens and Wang, 2007).	44
Figure 4.2 The plan view of the LSTF and alongshore locations of measurements of Test 1 (<i>T1C1 in this study</i>) (Gravens and Wang, 2007).....	44
Figure 4.3 The plan view of the LSTF and alongshore locations of measurements of Test 3 (<i>T3C1 in this study</i>) (Gravens and Wang, 2007).....	45
Figure 4.4 Averaged bed profile for BC1.....	46
Figure 4.5 Two dimensional model domains for T1C1 (<i>left</i>) and T3C1 (<i>right</i>)	47
Figure 4.6 Comparison between the alongshore velocities of LSTF data and the computed data with jointly varied ' <i>hmin</i> ' and ' <i>eps</i> ' parameters	51
Figure 4.7 Comparison of computed bed profiles of BC1 with variable ' <i>facua</i> ' shown in whole profile.....	54
Figure 4.8 Comparison of computed bed profiles of BC1 with varying ' <i>dzmax</i> '	55
Figure 4.9 Comparison of computed bed profiles of BC1 with varying ' <i>hswitch</i> ' ...	56
Figure 4.10 Bottom velocity for monochromatic <i>TnT</i> , <i>UwTn2H</i> and random <i>TnTz</i> , <i>UrmsTnHs</i> waves (Soulsby, 1997).	62
Figure 4.11 Modeled bathymetries and the cross sections for T1C1 and T3C1	66
Figure 4.12 Root mean squared wave height comparison for BC1.....	67
Figure 4.13 Wave induced longshore velocity comparison for BC1	68
Figure 4.14 Mean water level comparison for BC1	69
Figure 4.15 Measured initial bed level and computed and measured final bed level comparison for BC1	70
Figure 4.16 T1C1 Measured and computed <i>Hrms</i> values for y=18 m and y=22 m..	71
Figure 4.17 T1C1 Measured and computed <i>Hrms</i> values for y=24 m and y=26 m..	71

Figure 4.18 T1C1 Measured and computed <i>Hrms</i> values for $y=28$ m and $y=34$ m..	72
Figure 4.19 T1C1 Measured and computed ' v ' values for $y=18$ m and $y=22$ m	72
Figure 4.20 T1C1 Measured and computed ' v ' values for $y=24$ m and $y=26$ m.....	73
Figure 4.21 T1C1 Measured and computed ' v ' values for $y=28$ m and $y=34$ m.....	73
Figure 4.22 T1C1 Measured and computed ' <i>eta mean</i> ' values for $y=18$ m and $y=22$ m	74
Figure 4.23 T1C1 Measured and computed ' <i>eta mean</i> ' values for $y=24$ m and $y=26$ m	74
Figure 4.24 T1C1 Measured and computed ' <i>eta mean</i> ' values for $y=28$ m and $y=34$ m	74
Figure 4.25 Measured initial and final bed and computed final bed level comparison for T1C1	75
Figure 4.26 T3C1 Measured and computed <i>Hrms</i> values for $y=18$ m and $y=22$ m..	78
Figure 4.27 T3C1 Measured and computed <i>Hrms</i> values for $y=24$ m and $y=26$ m..	78
Figure 4.28 T3C1 Measured and computed <i>Hrms</i> values for $y=28$ m and $y=34$ m..	78
Figure 4.29 T3C1 Measured and computed v values for $y=18$ m and $y=22$ m.....	79
Figure 4.30 T3C1 Measured and computed v values for $y=24$ m and $y=26$ m.....	79
Figure 4.31 T3C1 Measured and computed v values for $y=28$ m and $y=34$ m.....	80
Figure 4.32 T3C1 Measured and computed ' <i>eta mean</i> ' values for $y=18$ m and $y=22$ m	80
Figure 4.33 T3C1 Measured and computed ' <i>eta mean</i> ' values for $y=24$ m and $y=26$ m	81
Figure 4.34 T3C1 Measured and computed ' <i>eta mean</i> ' values for $y=28$ m and $y=34$ m	81
Figure 4.35 Measured initial and final bed and computed final bed level comparison for T3C1	82
Figure 4.36 Root mean squared wave height comparison for BC1 (<i>rescaled</i>)	84
Figure 4.37 Longshore velocity comparison for BC1 (<i>rescaled</i>).....	85
Figure 4.38 Mean water level comparison for BC1 (<i>rescaled</i>).....	86
Figure 4.39 Measured initial bed level and computed and measured final bed level comparison for BC1 (<i>rescaled</i>).....	87

Figure 4.40 T1C1 Measured and computed <i>Hrms</i> values for $y=18\text{ m}$ and $y=22\text{ m}$ (<i>rescaled</i>).....	88
Figure 4.41 T1C1 Measured and computed <i>Hrms</i> values for $y=24\text{ m}$ and $y=26\text{ m}$ (<i>rescaled</i>).....	88
Figure 4.42 T1C1 Measured and Computed <i>Hrms</i> values for $y=28\text{ m}$ and $y=34\text{ m}$ (<i>rescaled</i>).....	89
Figure 4.43 T1C1 Measured and computed v values for $y=18\text{ m}$ and $y=22\text{ m}$ (<i>rescaled</i>).....	89
Figure 4.44 T1C1 Measured and computed v values for $y=24\text{ m}$ and $y=26\text{ m}$ (<i>rescaled</i>).....	90
Figure 4.45 T1C1 Measured and computed v values for $y=28\text{ m}$ and $y=34\text{ m}$ (<i>rescaled</i>).....	90
Figure 4.46 T1C1 Measured and Computed ' <i>eta mean</i> ' values for $y=18\text{m}$ and $y=22\text{m}$ (<i>rescaled</i>)	91
Figure 4.47 T1C1 Measured and Computed ' <i>eta mean</i> ' values for $y=24\text{m}$ and $y=26\text{m}$ (<i>rescaled</i>)	91
Figure 4.48 T1C1 Measured and Computed ' <i>eta mean</i> ' values for $y=28\text{m}$ and $y=34\text{m}$ (<i>rescaled</i>)	91
Figure 4.49 Measured initial and final bed and computed final bed level comparison for T1C1 (<i>rescaled</i>).....	92
Figure 4.50 T3C1 Measured and computed <i>Hrms</i> values for $y=18\text{ m}$ and $y=22\text{ m}$ (<i>rescaled</i>).....	94
Figure 4.51 T3C1 Measured and computed <i>Hrms</i> values for $y=24\text{ m}$ and $y=26\text{ m}$ (<i>rescaled</i>).....	94
Figure 4.52 T3C1 Measured and computed <i>Hrms</i> values for $y=28\text{ m}$ and $y=34\text{ m}$ (<i>rescaled</i>).....	94
Figure 4.53 T3C1 Measured and computed v values for $y=18\text{ m}$ and $y=22\text{ m}$ (<i>rescaled</i>).....	95
Figure 4.54 T3C1 Measured and computed v values for $y=24\text{ m}$ and $y=26\text{ m}$ (<i>rescaled</i>).....	95

Figure 4.55 T3C1 Measured and computed v values for $y=28$ m and $y=34$ m (<i>rescaled</i>).....	96
Figure 4.56 T3C1 Measured and Computed ‘ <i>eta mean</i> ’ values for $y=18$ m and $y=22$ m (<i>rescaled</i>)	96
Figure 4.57 T3C1 Measured and computed ‘ <i>eta mean</i> ’ values for $y=24$ m and $y=26$ m (<i>rescaled</i>)	97
Figure 4.58 T3C1 Measured and computed ‘ <i>eta mean</i> ’ values for $y=28$ m and $y=34$ m (<i>rescaled</i>)	97
Figure 4.59 Measured initial and final bed and computed final bed level for T3C1 (<i>rescaled</i>).....	98
Figure 5.1 Manavgat province and Manavgat river mouth location in Turkey	102
Figure 5.2 The most recent Google Earth Image for the study area, Manavgat river mouth	103
Figure 5.3 Oymapınar and Manavgat Dams and the river gage station locations on Manavgat River.....	105
Figure 5.4 Shoreline measurement of Manavgat river mouth on December 4 th , 1998 (Guler et al., 2003).	107
Figure 5.5 Shoreline measurement of Manavgat river mouth on December 15 th , 1998 (Guler et al., 2003).	107
Figure 5.6 Initial bathymetry according to the measurements of DLH for date 4.12.1998.....	108
Figure 5.7 A closer look to the bathymetry between $x= 2500$ m – 3300 m and $y=$ 1000 m – 2500 m.	109
Figure 5.8 Determination of the effective fetch lengths (Google Earth, 2016).	110
Figure 5.9 Daily Mean River Discharge Data (red line), concurrent hourly averaged deep water significant wave heights (large blue dots) and the time steps at which the hydrodynamic and morphologic conditions are presented (purple small dots) between December 4 th and 15 th , 1998.	112
Figure 5.10 Root Mean Squared Wave Height Distribution after 55 hours of simulation.....	120
Figure 5.11 Depth Averaged Flow Velocity Field after 55 hours of simulation	121

Figure 5.12 Initial shoreline (black dotted line), computed bed levels and shoreline (brown dashed line) after 55 hours of simulation	122
Figure 5.13 Depth Averaged Flow Velocity Field after 95 hours of simulation.....	123
Figure 5.14 Initial shoreline (black dotted line), computed bed levels and shoreline (brown dashed line) after 95 hours of simulation	124
Figure 5.15 Root Mean Squared Wave Height Distribution after 126 hours of simulation	125
Figure 5.16 Depth Averaged Flow Velocity Field after 126 hours of simulation...	126
Figure 5.17 Initial shoreline (black dotted line), computed bed levels and shoreline (brown dashed line) after 126 hours of simulation	127
Figure 5.18 Depth Averaged Flow Velocity Field after 143 hours of simulation...	128
Figure 5.19 Initial shoreline (black dotted line), computed bed levels and shoreline (brown dashed line) after 143 hours of simulation	129
Figure 5.20 Root Mean Squared Wave Height Distribution after 157 hours of simulation	130
Figure 5.21 Depth Averaged Flow Velocity Field after 157 hours of simulation...	131
Figure 5.22 Initial shoreline (black dotted line), computed bed levels and shoreline (brown dashed line) after 157 hours of simulation	132
Figure 5.23 Depth Averaged Flow Velocity Field after 175 hours of simulation...	133
Figure 5.24 Initial shoreline (black dotted line), computed bed levels and shoreline (brown dashed line) after 175 hours of simulation	134
Figure 5.25 Depth Averaged Flow Velocity Field after 239 hours of simulation...	135
Figure 5.26 Initial shoreline (black dotted line), computed bed levels and shoreline (brown dashed line) after 239 hours of simulation	136
Figure 5.27 Cumulative sediment accretion/erosion scheme at the end of the simulation	137
Figure 5.28 Initial (red dashed line) resulting measured (blue line), and final computed (brown dashed line, main color map in the figure) after 288 hours of simulation	138

CHAPTER 1

INTRODUCTION

Water environments consisting of rivers, lakes, wetlands, seas and oceans are the invaluable heritages of nature. From the early times of history until now, humankind has always been in contact with water for living, food, transportation, agriculture and many other necessities. Therefore, it is realized that stability and sustainability of these vulnerable, yet significant areas are of great attention especially in the recent decades.

Half the world's population lives within 60 km of the sea, and three-quarters of all large cities are located on the coast (“Cities and Coastal Areas”, n.d., para. 1). This makes the coastal areas are of great significance not only for the continuity of peace in nature, but also for the prevention of disastrous effects that may come into picture. Therefore, it is considered as necessary to develop sustainability and risk mitigation strategies for coasts. In order to estimate the shoreline behavior and response, and thus, to prevent adverse effects and to provide beach protection, coastal engineers and researchers developed formulations, numerical models, monitoring techniques and conducted laboratory experiments and put into place regulations for building coastal structures in the light of these investigations and previous experiences.

Understanding the processes that take place near a coastal area requires clear definition of the terms. Figure 1.1 shows these terms describing a typical beach profile.

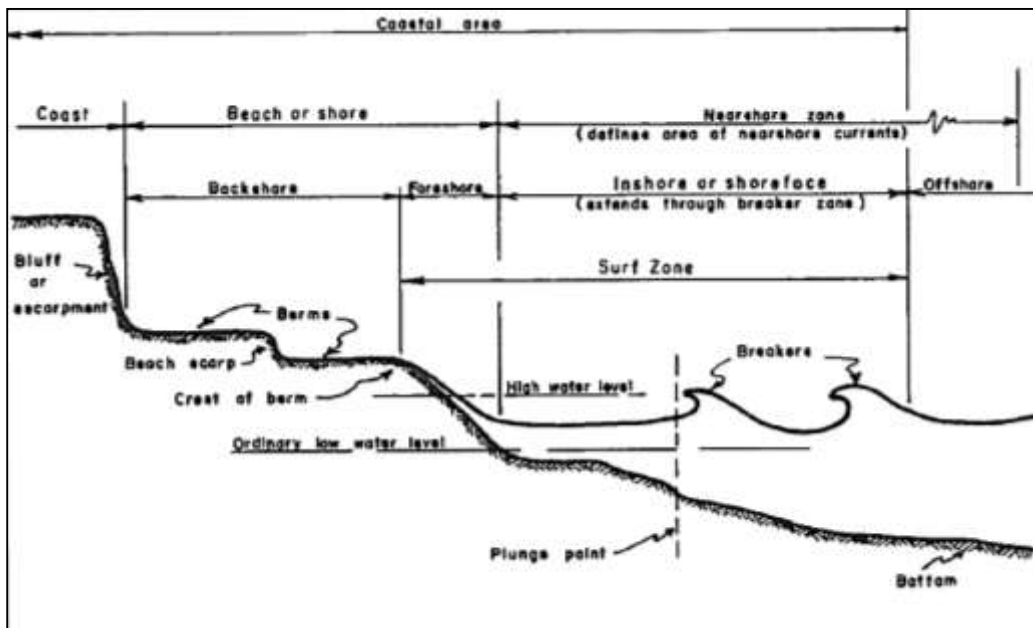


Figure 1.1 Terms describing a typical beach profile (SPM, 1984).

One of the governing processes that influences the shoreline and beach profile evolution is sediment transport or coastal sedimentation which occurs mainly in the nearshore zone. As the waves approach to the shore, wave height to wave length ratio increases up to some limiting value and wave breaking occurs resulting in wave induced longshore currents (currents flowing parallel to the shoreline) and wave setup (increase in the mean water level due to waves). Similarly, as the waves attack, there are also cross-shore currents (currents flowing perpendicular to the shoreline). These wave and/or current actions in the nearshore zone induce sediment transport near coastal areas, or in short, coastal sedimentation. Soulsby (1997) states that ‘The movement of sand influences: the construction of economically viable harbours (dredging costs for harbours and approach channels are often critical to viability), the construction of coastal power stations and refineries (sand may enter the cooling water intakes), coastal flood defence (integrity of beaches and offshore banks is crucial to dissipate wave attack), the loss or growth of amenity beaches (crucial to the success of many holiday resorts), the safety of offshore platforms and pipelines

(sea bed scour can lead to toppling of platforms or breakage of pipelines), and many other applications.’

As a part of coastal environments, river mouths and deltas where rivers meet with the seas or oceans are among the most fertile and productive ecosystems and housing half a billion people. However, the development and evolution of such areas are insufficiently understood (Syvitski and Saito, 2007; Fagherazzi and Overeem, 2007; Nardin and Fagherazzi, 2012). Understanding sediment transport driven by waves, and its relationship to the discharge of river sediments, is crucial for the morphological evolution of bars and therefore of the entire delta (Nardin and Fagherazzi, 2012). Near the river mouth, the topography of a sand bar is continuously affected by river runoff, ocean currents and sea wave action. Disruptions in any of these factors can alter the geometry of the sand bar, causing sedimentation problems and increased risk of flooding. In order to mitigate the risks associated with such changes, it is important to understand the characteristics of the topographic changes of river-mouth bars, and to develop a method for controlling the bar geometry. Especially in coastal areas where tidal forcing is not a governing behavior, river mouth bars tend to develop under conditions of longshore sediment transport, and blocking of river-mouths is frequent. Floods tend to breach the river-mouth bars that develop during dry periods, and complex changes occur in bar behavior during floods and in post-flushing river-mouth channel width. These changes vary depending on flood hydrodynamics, fluvial morphology near the river mouth, and the presence or absence of harbor facilities and other man-made structures along the coast (Ochi et al., 2015).

Coastal erosion or accretion is one of the most common yet significant problems that are faced with across the coasts. These problems are due to the imbalance of the sediment budget of the coastal areas. Either nature’s behavior or human interference may cause this imbalance (CIRIA, 1996). In order to understand the behavior and estimate the consequences of these actions, formulations and numerical models have

been developed while physical experiments play significant role both in estimation of a future design or supporting a formula or a numerical model.

In this study the main objective is to investigate the capabilities of the numerical model XBeach in laboratory and field conditions. Modeled laboratory data are adopted from the experiments that were conducted in the Large-Scale Sediment Transport Facility (LSTF) and these experiments were conceived and supported by the Coastal Inlets Research Program (CIRP) administered at the U.S. Army Engineer Research and Development Center (ERDC), Coastal and Hydraulics Laboratory (CHL) under the Navigation Systems Program for Headquarters, U.S. Army Corps of Engineers (HQUSACE). The experiments were aimed to estimate the coastal sedimentation quantitatively in the vicinity of the coastal structures (Hamilton et al., 2001; Gravens and Wang, 2007). On the other hand, field data, which is taken during the construction stages of river mouth jetties, consists of Manavgat river mouth for 12-day-bathymetric-data adopted from General Directorate of Railways, Harbors and Airports Construction (DLH). The applied numerical model, XBeach, is a two-dimensional model for wave propagation, long waves and mean flow, sediment transport and morphological changes of the nearshore area, beaches, dunes and backbarrier during storms and it is a public domain model developed with major funding from the US Army Corps of Engineers, Rijkswaterstaat and the EU, supported by a consortium of UNESCO-IHE, Deltares (formerly WL|Delft Hydraulics), Delft University of Technology and the University of Miami.

In Chapter 2, a detailed literature survey is presented about the coastal sediment transportation types, namely, longshore sediment transportation, cross-shore sediment transportation and sediment transport at the river mouths and the state-of-art numerical models that are developed within the scope of coastal sediment transport are introduced and the main idea and purposes of the models are presented.

Chapter 3 gives brief information about the definitions and the structure of the formulations used in XBeach numerical model about hydrodynamic and morphology

parameters that are; wave transformation, surface roller concept, non-linear shallow water equations, sediment transport and morphology update scheme and boundary condition options.

In Chapter 4, Large-Scale Sediment Transport Facility (LSTF) basin properties, the experiments and the purpose of these experiments are introduced. Model bathymetry setup and hydrodynamic and morphology parameters that are calibrated and used as input data in XBeach are explained in detail and discussed in the sense of applicability. Scale dependency and the consequent scaled hydrodynamic and morphology parameters are presented. In the final section, the comparison of the modeled and measured LSTF data and the discussions of results are given.

Chapter 5 consists of the case study Manavgat river mouth morphology modeling between the dates 4th and 15th December, 1998. The study area is introduced and the model setup and the input parameters are presented. The final morphologies are compared between the measured and the modeled output bathymetries. The similarities and differences are determined and the possible reasons of the differences are discussed.

In the last chapter, the work done is summarized and concluded according to the previous results and discussions. Further recommendations in the light of the numerical modeling studies especially with XBeach, are given.

CHAPTER 2

LITERATURE REVIEW

In this section, literature review is presented regarding to coastal sedimentation processes in alongshore and cross-shore directions and sediment transport at the river mouths that exist in literature. Also, studies that are within the scope of numerical modeling of coastal sedimentation, bed evolution and morphology are given.

2.1 Coastal Sediment Transport Processes

Sediment motion due to wind, waves, currents, tides, sea level fluctuations or many other phenomena is the main factor in coastal sedimentation and the transport processes. Shoreline stability, erosion or accretion is dependent on the rate of supplied or removed sediment amount. Excessive erosion or accretion may cause danger to the structural integrity, functional usefulness of a beach or of other structures (SPM, 1984). Therefore, it is important to understand, compute and estimate the coastal sediment transport processes. Here, the coastal sediment transport processes literature reviews are categorized as longshore sediment transport, cross-shore sediment transport and sediment transport at the river mouths.

2.1.1 Alongshore Sediment Transport

Alongshore (also littoral or longshore) sediment transport is the shore-parallel movement of the sediment particles in the nearshore area and may be caused by wave action, tide, wind or combination of them. The main driving factor of the

longshore sediment transport is the oblique incident waves and the resulting longshore currents. Also, wave diffraction caused by the coastal structures such as jetties, groins etc. may result in a diffraction induced currents generated by alongshore gradients in breaking wave height at the downdrift side of the structure (CEM, 2003).

Savage (1962) derived an equation later used by US Army Corps of Engineers in a 1966 coastal design manual, namely “CERC formula” (CEM, 2003).

Komar and Inman (1970) calibrated the available field data into the Inman and Bagnold’s (1963) immersed weighted longshore transport rate rather than the volumetric rate. Depending on the Komar and Inman’s (1970) equation, the CERC formula is derived in order to calculate the littoral sand transport rate (CEM, 2003) and it is given as:

$$I_l = K \left(\frac{\rho g^{3/2}}{16\kappa^{1/2}} \right) H_b^{\frac{5}{2}} \sin(2\alpha_b) \quad (2.1)$$

where I_l is the immersed weight longshore transport rate, K is the empirical proportionality coefficient, ρ is the density of water, g is the acceleration of gravity, H_b is the breaking wave height, κ is the breaker index and calculated by H_b/d_b where d_b is the breaking depth, and α_b is the wave breaker angle relative to the shoreline. Here, the main idea is to determine the potential longshore sediment transport rate that is related with the wave energy flux with the constant K explained above. This parameter is dimensionless and may be determined by directly applying the SPM value which is

$$K_{SPM,rms} = 0.92 \quad (2.2)$$

based on root-mean-squared wave height. Moreover, K may be determined by methods that are varied with median grain size and surf similarity methods. An example for the median grain size based method for calculating K parameter is suggested by del Valle, Medina and Losada (1993) as the following equation:

$$K = 1.4e^{(-2.5D_{50})} \quad (2.3)$$

Here, e is the logarithmic constant and D_{50} is the median grain size ranging between (0.40~1.50 mm). It is also indicated that K is proportional with the surf similarity parameter as mentioned above, as the surf similarity, ξ , is

$$\xi = m/(H_b/L_o)^{1/2} \quad (2.4)$$

where m is the bed slope and L_o is the deep water wave length. As the waves tend to show collapsing rather than spilling breaking behavior, which means while ξ increases, K also increases (Kamphuis and Readshaw, 1978).

Longuet-Higgins (1970) defined the mechanism of radiation stress based wave induced longshore current concept (Goda, 2010). Battjes (1974) proposed the calculation of the irregular wave induced longshore velocity based on the radiation stress description.

Kamphuis (1991) gave the relation between wave steepness, beach slope, relative grain size, breaking angle and the longshore sediment transport rate derived from dimensional analysis depending on set of three dimensional laboratory measurements consisting of both regular and irregular waves.

Bayram et al. (2007) developed a predictive formula for longshore sediment transport rate employing six high-quality data sets on hydrodynamics and sediment transport. The formula showed that the total transport rate is proportional to the

longshore current speed and the incoming wave-energy flux, and that the rate is inversely proportional to the sediment fall velocity. Comparing to most previous formulas for the total longshore sediment transport rate, the formula proposed in this study exhibit a dependence on the grain size. In addition, transport generated by currents of other origin than from breaking waves, such as tide- and wind-generated currents, may be predicted. It is concluded that, Bayram et al.'s formula (2007) is well suited for practical applications in coastal areas, as well as for numerical modeling of sediment transport and shoreline change in the nearshore.

2.1.2 Cross-shore Sediment Transport

Equilibrium beach profile is a significant concept in the coastal sedimentation problems and the nearshore activities. According to Dean (1991), some characteristic properties of the equilibrium beach profile may be given as, i) they tend to be concave upwards, ii) smaller diameters result in milder slopes whereas the larger diameters result in steeper, iii) beach face is nearly planar and iv) steep waves result in milder slopes and a tendency for bar formation.

Bruun (1954) analyzed profiles from Danish North Sea Coast and Mission Bay, California and proposed the following equation:

$$h(y) = Ay^{2/3} \quad (2.5)$$

where h is the water depth and a function of, y , seaward distance multiplied with the scale parameter A depending on sediment properties.

Dean (1977) gave a similar relation to Eq. 2.5 concluding that the exponential part of equation gives consistent results with the value $2/3$ with uniform energy dissipation per volume, D_* , which is computed as the following equation:

$$D_* = \frac{1}{h} \frac{\partial}{\partial y} (E C_g) \quad (2.6)$$

where h is the water depth at the specific seaward distance, y , E is the wave energy density and C_g is the group velocity. Also, the sediment scale parameter, A , can be calculated from Eq. 2.7:

$$A = \left[\frac{24D_*(D)}{5\rho g^{3/2}\kappa^2} \right] \quad (2.7)$$

where ρ is the water mass density, g is the gravitational acceleration and D is sediment particle diameter and κ is a constant that relates wave height to water depth within the surf zone.

Dean (1987) has proposed that the sediment scale parameter A is a function of fall velocity, w_s , rather than sediment diameter, D with a linear relation. Shortly after, Dean (1991) indicated methods in order to determine the shoreline response with high water levels and wave heights on natural and seawall built shorelines. Moreover, the author computed the nourishment quantities with uniform but arbitrary sand diameters and presented the corresponding results.

2.1.3 Sediment Transport at the River Mouths

River mouths where coastal waters meet fluvial flows are vulnerable zones that need special attention in the sediment transportation point of view. Near such coastal area, sands are expected to be affected by mainly two important forcings: waves and currents.

Sediment transportation in rivers may be due to bed load transport, suspension or the combination of both. Bed ripples or dunes are typical resultants of the sediment

transportation in alluvial beds. Moreover, tidal and density-induced effects may be observed in the lower reaches of the rivers (Van Rijn, 1993).

Sediment transportation in coastal seas mainly occurs due to oscillatory behavior of short (low-frequency) waves. The sand particles are stirred by the wave action and in the end transported by mean currents (Van Rijn, 1993).

Van Rijn (2007a) analyzed high-quality bed load transport data sets given for the sand range of the particle size the bed-load transport rate is proportional to the velocity with the power of 2.5, where this rate is not affected by particle size. Bed load transport formulas are given for a quick estimate in river and coastal flows and the model can estimate the bed load transport within the range of fine silt to coarse sand. In the model, only basic hydrodynamic conditions and sediment characteristics need to be known. The prediction of the effective bed roughness is an integral part of the model.

Soulsby (1997) indicated that combined action of waves and currents are considered, for example, within the coastal and offshore sites in depths between 5 m and 40 m, estuaries exposed to open sea or with long and/or wide stretches exposed to strong winds. For computing the combined effects of waves and currents, the author proposed three main approaches: *i*) design wave and tide approach where a single tidal height and current and a single wave condition are considered *ii*) probabilistic approach where all possible combinations of events summed with a weighting depending on the frequency of the events, and *iii*) sequential approach where the current (or surface elevations) and waves are given as input at every time step through a long-term simulation.

2.2 Numerical Modeling of Coastal Sedimentation

Numerical models play crucial roles in estimating the beach profile and morphologies. Predicting the beach evolution, where planned or existing engineering projects come into picture, is significant in quantitative comprehension of beach profile change (Larson and Kraus, 1989). It is important to decide for the appropriate numerical model for the area of concern, duration of the event and precision level that is necessary to be computed. Therefore, the ultimate goal should be clarified for the aiming study.

The area of concern is important for the decision of which sediment transport formulations govern: longshore or cross-shore.

Time scale for the event of interest may be categorized as storm-induced, which is in the order of 1-3 days, and beach fill adjustment, which may take several weeks to several months to observe (Larson and Kraus, 1989).

The precision level of the study covers the resolution of hydrodynamic and bathymetric data. For accurate, stable and effective computing procedure, it is important to choose the correct dimensional characteristics, whether the model should be one dimensional, two dimensional and depth averaged, quasi-3D or fully 3D.

As an example of the decision process, Baykal (2012) states that “the long term changes in the shoreline could be studied fastest using one-line models, whereas dune erosion, bar formation or seasonal changes in the shoreline, swash zone dynamics could be studied with medium- or short-term beach evolution models.”

One of the earliest studies of beach evolution modeling is done by Pelnard-Considere (1956). Here, it is assumed that even though the cross-shore profile varies with the seasonal changes, the overall variation is negligible in a longer period. Therefore, the

beach profile shape stays the same in an event of erosion or accretion. Consequently, the change observed is only the shoreline evolution and this model is often called ‘one-line model’. Another assumption is the seaward and shoreward limits of the transportation process, namely, berm height and depth of closure. Between these two limits, the rate of change of sediment volume is basically calculated and in the case of variation in the net sediment volume, then the profile is regenerated within the chosen longshore intervals. Bakker (1968) extended the concept to account for possible on – offshore transport and formulated a two-line schematisation of the profile. Additional contributions to such models have been produced by Le Méhauté and Soldate (1978) for the inclusion of wave refraction and diffraction and by Fleming and Hunt (1976) for the bathymetry modification as a change in depths at a set of schematised grid points (Capobianco et al., 2002).

GENESIS is the shoreline change model that is developed in order to simulate the shoreline changes computing longshore sand transport. Similar to the one-line model, the cross-shore changes due to short-term storm actions and seasonal variations across the bed profile cannot be indicated within this numerical model, since it is assumed that these variations cancel out in long-term period (Hanson and Kraus, 1989). Similarly, ONELINE numerical model is also based on the one-line theory of shoreline change, but does not make any small angle assumption with respect to the incident wave angle and shoreline direction (Dabees and Kamphuis, 1998).

The main assumption of the one-line models is the ignorance of the beach profile change due to storm-induced actions and seasonal variations. However, when considering short-term applications of the morphological behavior, bed profile changes should be taken into account. Capobianco et al. (2002) indicates that there are several models that computes such bed profile response that both for the emerged (Kriebel and Dean, 1985) and the submerged parts (Larson and Kraus, 1989; Larson et al., 1990a,b).

Lin and Wang (1984) proposed a numerical model for predicting long-term shoreline evolution around a river mouth by incorporation certain river parameters into the Willis (1978) beach evolution model.

The Coastal Modeling System (CMS) is an integrated numerical modeling system for simulating nearshore waves, currents, water levels, sediment transport, and morphology change (Militello et al. 2004; Buttolph et al. 2006; Lin et al. 2008; Reed et al. 2011). The system was developed and continues to be supported by the Coastal Inlets Research Program (CIRP), a research and development program of the U.S. Army Corps of Engineers (USACE) that is funded by the Operation and Maintenance Navigation Business Line of the USACE. CMS is designed for coastal inlets and navigation applications including channel performance and sediment exchange between inlets and adjacent beaches. CMS-Flow and CMS-Wave are coupled flow and wave models, respectively where CMS-Flow is a two dimensional depth averaged nearshore circulation model (2DH) that calculates currents and water levels including physical processes such as advection, turbulent mixing, combined wave-current bottom friction; wind, wave, river, and tidal forcing forcing; Coriolis force; and the influence of coastal structures (Buttolph et al. 2006; Wu et al. 2011) and CMS-Wave is a spectral wave transformation model, solving the wave action balance equation using a forward marching Finite Difference Method (Mase et al., 2005; Lin et al. 2008) and includes physical processes such as wave shoaling, refraction, diffraction, reflection, wave-current interaction, wave breaking, wind wave generation, white capping of waves, and the influence of coastal structures.

SISYPHE is a sediment transport and morphodynamic module of TELEMAC modelling system (Hervouet and Bates, 2000) which consists of 2D and 3D flow modules that are coupled with the SISYPHE module, namely, TELEMAC-2D and TELEMAC-3D and a spectral wave propagation model (TOMAWAC) (Luo et al., 2013). SISYPHE uses the depth-averaged hydrodynamic parameters taken from the TELEMAC-2D or TELEMAC-3D modules.

Nam et al. (2009) studied the Longshore Sediment Transport Facility (LSTF) model basin with EBED and Modified-EBED models for wave heights, (Dally and Brown, 1995); Larson and Kraus (2002) wave energy balance equations for surface roller model, Militello et al. (2004) approach for nearshore currents, Larson and Wamsley (2007) formula for swash zone sediment transport and Camenen and Larson (2005, 2007, 2008) formulation for the nearshore zone (offshore and surf zone) sediment transport processes.

Baykal (2012) developed a two-dimensional depth averaged beach evolution numerical model studying the medium and long term nearshore sea bottom evolution wind wave induced sediment transport over the arbitrary land and sea topographies around existing coastal structures and formations. The model consists of four sub-models: i) wave characteristics are determined by nearshore spectral wave transformation model based on energy balance equation given by Mase (2001) including random wave breaking and diffraction terms, ii) nearshore depth averaged wave induced current velocities and mean water level changes are computed by nearshore wave-induced circulation model based on the non-linear shallow water equations, iii) formulation given by Watanabe (1992) for wind wave induced local total sediment transport rates given by a sediment transport model and iv) bed level changes due to the longshore and cross-shore sediment transport rate gradients modeled by a bottom evolution model. The model is applied to several theoretical and conceptual benchmark cases as well as an extensive data set of laboratory and field measurements. Baykal (2014) successfully applied the model to the SANDYDUCK field experiments and to some conceptual benchmark cases. The numerical model gave results in agreement with the measurements both qualitatively and quantitatively and reflected the physical concepts well for the selected conceptual cases. Similarly, Baykal et al (2013) validated the model by the LSTF from Wang et al. (2002) and from Gravens and Wang (2007) and applied to a case study near Kızılırmak river mouth following the validation studies. It is concluded that the measured field data and the model outputs are in agreement.

Bolle et al. (2010) applied XBeach numerical model to three field sites with specific problems ranging from 1D cross-shore profiles to 2D curved beaches. Other examples are for high energy coasts (with long swell waves). Applications such as the design of a new coastal protection scheme as well as the study of a sedimentation patterns in a shallow harbor surrounded by breakwaters and beaches. It is concluded that XBeach is a powerful tool to compute such complex situations.

Van Dongeren et al. (2009) have compared the beach profile model outputs of XBeach and the field data measured at different European sites. The model is found to be successful in computing the beach profile whereas the erosion around the mean water line and the depositions at the lower beach face are overpredicted.

With the progress of the computational power in the recent years, it is possible to determine the beach evolution and nearshore morphology with 2DH (two dimensional depth averaged), Quasi-3D or fully 3D numerical models. Here, Quasi-3D model is defined as two dimensional depth averaged numerical model with one dimensional vertical profile in order to take the return flows (undertow) into account (Briand and Kamphuis, 1993) where a fully 3D numerical model solves the governing hydrodynamic equations in three directions (Warner et al., 2008).

DELFT-3D (FLOW) that is the flow module of DELFT3D modelling package solves the depth-averaged or 3D shallow water equations. FLOW module is coupled with the WAVE module online at regular interval to account for the effects of waves on the flow and to provide flow boundary conditions for the wave transformation. Sediment transport under combined waves and currents is computed with an advection-diffusion equation (Trouw et al., 2012).

Nardin and Fagherazzi (2012) modeled the river bar formation with the coupled sediment transport and wave model DELFT3D-SWAN. It is concluded that wave characteristics (height, period, and direction) play an important role in the formation of mouth bars. In the numerical experiments waves affect bar development in three

ways: by modifying the direction of the river jet, by increasing bottom shear stresses at the river mouth, and by changing bottom friction and hence increasing jet spreading. Moreover, it is further shown that high waves with long period prevent the formation of mouth bars; in particular, wave angles between 45° and 60° are the least favorable to bar formation, likely producing a deflected river mouth.

In this study, XBeach, that is a two dimensional depth averaged numerical including hydrodynamic and morphodynamic processes, is applied for the modeling purposes.

CHAPTER 3

XBEACH NUMERICAL MODEL DESCRIPTION

In this chapter, the model structure of XBeach and the formulations that are used in the numerical model within the scope of this study are introduced.

3.1 Model Definition

XBeach is an open-source two-dimensional, depth-averaged numerical model developed to simulate the hydrodynamic and morphodynamic processes and impacts on coasts (Roelvink et al., 2015). The model consists of hydrodynamic formulations such as short wave transformation, long wave (infra-gravity waves) transformation, wave-induced setup and unsteady currents, as well as overwash and inundation. Morphodynamic formulations include bed load and suspended sediment transport, dune face avalanching, bed update and breaching (Roelvink et al., 2015).

The model requires mainly three input in order to simulate the hydrodynamics and/or morphology of a nearshore region: i) a structured (rectangular) grid bathymetry, ii) wave and flow boundary conditions and iii) relevant controlling parameters. Once the input parameters and the boundary conditions are defined, numerical model starts first solving the time dependent wave action balance equation given in Eq. 3.1, to compute nearshore wave characteristics. Next, roller energy balance equation is solved to compute the growth and decay of the kinetic energies of the surface rollers, and contribution of rollers to the wave-induced stresses on the nearshore currents and mean sea level. Later, the non-linear shallow water equations given in Eq.s 3.25 and

3.26 and the continuity equation given in 3.27 are solved to compute the nearshore currents and changes in the mean sea level.

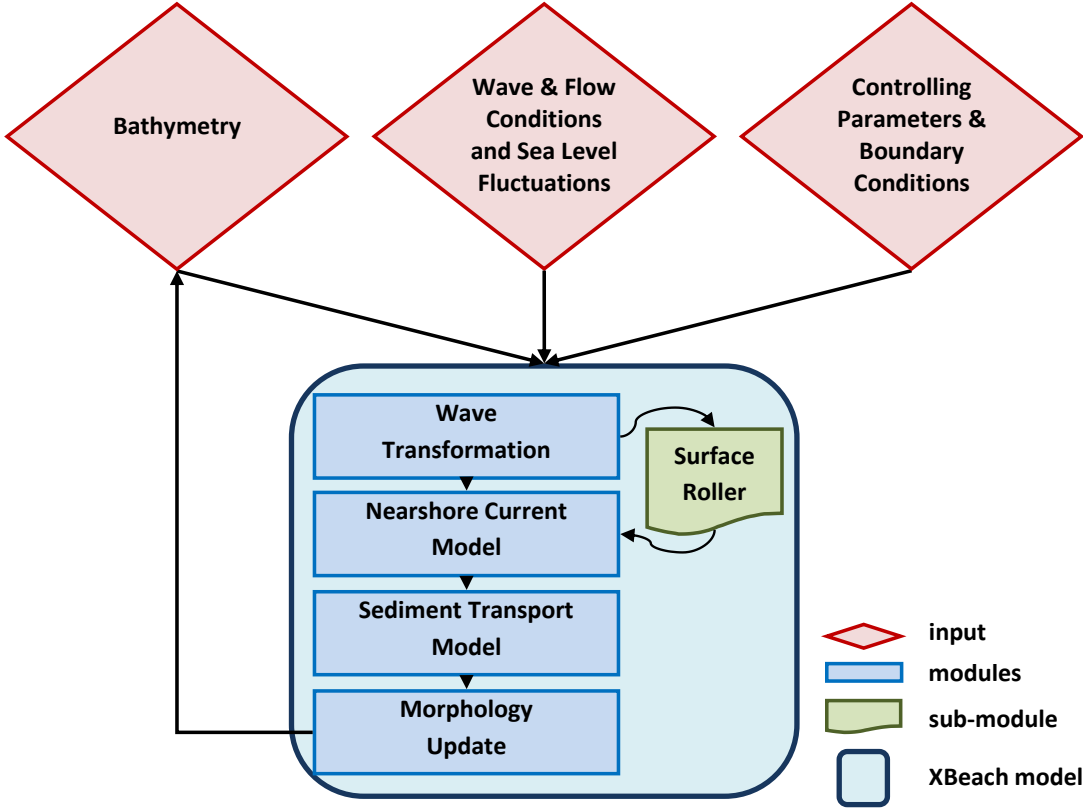


Figure 3.1 XBeach model structure flowchart

3.2 Wave Transformation Model

The wave model includes stationary, instationary (surfbeat) and non-hydrostatic modes for the wave transformation calculations.

- Stationary mode is used to solve wave-averaged formulations and wave action balance equation where the infragravity waves are excluded. In this study, stationary wave model is used for all cases.

- Surfbeat mode, which is also called instationary mode, is used in order to resolve short wave variations and the long waves associated with them.
- Non-hydrostatic mode is used in order to simulate the individual wave propagation and dissipation. The process is performed by solving the non-linear shallow water equations with a pressure corrected term included.

3.2.1 Short Wave Action Balance

Short wave transformation is solved with the Short Wave Action Balance equation developed by Delft University. Here, the time dependent wave action parameter is considered with directional distribution of the wave action where frequency spectrum is represented by a single characteristic frequency (Van Thiel de Vries, 2009).

The time dependent wave action balance equation both in x and y direction is followed by the Eq. 3.1:

$$\frac{\partial A}{\partial t} + \frac{\partial c_x A}{\partial x} + \frac{\partial c_y A}{\partial y} + \frac{\partial c_\theta A}{\partial \theta} = - \frac{D_w + D_f + D_v}{\sigma} \quad (3.1)$$

where t is time (in sec), θ is the angle of incidence with respect to x-axis, c_x and c_y are wave group celerities in x and y directions and c_θ is the wave propagation speed in θ -space. In Eq. 3.1 dissipation factors are defined as, D_w , wave breaking, D_f , bottom friction and D_v , vegetation. In this study, energy dissipation due to vegetation is not taken into consideration.

The wave action, A , is calculated by:

$$A(x, y, t, \theta) = \frac{S_w(x, y, t, \theta)}{\sigma(x, y, t)} \quad (3.2)$$

in which S_w is the wave energy density in each directional bin and σ is the intrinsic wave frequency. The propagation speeds are defined as in Eqs. 3.3, 3.4 and 3.5:

$$c_x(x, y, t, \theta) = c_g \cos \theta \quad (3.3)$$

$$c_y(x, y, t, \theta) = c_g \sin \theta \quad (3.4)$$

$$c_\theta(x, y, t, \theta) = \frac{\sigma}{\sin(2kt)} \left(\frac{\partial \theta}{\partial x} \sin \theta - \frac{\partial \theta}{\partial x} \cos \theta \right) \quad (3.5)$$

Here, t is defined as specified time, k is the wave number, h is the local water depth, θ is defined as the angle of incidence with respect to x-axis, σ may be obtained from the Eq. 3.6.

$$\sigma = \sqrt{gk \tanh(kh)} \quad (3.6)$$

where g is the acceleration due to gravity.

3.2.2 Wave Breaking

In XBeach model, wave breaking is solved for five different formulations which are Roelvink (1993), Roelvink (1993) extended, Daly et al. (2010), Baldock et al. (1998) and Janssen and Battjes (2007). The last two formulations are for the stationary waves condition and in this study only the Baldock et al. (1998) formulation is selected. Therefore, only Baldock et al. (1998) formulation is going to be defined in this chapter.

3.2.2.1 Wave Breaking for Baldock et al. (1998)

Baldock et al. (1998) formulation used in XBeach for stationary waves is given as:

$$\bar{D}_w = \frac{1}{4} \alpha Q_b \rho g f_{rep} (H_b^2 + H_{rms}^2) \quad (3.7)$$

$$Q_b = \exp \left[- \left(\frac{H_b^2}{H_{rms}^2} \right) \right] \quad (3.8)$$

$$H_b = \frac{0.88}{k} \tanh \left[\frac{\gamma kh}{0.88} \right] \quad (3.9)$$

Here, the wave breaking parameters are defined as α , wave dissipation coefficient, Q_b , the fraction of breaking waves, f_{rep} , representative frequency, H_b , breaking wave height, H_{rms} , root mean squared wave height, γ , breaker index and ρ , density of water.

3.2.3 Bottom Friction

The bottom friction dissipation (D_f) equation that is considered in the wave model separately from the momentum equations is shown in Eq. 3.10 (Jonsson, 1966).

$$D_f = \frac{2}{3\pi} \rho f_w \left(\frac{\pi H_{rms}}{T_{m01} \sinh kh} \right)^3 \quad (3.10)$$

Here, f_w is the short-wave friction coefficient and T_{m01} is the mean wave period defined by zeroth and first moment of the wave spectrum.

The dissipation parameter (D_f) is only considered in the wave action equation, which is not valid for the flow equations' bed friction parameters. According to Lowe et al. (2007), f_w should be larger than the friction coefficient due to flow depending on the

frequency of the wave motion. Thus, for the stationary case, the dissipation parameter is calculated as followed by Eq. 3.11.

$$\langle \widetilde{D}_f \rangle = 0.28 \rho f_w u_{orb}^3 \quad (3.11)$$

The parameter u_{orb} is defined as the orbital velocity amplitude and calculated from Eq. 3.12.

$$u_{orb} = \frac{\pi H_{rms}}{T_p \sinh(kh)} \quad (3.12)$$

Here, H_{rms} is the root mean square wave height, T_p is defined as the peak period, k is the wave number and h is the water depth .

3.2.4 Radiation Stresses

Radiation stress concept is defined by Longuet-Higgins and Stewart (1964) as the excess momentum flow caused by the wave motion itself derived from the momentum balance equation.

The change of radiation stress after the wave breaking process causes differences between the mean water levels, namely, wave set-up. Before the waves break, as the waves are shoaling, the mean water level lowered due to no loss of energy and steady increase of the radiation stress, which is also called wave set-down (Longuet-Higgins and Stewart, 1964).

Moreover, oblique incident waves induce longshore current in the surf zone. This causes the radiation stress variations of S_{xy} component over the width of the surf zone, which in the end, forces longshore current and hence longshore sediment transport.

Also, ‘surf beat’, which leads to a standing wave-pattern due to long waves, are the liberated long waves from the dissipated (due to friction and breaking) primary waves, i.e. wind-sea and swell (CIRIA, 2007). This phenomenon is also described by the radiation stress concept.

Moreover, wave-current interaction, non-linear wave interaction and damping of gravity waves by capillary waves are also explained by radiation stress terms.

The radiation stresses, (S), are defined as the Eqs. 3.13, 3.14 and 3.15:

$$S_{xx,w}(x, y, t) = \int \left(\frac{c_g}{c} (1 + \cos^2 \theta) - \frac{1}{2} \right) S_w d\theta \quad (3.13)$$

$$S_{xy,w}(x, y, t) = S_{yx,w}(x, y, t) = \int \sin \theta \cos \theta \frac{c_g}{c} S_w d\theta \quad (3.14)$$

$$S_{yy,w}(x, y, t) = \int \left(\frac{c_g}{c} (1 + \sin^2 \theta) - \frac{1}{2} \right) S_w d\theta \quad (3.15)$$

Here, parameters $S_{xx,w}$, $S_{xy,w}$, $S_{yx,w}$, and $S_{yy,w}$ are the radiation stresses due to the wave contribution in xx, xy, yx and yy directions and c_g and c are defined as wave group velocity and wave celerity, respectively.

3.2.5 Wave Shape

As waves propagate from deep water onto beach, the orbital motion become increasingly non-linear and waves approaching to shoreline become skewed in the shoaling region and become asymmetrical in the surf zone (Ruessink et al., 2012; Miles, 2013).

In XBeach model, two types of wave shape formulations are taken into account: i) A formulation of Ruessink et al. (2012) based on a parameterization with the Ursell

number and ii) A formulation of Van Thiel de Vries (2009) based on the parameterized wave shape model of Rienecker and Fenton (1981).

In this study, wave shape formulations of Van Thiel de Vries (2009), shown in Eq. 3.16 is considered in all runs.

$$u_{bed} = \sum_{i=1}^{i=8} wA_i \cos(i\omega t) + (1 - w)A_i \sin(i\omega t) \quad (3.16)$$

Here short wave shape is defined with the near-bed short wave flow velocity, u_{bed} . In this equation, i refers to the i^{th} harmonic, ω is the angular wave frequency, A_i is the amplitude of a specific harmonic and w is a weighting function affecting the wave shape.

The wave skewness is found by the Eq. 3.17:

$$S_k = \frac{\overline{u_{bed}^3}}{\sigma_{u_{bed}}^3} \quad (3.17)$$

The wave asymmetry can be found by replacing S_k with A_s and u_{bed} with its Helbert transformed value.

3.3 Surface Rollers

Aerated region of a breaking wave plays significant role on the longshore and cross-shore current velocities as well as the wave action itself. The landward shift of the longshore and cross-shore peak velocities is caused by this behavior (Dally and Osiecki, 1994). Thus, the behavior of the rollers in the nearshore area necessitates great attention especially when the purpose is to reveal the nearshore processes.

In XBeach, the surface roller energy balance is coupled to the wave action/energy balance where dissipation of wave energy serves as a source term for the roller energy balance (Roelvink et al, 2015).

3.3.1 Roller Energy Balance

The roller energy balance is given as:

$$\frac{\partial E_r}{\partial t} + \frac{\partial E_r c \cos \theta}{\partial x} + \frac{\partial E_r c \sin \theta}{\partial y} = D_w - D_r \quad (3.18)$$

where D_w is the dissipation caused by wave breaking and D_r is the dissipation caused by roller.

The wave dissipation parameter (D_w) is considered as the source term for the roller parameter.

Here, D_r is given in Eq. 3. 19:

$$D_r = \frac{2g\beta_r E_r}{c} \quad (3.19)$$

The roller contribution to the radiation stress is:

$$S_{xx,r}(x, y, t) = \int \cos^2 \theta S_r d\theta \quad (3.20)$$

$$S_{xy,r}(x, y, t) = S_{yx,r}(x, y, t) = \int \sin \theta \cos \theta S_r d\theta \quad (3.21)$$

$$S_{yy,r}(x, y, t) = \int \sin^2 \theta S_r d\theta \quad (3.22)$$

Here, the subscript “r” is denoted for the roller effect in radiation stress term “S”.

3.4 Non-Linear Shallow Water Equations

In order to consider the non-linear shallow water equations (NLSWE), the basic assumption is that the wave length (low frequency waves) is larger than the water depth. Also, mean flows can be computed using NLSWE.

In XBeach model, wave-induced mass-flux and the subsequent return flow are casted into Generalized Lagrangian Mean (GLM) formulation and the momentum and continuity equations are formulated in terms of Lagrangian velocity u^L and v^L which is defined as the distance a water particle travels in one wave period, divided by that period in x and y directions, respectively (Roelvink, 2015).

$$u^L = u^E + u^S \text{ and } v^L = v^E + v^S \quad (3.23)$$

$$u^S = \frac{E_w \cos \theta}{\rho h c} \text{ and } v^S = \frac{E_w \sin \theta}{\rho h c} \quad (3.24)$$

Here, u^E and v^E are the Eulerian velocity component where u^S and v^S are the Stokes' drift component, in x and y directions, respectively.

The resulting GLM-momentum Eq.s, 3.25, 3.26 and the continuity equation 3.27 are given by:

$$\frac{\partial u^L}{\partial t} + u^L \frac{\partial u^L}{\partial x} + v^L \frac{\partial u^L}{\partial y} - f v^L - v_h \left(\frac{\partial^2 u^L}{\partial x^2} + \frac{\partial^2 u^L}{\partial y^2} \right) = \frac{\tau_{sx}}{\rho h} - \frac{\tau_{bx}^E}{\rho h} - g \frac{\partial \eta}{\partial x} + \frac{F_x}{\rho h} - \frac{F_{v,x}}{\rho h} \quad (3.25)$$

$$\frac{\partial v^L}{\partial t} + u^L \frac{\partial v^L}{\partial x} + v^L \frac{\partial v^L}{\partial y} - f u^L - v_h \left(\frac{\partial^2 v^L}{\partial x^2} + \frac{\partial^2 v^L}{\partial y^2} \right) = \frac{\tau_{sy}}{\rho h} - \frac{\tau_{by}^E}{\rho h} - g \frac{\partial \eta}{\partial y} + \frac{F_y}{\rho h} - \frac{F_{v,y}}{\rho h} \quad (3.26)$$

$$\frac{\partial \eta}{\partial t} + \frac{\partial hu^L}{\partial x} + \frac{\partial hv^L}{\partial y} = 0 \quad (3.27)$$

where τ_{sx} and τ_{sy} are the wind shear stresses, τ_{bx}^E and τ_{by}^E are the Eulerian bed shear stresses, η is the water level, F_x and F_y are the wave-induced stresses, $F_{v,x}$ and $F_{v,y}$ are the stresses induced by vegetation, ν_h is the horizontal viscosity and f is the Coriolis coefficient. It should be noted that, in this study, wind, vegetation and Coriolis effects are not taken into account.

The wave induced (radiation) stresses are calculated as the following Eqs. 3.28 and 3.29 :

$$F_x(x, y, t) = - \left(\frac{\partial S_{xx,w} + S_{xx,r}}{\partial x} + \frac{\partial S_{xy,w} + S_{xy,r}}{\partial y} \right) \quad (3.28)$$

$$F_y(x, y, t) = - \left(\frac{\partial S_{yx,w} + S_{yx,r}}{\partial x} + \frac{\partial S_{xy,w} + S_{yy,r}}{\partial y} \right) \quad (3.29)$$

3.4.1 Horizontal Viscosity

Horizontal (lateral) viscosity is the parameter caused by the lateral shear stress due to lateral transfer of the momentum and consists of horizontal velocity gradients that may develop from the no-slip conditions at the boundaries (Colbo, 2006). It is calculated by Smagorinsky (1963) model and given in Eq 3.30:

$$\nu_h = c_s^2 2^{\frac{1}{2}} \sqrt{\left(\frac{\delta u}{\delta x}\right)^2 + \left(\frac{\delta v}{\delta y}\right)^2 + \frac{1}{2}\left(\frac{\delta u}{\delta x} + \frac{\delta v}{\delta y}\right)^2} \Delta x \Delta y \quad (3.30)$$

In Eq. 3.30, ν_h is the horizontal viscosity where c_s is the Smagorinsky constant. In this study, the Smagorinsky horizontal viscosity is not switched on. Instead, the ν_h parameter is multiplied by a factor to reduce the alongshore viscosity for calibration purposes (See Section 4.3.1).

3.4.2 Bed Shear Stress

The bed friction associated with mean currents and long waves is included via the formulation of the bed shear stress, τ_b . Using the approach of Ruessink et al. (2001) the bed shear stress is calculated with (Roelvink, 2015):

$$\tau_{bx}^E = c_f \rho u_E \sqrt{(1.16 u_{rms})^2 + (u_E + v_E)^2} \quad (3.31)$$

$$\tau_{by}^E = c_f \rho v_E \sqrt{(1.16 u_{rms})^2 + (u_E + v_E)^2} \quad (3.32)$$

In XBeach model, there are five different formulations in order to determine the dimensionless bed friction coefficient, c_f : *i*) Dimensionless friction coefficient, *ii*) Chézy, *iii*) Manning, *iv*) White-Colebrook and *v*) White-Colebrook grain size.

In this study, dimensionless friction coefficient is used for simulations, that is,

$$c_f = \frac{g}{C^2} \quad (3.33)$$

where C is the Chézy value.

3.5 Sediment Transport and Morphology Update

3.5.1 Parameters

In order to calculate the sediment concentrations, Galappatti and Vreugdenhil (1985) depth-averaged advection-diffusion scheme with a source-sink based on equilibrium sediment concentrations is solved (Roelvink et al., 2015) and the Eq. 3.34 is given as the following:

$$\frac{\partial hc}{\partial t} + \frac{\partial hc u^E}{\partial x} + \frac{\partial hc v^E}{\partial y} + \frac{\partial}{\partial x} \left[D_h h \frac{\partial C}{\partial x} \right] + \frac{\partial}{\partial y} \left[D_h h \frac{\partial C}{\partial y} \right] = \frac{hc_{eq} - hc}{T_s} \quad (3.34)$$

In Eq. 3.34, D_h is the sediment diffusion coefficient, C represents the sediment concentration whereas subscript “ eq ” is denoted for the equilibrium, h is the local water depth and T_s is the adaptation time which is determined by:

$$T_s = \max\left(f_{T_s} \frac{h}{w_s}, T_{s,min}\right) \quad (3.35)$$

The equilibrium sediment concentration (C_{eq}) is the threshold value which determines whether the sediment entrainment or deposition occur and it is calculated with several formulae of equilibrium transport rate in literature. C_{eq} is dependent on the following parameters:

- i) v_{mg} , velocity magnitude,
- ii) u_{rms} , orbital velocity and
- iii) w_s , fall velocity.

The velocity magnitude, v_{mg} , determined separately depending on the long wave stirring (lws) option is either on or off. In our case, lws is turned off, therefore the velocity is determined by the following Eq. 3.36:

$$v_{mg} = \left(1 - \frac{dt}{f_{cats} T_{rep}}\right) v_{mg}^{n-1} + \frac{dt}{f_{cats} T_{rep}} \sqrt{(u^E)^2 + (v^E)^2} \quad (3.36)$$

Here, f_{cats} is the averaging factor and T_{rep} is the representative wave period where the user could choose to define T_{rep} as T_{m01} or $T_{m-1,0}$ by input file.

The root mean squared orbital velocity, u_{rms} , is determined by Eq. 3.37:

$$u_{rms} = \frac{\pi H_{rms}}{T_{rep} \sqrt{2} \sinh(k(h + \delta H_{rms}))} \quad (3.37)$$

The fall velocity, w_s , is determined by Eq. 3.38:

$$w_s = \alpha_1 \sqrt{\Delta g D_{50}} + \alpha_2 \frac{\Delta g D_{50}^2}{v} \quad (3.38)$$

where the parameters, α_1 and α_2 , are given as:

$$\alpha_1 = 1.06 \tanh(0.016A^{0.50} \exp(-120/A)) \quad (3.39)$$

$$\alpha_2 = 0.055 \tanh(12A^{-0.59} \exp(-0.0004A)) \quad (3.40)$$

Wave breaking induced turbulence at the water surface has to be transported towards the bed in order to affect the up-stirring of sediment. There are three formulations of turbulence variance at the bed; i) wave averaged, ii) bore averaged and iii) none (turbulence is not considered at the bed). It should be noted that in this study, both long wave and short wave turbulences are not taken into account.

3.5.2 Formulations

In XBeach sediment transport module, there are two options of the formulations, namely, i) Soulsby-Van Rijn and ii) Van Thiel-Van Rijn. Both equations require sediment equilibrium value. The formulation of the equilibrium sediment concentration is calculated as the following Eq. 3.41:

The equilibrium concentrations of bed load and suspended load are compared to half of the maximum value of concentration, C_{max} , and summed up for the total equilibrium concentration in Eq. 3.41.

$$C_{eq} = \max \left[\min \left(C_{eq,b}, \frac{1}{2} C_{max} \right) + \min \left(C_{eq,s}, \frac{1}{2} C_{max} \right), 0 \right] \quad (3.41)$$

3.5.2.1 Formulation of Soulsby - Van Rijn (Van Rijn, 1984; Soulsby, 1997)

Sediment transport formulations of “Soulsby - Van Rijn” are considered and the formulations are given as (van Rijn, 1984a,b; Soulsby, 1997):

$$C_{eq,b} = \frac{A_{sb}}{h} \left(\sqrt{v_{mg}^2 + 0.018 \frac{u_{rms,2}^2}{c_d}} - U_{cr} \right)^{2.4} \quad (3.42)$$

$$C_{eq,s} = \frac{A_{ss}}{h} \left(\sqrt{v_{mg}^2 + 0.018 \frac{u_{rms,2}^2}{c_d}} - U_{cr} \right)^{2.4} \quad (3.43)$$

where

$$A_{sb} = 0.005h \left(\frac{D_{50}}{h\Delta g D_{50}} \right)^{1.2} \quad A_{sb} = 0.012D_{50} \frac{D_*^{-0.6}}{(\Delta g D_{50})^{1.2}} \quad (3.44)$$

In Eq. 3.44, D_* parameter can be calculated by:

$$D_* = \left(\frac{\Delta g}{v^2} \right)^{1/3} D_{50} \quad (3.45)$$

The critical velocity, U_{cr} , is the critical velocity where depth averaged velocity sediment motion is initiated:

$$U_{cr} = \begin{cases} 0.19D_{50}^{0.1} \log 10 \left(\frac{4h}{D_{90}} \right) & \text{for } D_{50} \leq 0.0005 \text{ m} \\ 8.5D_{50}^{0.6} \log 10 \left(\frac{4h}{D_{90}} \right) & \text{for } D_{50} > 0.05 \text{ m} \end{cases} \quad (3.46)$$

The drag coefficient, C_d , is calculated by Eq. 3.47:

$$C_d = \left(\frac{0.40}{\ln\left(\frac{\max(h, 10z_0)}{z_0}\right) - 1} \right)^2 \quad (3.47)$$

3.5.2.2 Formulation of Van Thiel - Van Rijn (Van Rijn, 2007; Van Thiel de Vries, 2009)

Sediment transport formulations of “Van Thiel-Van Rijn” are considered and the formulations are given as (van Rijn, 2007a,b,c; van Thiel de Vries, 2009):

$$C_{eq,b} = \frac{A_{sb}}{h} \left(\sqrt{v_{mg}^2 + 0.64u_{rms,2}^2} - U_{cr} \right)^{1.5} \quad (3.48)$$

$$C_{eq,s} = \frac{A_{ss}}{h} \left(\sqrt{v_{mg}^2 + 0.64u_{rms,2}^2} - U_{cr} \right)^{2.4} \quad (3.49)$$

The coefficients of bed load and suspended load in Eqs above, A_{sb} and A_{ss} , are calculated as the following formulae:

$$A_{sb} = 0.015h \frac{(D_{50}/h)^{1.2}}{(\Delta g D_{50})^{0.75}} \quad A_{ss} = 0.012D_{50} \frac{D_*^{-0.6}}{(\Delta g D_{50})^{1.2}} \quad (3.50)$$

The critical velocity is computed as in Eq. 3.51 (Van Rijn, 2007a):

$$U_{cr} = \beta U_{crc} + (1 - \beta) U_{crw} \quad (3.51)$$

Here, β coefficient is found from:

$$\beta = \frac{v_{mg}}{v_{mg} + u_{rms}} \quad (3.52)$$

In Eq. 3.50, U_{crc} and U_{crw} are defined as critical velocities for current and waves, respectively. U_{crc} is computed from Shields' criterion (1936) and U_{crw} is based on Komar and Miller's formulation (1975) and given in Eqs. 3.53 and 3.54:

$$U_{crc} = \begin{cases} 0.19D_{50}^{0.1} \log 10 \left(\frac{4h}{D_{90}} \right) & \text{for } D_{50} \leq 0.0005 \text{ m} \\ 8.5D_{50}^{0.6} \log 10 \left(\frac{4h}{D_{90}} \right) & \text{for } D_{50} \leq 0.002 \text{ m} \\ 1.3 \sqrt{\Delta g D_{50} \left(\frac{h}{D_{50}} \right)} & \text{for } D_{50} > 0.002 \text{ m} \end{cases} \quad (3.53)$$

$$U_{crw} = \begin{cases} 0.24(\Delta g)^{2/3} (D_{50} T_{rep})^{1/3} & \text{for } D_{50} \leq 0.0005 \text{ m} \\ 0.95(\Delta g)^{0.57} (D_{50})^{0.43} T_{rep}^{0.14} & \text{for } D_{50} > 0.0005 \text{ m} \end{cases} \quad (3.54)$$

3.5.3 Wave Non-linearity

XBeach model considers the wave energy of short waves as averaged over their length, hence does not simulate the wave shape. A discretization of the wave skewness and asymmetry was introduced by Van Thiel de Vries (2009), to affect the sediment advection velocity given in Eq. 3.55:

$$u_a = (f_{Sk} S_k - f_{As} A_s) u_{rms} \quad (3.55)$$

Here, u_a is a parameter depending on the wave skewness, S_k , wave asymmetry, A_s , root mean square velocity, u_{rms} and calibration factors for asymmetry and skewness, f_{As} and f_{Sk} . These calibration factors are defined by user and values should be between 0 and 1. Moreover, for simplicity, u_a parameter can be defined in advance ('*facua*' parameter). The higher values of u_a , the stronger onshore sediment transport component is derived (Roelvink et al, 2015).

3.5.4 Bed Update and Morphology

XBeach model simulates the bed level changes solving the Exner equation:

$$\frac{\partial z_b}{\partial t} + \frac{f_{mor}}{(1-p)} \left(\frac{\partial q_x}{\partial x} + \frac{\partial q_y}{\partial y} \right) = 0 \quad (3.56)$$

Here, z_b is the bed level, p is the porosity, f_{mor} is the morphological acceleration factor, q_x and q_y are the rates of sediment transport.

The morphological acceleration factor, f_{mor} , is used in order to save computational time. As an example, for 60 hydrodynamic minutes of simulation, if one selects f_{mor} as 6, the model runs for 10 minutes updating the bed level at each step by multiplying the transport rate by 6. This is recommended for short term simulations. It should be noted that, in XBeach, the morphological acceleration factor, f_{mor} , is used in two ways. However, the use of, f_{mor} , applied in this study is only described above.

Avalanching of the bed is introduced as another factor in the morphological update. It is significant to determine the critical bed slope in order to determine the amount of slumping. It is considered that inundated areas are much more prone to slumping and therefore two separate critical slopes for dry (*dryslp* term) and wet points (*wetslp* term) are used in XBeach (Roelvink et al., 2015) and the relation is shown in Eq. 3.57.

$$\left| \frac{\partial z_b}{\partial x} \right| > m_{cr} \quad (3.57)$$

When the critical slope, m_{cr} , is exceeded, the sandy material is exchanged between the adjacent cells to the amount needed to bring the slope back to the critical slope (Roelvink et al., 2015).

3.6 Boundary Conditions

The boundary conditions are classified and explained for i) Wave conditions, ii) Shallow water equations and iii) Sediment transport equations.

3.6.1 Waves

XBeach model wave boundary conditions are defined in two conditions: *i*) spectral and *ii*) non-spectral. User may also choose to define other special types of boundary conditions such as bichromatic waves, reuse of previous boundary conditions or may switch off the wave action in the whole domain. Since, the spectral wave boundary conditions are not taken into account in this study, only non-spectral wave boundary conditions will be discussed here.

Non-spectral wave boundary conditions are divided into two main options, *i*) Stationary wave boundary conditions and *ii*) Time series of waves. For the scope of this study, stationary wave boundary conditions are applied in the simulations. In order to define wave conditions, H_{rms} , T_{m01} , direction and power of the directional distribution function are introduced as wave input. In stationary waves, there are two possibilities to define the waves, namely, specifying the single sea state and specifying the series of sea states. In other words, wave conditions are applied for one sea state throughout the predefined duration or they are introduced as sub-time periods of different sea states in that duration.

Lateral boundary conditions are considered in order to determine the lateral end points of the wave action. There are three kind of lateral boundary conditions in XBeach model, which are *i*) Neumann, *ii*) Wave crests and *iii*) Cyclic. Neumann boundary condition where the longshore gradient is set to zero is applied in this study.

3.6.2 Shallow Water Equations

There are four boundary conditions for shallow water equations, namely, i) offshore, ii) lateral, iii) water level and iv) river-point discharge boundary conditions.

3.6.2.1 Offshore Boundary Conditions

An offshore boundary in XBeach indicates the wave and flow boundary conditions at the offshore of the model domain. There are six options for offshore boundary conditions: i) one dimensional absorbing-generating, ii) two dimensional absorbing generating wave model, iii) no flux wall, iv) water level specification, v) non-hydrostatic and vi) radiation boundary condition.

In this study, *two dimensional absorbing generating wave model* is applied as offshore boundary.

3.6.2.2 Lateral Boundary Conditions

Lateral boundaries are the boundaries perpendicular to the coastline. Usually these are artificial, because the model domain is limited but the physical coast will continue (Roelvink et al., 2015). The boundary condition is separated left and right which are the lateral boundaries that are perpendicular to the offshore boundary condition. There are five options: i) Neumann, ii) no flux wall, iii) only advective terms added velocity, iv) copy of adjacent velocity and v) cyclic boundary conditions.

In this study, *Neumann* is applied as lateral boundary conditions.

3.6.2.3 Water Level Boundary Condition

XBeach model allows defining the water level boundary conditions. In other words, tidal fluctuations may be introduced in the model input. There are four options for the boundary condition, namely, uniform water level, one time-varying, two time-varying and four time-varying water levels may be applied. In this study, one time-varying is applied as water level boundary condition.

3.6.2.4 River and Point Discharge Boundary Condition

Simulation of river and/or point discharge can be performed in XBeach numerical model. Discharge model is produced in a single discharge input or as a time series.

3.6.3 Sediment Transport

The boundary conditions for sediment transport are Neumann boundaries everywhere, implying that the cross-boundary gradients in the advection-diffusion equation are set to zero, as well as the gradients of the bed load transports in that direction. Cross-shore profile changes due to cross-shore transport gradients are possible, allowing the boundary to smoothly follow the rest of the model (Roelvink et al., 2015)

CHAPTER 4

COMPARISON OF LABORATORY DATA TO XBEACH NUMERICAL MODEL OUTPUT

Physical model experiments play crucial roles on verification and validation of constantly improving numerical models where sediment transport and coastal sedimentation dominated problems come into picture. Moreover, application of numerical models comparing the measured laboratory outputs provides valuable discussions and conclusions both on numerical and physical models.

In this section, an experimental data set at laboratory scale is compared with the XBeach numerical model in two aspects; the numerical model is first applied to the experimental data set in the original laboratory scale and later the numerical model is applied to the experimental data set that is scaled up with Froude scaling to investigate scale effects in the numerical model. Both model results are compared and discussed by means of hydrodynamic and morphological properties.

4.1 Large-Scale Sediment Transport Facility (LSTF) Data

Five series of movable bed physical model experiments were conducted in the US-Army Corps of Engineers (USACE), Engineer Research and Development Center (ERDC), Coastal and Hydraulics Laboratory's (CHL's) Large-Scale Sediment Transport Facility (LSTF hereafter) basin (Gravens and Wang, 2007). The purpose of these experiments is to gather quality data sets in order to test and validate new sediment transport relationships (Hanson et al., 2001; Gravens and Wang, 2007) as

well as the new numerical model algorithms for the headland structures such as detached breakwaters and T-groins (Hanson et al. 2006; Gravens and Wang, 2007).

The laboratory scale model consists of four wave generators, producing spilling wave conditions, and a LSTF instrumentation bridge with 14 fiber optic backscatter sensors (FOBS) so that the wave height, wave period, cross-shore and longshore velocity and sediment concentration data can be determined at any longshore location, i.e. in y-direction. The bridge consists of FOBS at 3.125 m (x_1), 5.2 m (x_2), 6.3 m (x_3), 7.125 m (x_4), 8.73 m (x_5), 10.125 m (x_6), 11.525 m (x_7), 13.125 m (x_8), 14.625 m (x_9), and 16.125 m (x_{10}) seaward from the wall of the laboratory basin (x-direction). The measured wave and current data at gauges (FOBS) x_{12} , x_{13} and x_{14} are taken into account as an average value.

There are five cases that are done in the scope of these experiments. The first series of the experiments are the base cases (Base Case 1 and Base Case 2) which are conducted to validate the sediment transportation relationships in the LSTF basin (Figure 4.1). These experiments consist of 6 runs in a row lasting 160 minutes each. The second and third series of experiments (Test 1 and Test 2) are performed in order to model the “tombolo” formation behind the detached breakwater (Figure 4.2) in 16 runs in a row (8 runs for Test-1 and 8 runs for Test-2) lasting 190 minutes each. The fourth series (Test 3) are designed for tombolo development in the lee of the T-Groin consisting of 6 runs lasting for 180 minutes each (Figure 3). The fifth series of experiments (Test 4) are to investigate the tombolo formation behind the detached breakwater with different dimensions and location comparing to the Test-1 and Test-2. This experiment is performed in 4 runs of 180 minutes each (Gravens and Wang, 2007).

In this study, Base Case 1 (BC1), Test 1 - Case 1 (T1C1), and Test 3 - Case 1 (T3C1) experiments are compared with the XBeach model results in order to determine and to test the capabilities of the numerical model. The three cases are selected in order to understand the behavior of the nearshore hydrodynamic and morphodynamic

behavior as well as the visualization of the phenomenon of the coastal sedimentation in the vicinity of structures. Accordingly, these cases are modeled with XBeach and then the numerical model results are compared with the LSTF data.

For BC1, T1C1 and T3C1 experiments, root mean square wave height (H_{rms}), peak period (T_p) and the mean wave breaking angle (θ) measured in front of the wave generation system are shown in Table 4.1. It should be noted that the mean wave breaking angle is not the same as the wave generators alignment due to refraction.

Table 4.1 Average values of offshore wave parameters measured at the offshore boundary (x_{12} , x_{13} and x_{14}) for BC1, T1C1 and T3C1.

	H_{rms} (m)	T_p (s)	θ (°)
BC1	0.161	1.459	6.5
T1C1	0.163	1.457	6.5
T3C1	0.158	1.458	6.5

The base case (BC1) is introduced into the numerical model, XBeach, in order to calibrate the model input parameters such as wave data, sediment transport and morphology parameters. Initial bottom profile given in BC1 experiment corresponds to an equilibrium profile which is obtained by generating the wave conditions for several hours until an equilibrium profile is reached since it is significant to ensure a stable profile in order to obtain consistent alongshore sediment transport values (Wang, 2006). Later, inserting the respective structures, this profile is also used in T1C1 and T3C1 experiments.

The laboratory bed is fairly uniform in the alongshore direction (Nam et al., 2009). Although there are minor differences between H_{rms} and T_p parameters for each case, the same calibrated input parameters are applied into the numerical model for T1C1 and T3C1 as in BC1, for the sake of simplicity.

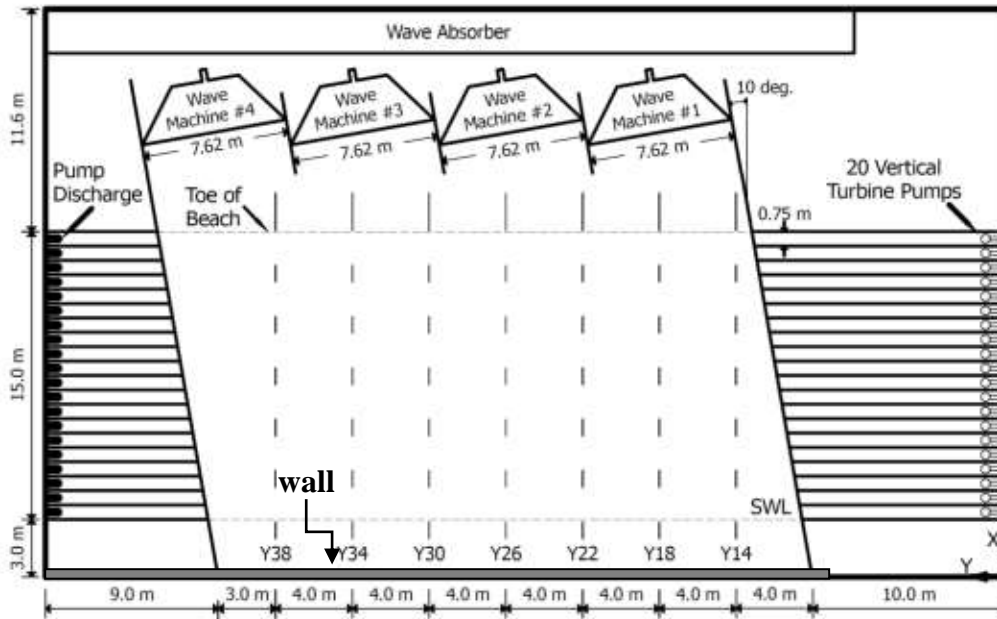


Figure 4.1 The plan view of the LSTF and alongshore locations of measurements of Base Case (BC1 in this study) (Wang et al., 2002; Gravens and Wang, 2007).

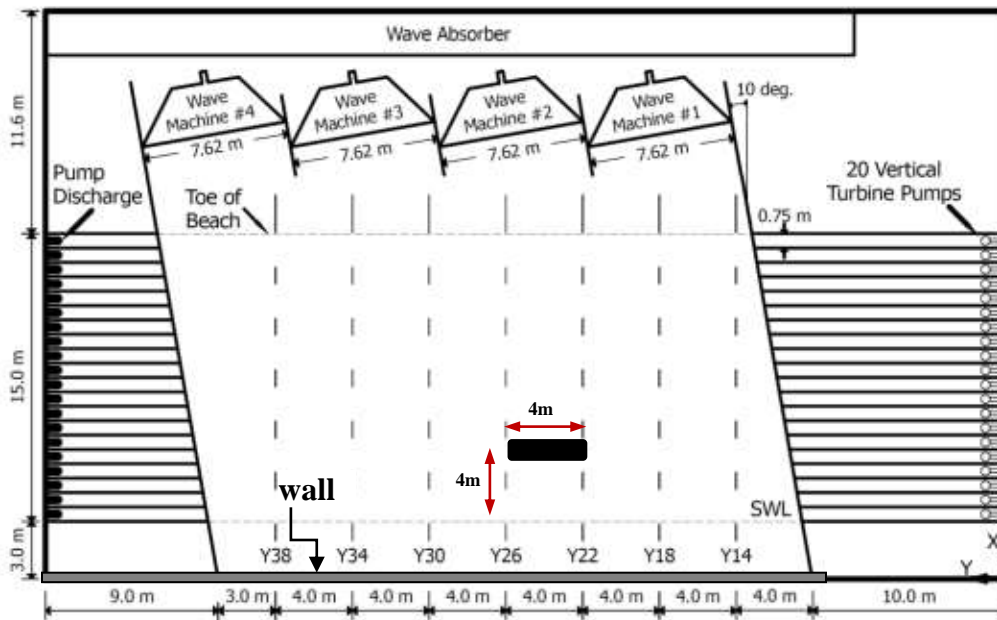


Figure 4.2 The plan view of the LSTF and alongshore locations of measurements of Test 1 (TIC1 in this study) (Gravens and Wang, 2007).

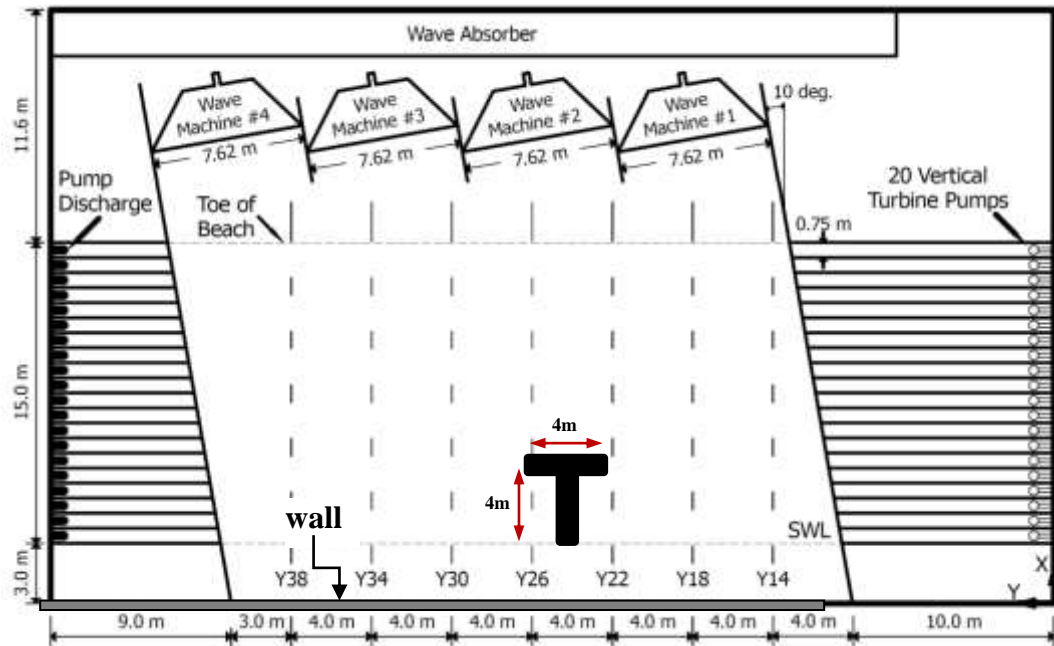


Figure 4.3 The plan view of the LSTF and alongshore locations of measurements of Test 3 (*T3C1* in this study) (Gravens and Wang, 2007).

4.2 Model Setup

LSTF laboratory dimensions are modeled and produced as in two types of bathymetric data, namely, one dimensional bathymetry, or profile, for BC1 and two dimensional bathymetries for T1C1 and T3C1. The bed level profile for BC1 is 18 m with 0.25 m grid size in x-direction shown in Figure 4.4. The bed level ranges approximately between -0.7 m up to +0.3 m from still water level.

Bed level consists of mainly uniform bottom contours in the alongshore direction (Nam et al., 2009). For the sake of simplicity, bathymetry bed level profiles are averaged, then, used as an input for the numerical model. In other words, the BC1 experiment bed levels are digitized as one dimensional (Figure 4.4) since BC1 bathymetry is the calibration experiment for the subsequent experiments and the

bathymetry consists of shore parallel bottom contour lines. Hydrodynamic and morphology parameters that are needed to be calibrated are applied on this 1D domain.

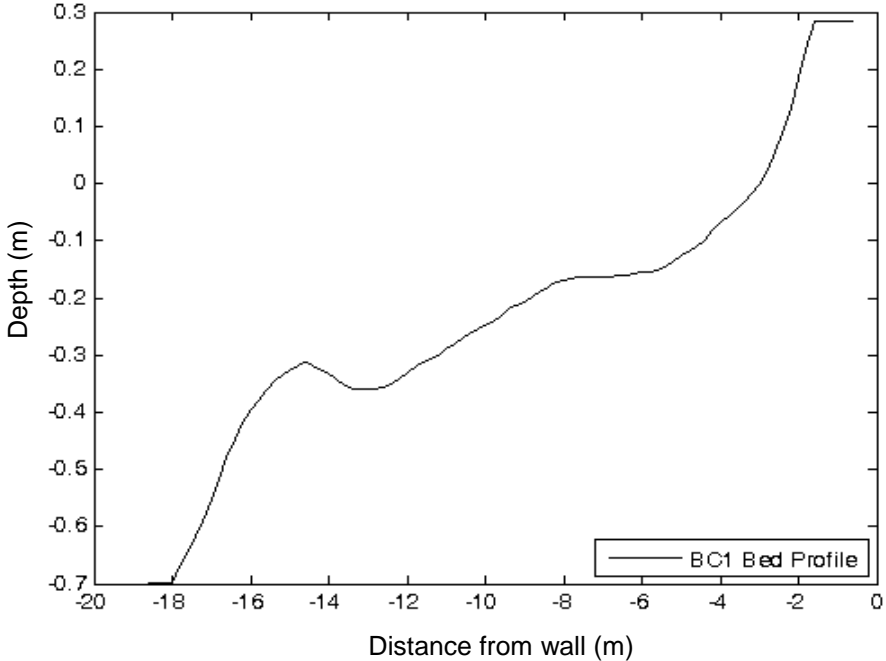


Figure 4.4 Averaged bed profile for BC1

For T1C1 and T3C1 runs, 18x27 m model bathymetries with 0.25 m grid size on both cross-shore and longshore directions are prepared. In order to interpolate between the model bed data, triangular interpolation is applied via Delft3D Graphical User Interface. Two dimensional model domains for T1C1 and T3C1 are shown in Figure 4.5.

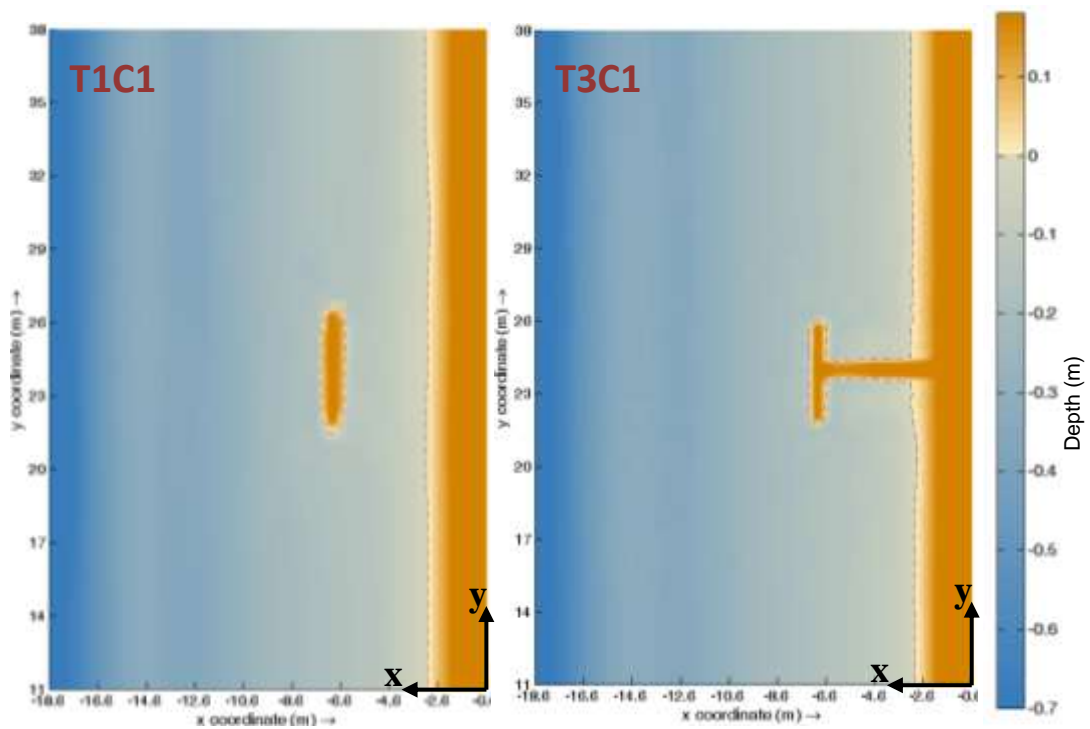


Figure 4.5 Two dimensional model domains for T1C1 (*left*) and T3C1 (*right*)

Here, it should be noted that cross shore direction is shown in negative values that, for example, the offshore boundary at $x = -18.6$ implies that it is 18.6 m from the wall shown in Figures 4.1, 4.2 and 4.3.

4.3 Model Calibration

The calibration process of wave, flow, sediment transport and morphology parameters for the BC1 case is revised until the measured BC1 wave, current and morphology output values are reached in the XBeach model output. The reason for taking into account BC1 for calibration is the simplicity of the model domain. Moreover, the purpose itself in the BC1 experiment is to set the basin to equilibrium both in hydrodynamically and morphologically in order to determine the coastal behavior in the presence of the structures such as detached breakwater and T-Groin.

When the adjustment and calibration of the parameters are finalized, BC1, T1C1 and T3C1 experiments are modeled according to the previously defined parameters.

4.3.1 Hydrodynamic Parameters

In this section, selection and calibration of the hydrodynamic parameters which are used as an XBeach input are going to be discussed for BC1, T1C1 and T3C1. Parameters other than discussed here are taken as the recommended values of the model.

The parameters that are related to the hydrodynamic conditions, the definitions of these parameters and the corresponding LSTF data for BC1, T1C1 and T3C1 are given in Table 4.2.

Table 4.2 Hydrodynamic parameters applied in the model for BC1, T1C1 and T3C1

PARAMETER	UNITS	DEFINITION	MODEL VALUES
<i>Hrms</i>	m	root mean square wave height	0.185
<i>Trep</i>	sec	representative wave period	1.459
<i>m</i>	-	directional distribution parameter	128
<i>break</i>	-	wave breaker type	Baldock
<i>gamma</i>	-	breaker index	0.94
<i>eps</i>	m	threshold water depth above which are considered wet	0.01
<i>hmin</i>	m	threshold water depth above which Stokes drift is included	0.1
<i>bedfriccoef</i>	-	bed friction coefficient	0.008
<i>nuhv</i>	-	longshore viscosity enhancement factor	0.05
<i>beta</i>	-	Breaker slope coefficient in roller model	0.016

' H_{rms} ', implying the root mean square wave height in XBeach model, is applied as 0.185 m at the toe of the basin shown in Figures 4.4 and 4.5. In the numerical model, the offshore boundary condition does not account for deep water depth for the given wave height which is considered as approximately 0.161 m for all cases as mentioned previously in Table 4.1. There is no data given about wave spectra in front of the wave generators. In fact, the only boundary condition for the waves is given in H_{rms} or H_{m0} parameters. Therefore, it is not possible to define a spectrum at the toe of the LSTF basin without assumptions. Consequently, the most appropriate solution is to apply a suitable H_{rms} value to the wave boundary condition that ensures the best fitting root mean squared wave height profile. Here, ' H_{rms} ' parameter in XBeach model is determined at the toe of the beach giving the closest value to the one at the far most gauge in the cross-shore direction (x_{10} which is 16.125 m from wall towards the sea). It should be noted that, elongating the bed profile until deep water wave conditions are reached may result in a deviation of the circulation pattern observed at the laboratory basin as well as unnecessarily long computational time.

' T_{rep} ', the representative wave period in the model, is assumed to be equal to the peak period measured in the experiments.

The directional distribution parameter, ' m ', is equal to $2s$ parameter in the following directional distribution function (Eq. 4.1):

$$D(\theta) = G(s) \left[\cos\left(\frac{\theta - \theta_0}{2}\right) \right]^{2s} \quad (4.1)$$

In Eq. 4.1, θ is the direction in radians, θ_0 is the mean wave direction, $D(\theta)$ is the angular spreading function, $G(s)$ is related to the gamma function and s is the directional spreading parameter. In the model, the directional parameter, m , is taken as 128 since the wave generation system is unidirectional in the laboratory.

The wave breaking type and the breaker index (*break* and *gamma* parameters, respectively) are taken same for all cases. The wave breaking type is chosen as the Baldock et al.'s approach (1998) that is explained in Section 3.2.2. The breaker index parameter is calibrated by trial and error with different values. For this formulation, it is assumed as 0.94 for all cases.

The parameter that is defined as the threshold water depth above which is considered wet is '*eps*'. In other words, '*eps*' parameter is used to determine the cell is whether dry or wet. This parameter is effective on the magnitude of current velocities. Several simulations are carried out for different values of '*eps*'. As it can be seen from Figure 4.7, the best value is selected as 0.01 m from the longshore velocity comparisons.

'*hmin*' parameter is the threshold water depth that is the limiter for the flow depth. Above this limit, Stokes' drift is included. The value is selected as 0.1 m for all cases. The comparison of XBeach output longshore velocities and LSTF data is shown in Figure 4.7 with varied values of '*hmin*' and '*eps*', between 0.01-0.1 for '*hmin*' and between 0.001-0.01 for '*eps*'.

In Figure 4.7, for the sake of simplicity, the longshore velocity profiles computed for the best matching values of *eps* and *hmin*, *eps*=0.01 m and *hmin*=0.1 m and for the minimum values of these parameters, *eps*=0.001 m and *hmin*=0.01.

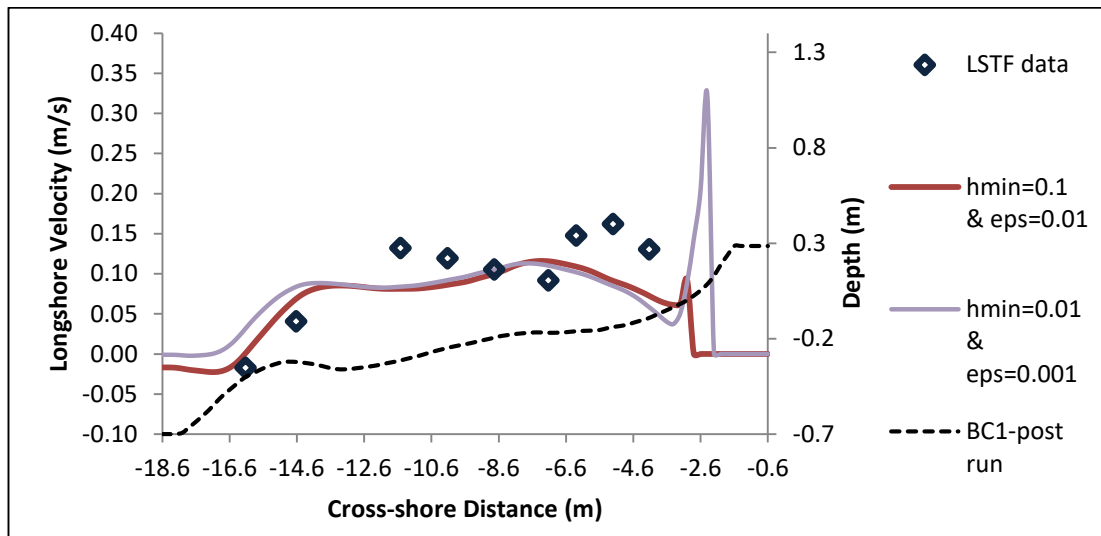


Figure 4.6 Comparison between the alongshore velocities of LSTF data and the computed data with jointly varied '*hmin*' and '*eps*' parameters

The selected values for '*hmin*' and '*eps*' parameters are not in agreement with the geometric dimensions of the experiments. One might expect to select them in accordance with the scale of experiment compared to the recommended values given for large scale or field scale cases. However, as seen from Figure 4.7, as '*hmin*' and '*eps*' values decrease, the flow velocities at the shoreline increase significantly. Also, it should be mentioned that, setting low values for '*hmin*' and '*eps*' parameters lengthens significantly the time required to reach the steady state solution of the velocities and mean water level for the given stationary wave field. Increase in the flow velocities at the shoreline amplifies the sediment transport and results in abrupt changes in the morphology here. From literature, the values used in this study are selected as the recommended values given for the field scale.

Bed friction is selected as '*cf*' formulation from available for the determination of the friction in wave-induced circulation as given in Section 3.2.3. The bed friction coefficient is applied as 0.008 and it is taken same for all cases.

'*nuhv*' parameter is the longshore viscosity enhancement factor and this parameter provides additional advective mixing in lateral directions when chosen higher than "1". However, here this factor is chosen smaller than unity in order to depreciate the cross-shore dispersion and to get higher values for wave induced velocity throughout the profile since these experiments are in the laboratory scale. Hence, for all cases and by trial and error, '*nuhv*' is chosen as 0.05 which gives the most appropriate solution for LSTF longshore velocity profile.

The last parameter that is to be selected is '*beta*' within the hydrodynamic parameters. This is the breaker slope coefficient in the roller model given in Section 3.3.1. The smaller the '*beta*' parameter, the more shoreward shift in wave induced setup, return flow and the alongshore current (Roelvink et al., 2015). The roller not only causes a shift in the peak of the longshore current towards the shoreline but it also increases the magnitude of the longshore current in the surf zone (Nam et al., 2009). Provided this information, '*beta*' is selected by trial and error as 0.016 which is far smaller than default, 0.1, in order to catch the longshore velocity trend that is observed in LSTF data.

4.3.2 Morphology Parameters

In this part, calibration of the morphology parameters which are used as XBeach model input are going to be discussed for BC1, T1C1 and T3C1. Morphology parameters include the sediment transport and bed update schemes and these parameters are given in Table 4.3. It should be indicated that the input bathymetry and hydrodynamic and morphology parameters are at laboratory scale here.

Table 4.3 Morphology parameters applied in the model for BC1, T1C1 and T3C1

PARAMETER	UNITS	DEFINITION	MODEL VALUES
<i>D50</i>	m	median grain size	0.00015
<i>form</i>	-	equilibrium sediment transport formulation	soulsby_vanrijn
<i>facua</i>	-	factor for setting wave asymmetry and skewness together	5
<i>dzmax</i>	m ³ /s/m	maximum erosion rate during avalanche	default
<i>hswitch</i>	m	water depth at which is switched from wet slope to dry slope	default
<i>turb</i>	-	short wave turbulence switch	0
<i>wetslp</i>	-	critical wet slope for the wet area	0.22
<i>dryslp</i>	-	critical dry slope for the dry area	0.23
<i>struct</i>	-	switch for the non-erodible structure	none

The median grain size parameter '*D50*' is given as 0.15 mm by Gravens and Wang (2007).

The sediment transport equilibrium formulations are selected as '*soulsby_vanrijn*' that uses the Soulsby and Van Rijn approach (Soulsby, 1997) for sediment concentration calculation. The reason for selecting this approach is that the '*vanthiel_vanrijn*' formulation did not give accurate results for the shoreline evolution and calculated extreme and wrong erosion scheme. Therefore, '*soulsby_vanrijn*' formulation is assumed to be more appropriate for this simulation. The '*facua*' parameter is the alias depending on the wave skewness and asymmetry and the parameter is the correspondent of the '*u_a*' in Eq. (3.49). The higher values of *u_a*, the stronger onshore sediment transport component is derived (Roelvink et al, 2015). The calibration of '*facua*' parameter consists of testing different values as

input while the other parameters stay the same. The aim here is to reveal the sensitivity of the *'facua'* parameter for the bed morphology. The best bed level between the computed and LSTF data corresponds to the value *'facua=5'* (Figure 4.8). On the other hand, the *'facua'* parameter is recommended to be selected between the values 0 and 1, according to Roelvink et al. (2015). It is seen that the numerical model overestimates the erosion rates for all of the cases and the accretion seemed to be insufficient when the parameter is chosen between the recommended range. Since increasing the value of the *'facua'* parameter yields to a higher onshore sediment transport rate, it needed to be increased further than unity, which is not a desirable aspect for this parameter.

The comparison of XBeach output bed profile for BC1 and LSTF measured bed profile is computed with varied values of *'facua'* between 0.1 - 5.0. In Figure 4.8, for the sake of simplicity, the longshore velocity profiles computed for the best matching values of *'facua=5'* and for the recommended values of this parameter, *'facua=0.1'*.

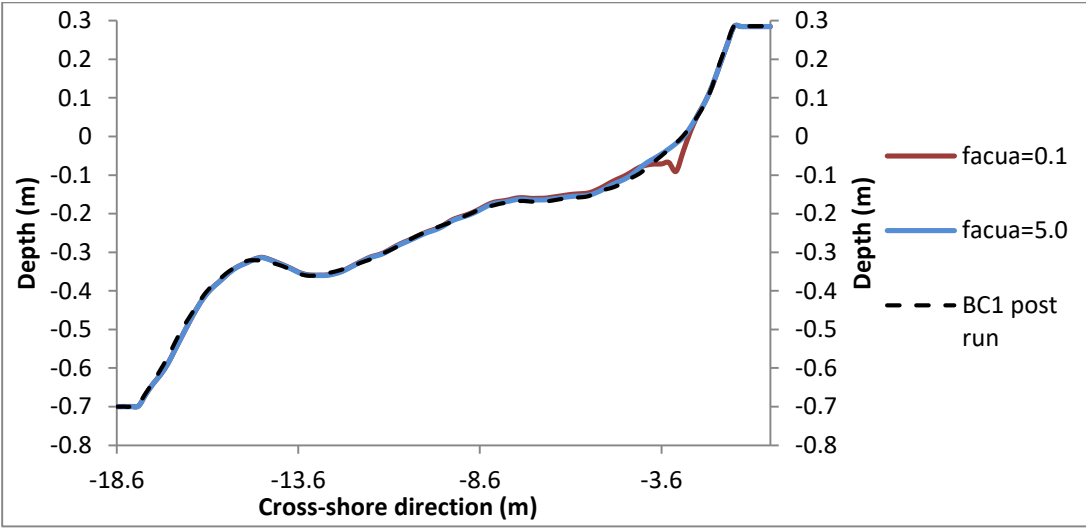


Figure 4.7 Comparison of computed bed profiles of BC1 with variable *'facua'* shown in whole profile.

The switches for short wave and long wave turbulence parameters, namely, '*turb*' and '*lwt*' are switched off due to high erosion rates when switched on.

The parameter to limit the maximum avalanching rate is the '*dzmax*' parameter in XBeach. Although Brandenburg (2010) suggests that the XBeach model is very sensitive to '*dzmax*' parameter for morphology computations, in Figure 4.9, the sensitivity analysis of '*dzmax*' parameter for the BC1 case shows that there is no significant difference between the bed morphology with varied '*dzmax*' value with these set of input parameters. Thus, '*dzmax*' parameter is remained as the recommended value of 0.05 for all cases in this study.

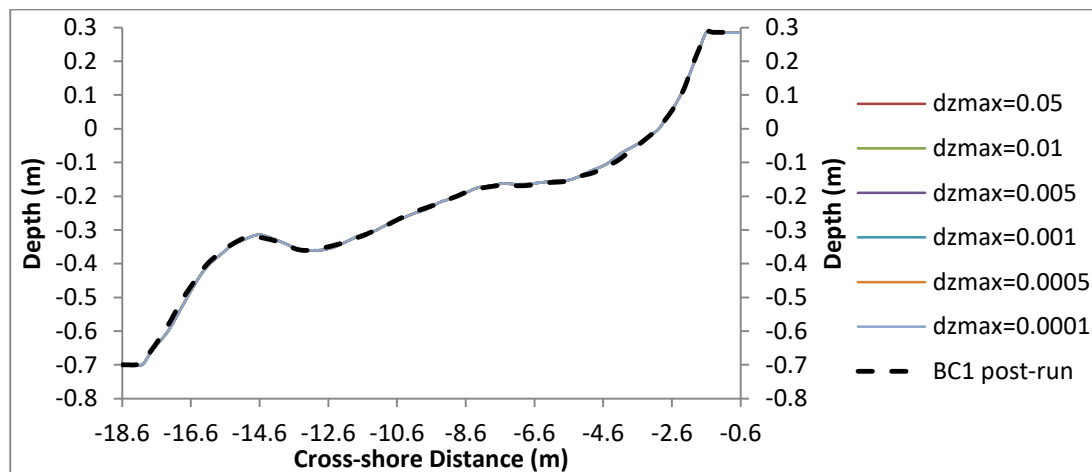


Figure 4.8 Comparison of computed bed profiles of BC1 with varying '*dzmax*'

'*hswitch*' parameter is defined as the limiter for the water depth which is switched from wet slope to dry slope. In other words, it is the minimum water depth where the wet slope avalanching is applied. It is indicated by Brandenburg (2010) that XBeach is sensitive to '*hswitch*' parameter in morphology calculations. However, in Figure 4.10, it is seen that there is no significant difference with this set of input parameters

between the varied values of 'hswitch'. Therefore, the parameter remained as 0.1 for all cases.

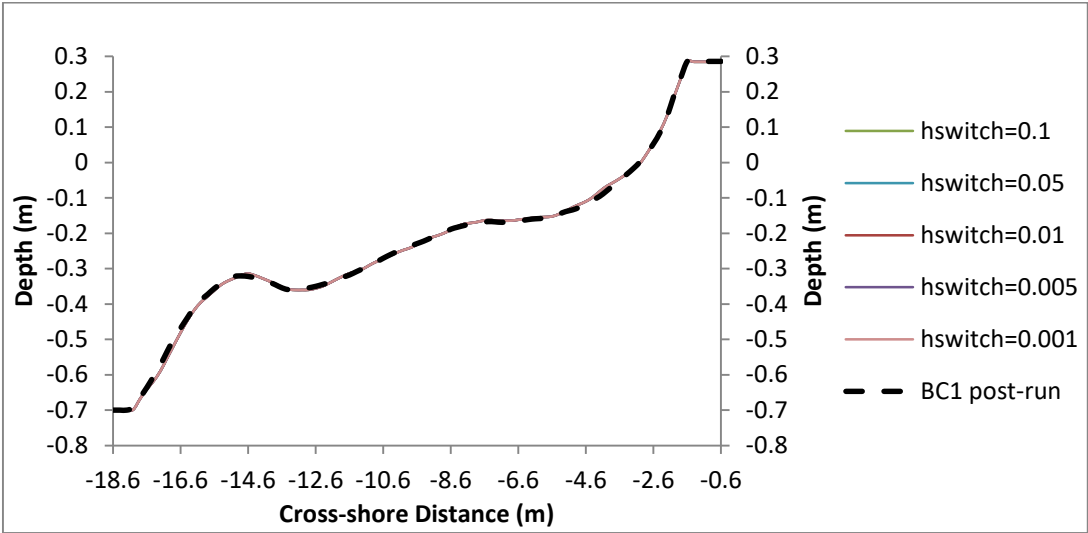


Figure 4.9 Comparison of computed bed profiles of BC1 with varying 'hswitch'

The parameters 'wetslp' and 'dryslp', defined as critical wet and dry slopes, are applied carefully because these parameters directly related with the avalanching process which is the main morphology behavior for these laboratory experiments. The selection of these parameters is done by the measured dimensions of the final morphology of LSTF bed level data. In this study, wetslp and dryslp are applied as 0.22 and 0.23, respectively, as given in Table 4.3.

Detached breakwater and T-Groin structures are defined as 'non-erodible layers' in XBeach. The distinction between erodible and non-erodible structures is introduced with a different bathymetry-like input format. The switch to introduce these structures on model bathymetry is 'struct' and turned on for T1C1 and T3C1 cases. Apparently, there is no need to define such a parameter in BC1.

4.4 Scale Dependency

XBeach numerical model is essentially developed for simulating hydrodynamic and morphological processes during short-term cross-shore sediment transport dominated events such as dune erosion or breaching due to strong storm waves action. Therefore, the recommended model parameters are more focused on the dune erosion processes and the formulations are inserted into the model according to the dune erosion scenarios in large model or prototype scales.

Brandenburg (2010) has done laboratory-scaled and prototype analyses in order to reveal the scale dependency of XBeach model. The experiments are done in the Deltares' wind and wave flumes facility. The data is determined with Froude scaling factors and they were $n_d=84$, $n_d=47$, $n_d=26$ for the small scaled experiments and $n_d=5$ for the large scaled experiment. Brandenburg (2010) compared the model results and the laboratory data for the above-mentioned laboratory scales. It is shown that XBeach hydrodynamic model scales to Froude and the foreshore wave heights estimated higher than the laboratory data when $n_d>26$.

Brandenburg (2010) proposed that '*dzmax*', '*hswitch*', '*hmin*' and '*eps*' parameters needed to be calibrated for variable laboratory scales. Moreover, the critical flow velocity may also be underestimated or the drag force on the sand grains is overrated, therefore the net effective flow velocity resulting in sediment transport is overestimated for small laboratory scales ($n_d>26$). Also the '*wetslp*' parameter, which is the critical wet slope, is needed to be calibrated in small scaled experiments. Combining these phenomena, the resulting morphology reveals overestimated sediment transport rates and hence increased erosion/accretion for small scale laboratory comparisons.

According to Brandenburg (2010), since the validation of the XBeach model with given default parameters are done by van Thiel de Vries (2009) with large experimental data, which is $n_d=6$, XBeach model is well compared with the large

scaled laboratory experiment data where the model is not sufficient for determining the small scaled data, ie. $n_d > 26$. The probable reasons for this may be explained with the limiters and some empirical model parameters that are causing significant errors in small-scale simulations and it is recommended that further calibration in the model composition may be done (Brandenburg, 2010).

Based on the information given above, the scale dependency issue in XBeach results in the overestimated erosion throughout the shoreline when compared to the LSTF data with the recommended parameters of the model. First attempt to reduce the effect of the overestimated erosion was adjusting the '*facua*' parameter which is increased nearly 50 times compared to the recommended value, given as between 0 and 1. The results of the sensitivity analysis for the parameter are given and discussed in Section 4.3.1. The second attempt was to scale the LSTF data to an assumed Froude scale factor (any scale was not given in LSTF data report) and it is assumed as $n_d = 25$ in this study. Input parameters are shown in Table 4.5 and 4.6. The purpose here by scaling the laboratory data to an assumed prototype is to reduce the negative scale effects and obtain more reasonable results from XBeach both for hydrodynamic outputs and the resulting morphology. Consequently, a model domain is regenerated based on the $n_d = 25$ Froude scale and input parameters are increased and/or adjusted according to this scaling factor. The results are scale back down to the original dimensions and these outputs are compared in Section 4.5.2.

According to Frostick et al. (2011), one should not use distorted models for longshore morphology planning as it is not known the scale effects that may influence the refraction pattern in the basin. Therefore, it is significant to note that the scale assumed in this study remained undistorted both for the bathymetry and other related wave and period parameters.

Table 4.4 Scaled hydrodynamic parameters applied in the model for BC1, TIC1 and T3C1 ($n_d=25$)

PARAMETER	UNITS	DEFINITION	MODEL VALUES
<i>Hrms</i>	m	root mean square wave height	4.63
<i>Trep</i>	sec	representative wave period (assumed as peak wave period)	7.3
<i>m</i>	-	directional distribution parameter	128
<i>break</i>	-	wave breaker type	Baldock
<i>gamma</i>	-	breaker index	0.94
<i>eps</i>	m	threshold water depth above which are considered wet	0.01
<i>hmin</i>	m	threshold water depth above which Stokes drift is included	0.1
<i>bedfriccoef</i>	-	bed friction coefficient	0.008
<i>nuhv</i>	-	longshore viscosity enhancement factor	0.005
<i>beta</i>	-	breaker slope coefficient in roller model	0.1

In the scaled runs, '*Hrms*' and '*Trep*' parameters are increased with the Froude scale $n_d=25$.

From Table 4.4, it is seen that '*nuhv*' parameter is decreased and '*beta*' parameter is increased in the scaled LSTF simulations comparing to the previous hydrodynamic parameters used in non-scaled runs (Table 4.2). The reason for this is the effects of the wave induced longshore velocity magnitudes and distribution throughout the laboratory basin. Since the wave heights and wave periods, thus, wave length is increased in the Froude scale of $n_d=25$, the wave induced longshore velocity magnitudes multiplied. In order to correctly demonstrate the longshore velocity

distribution, the horizontal viscosity further reduced in the scaled domain. On the other hand, '*beta*' parameter, that is responsible for the shoreward shift of the peak velocity in the roller model (Section 3.3.1), is taken as 0.1 since the shift is represented in the most appropriate value with the recommended '*beta*' value.

Table 4.5 Scaled morphology parameters applied in the model for BC1, T1C1 and T3C1 ($n_d=25$)

PARAMETER	UNITS	DEFINITION	MODEL VALUES
<i>D50</i>	m	median grain size	0.0004
<i>form</i>	-	equilibrium sediment transport formulation	vanthiel_vanrijn
<i>facua</i>	-	factor for setting wave asymmetry and skewness together	0.4
<i>dzmax</i>	m ³ /s/m	maximum erosion rate during avalanche	default
<i>hswitch</i>	m	water depth at which is switched from wet slope to dry slope	default
<i>turb</i>	-	short wave turbulence switch	0
<i>lwt</i>	-	long wave turbulence switch	0
<i>wetslp</i>	-	critical wet slope for the wet area	0.22
<i>dryslp</i>	-	critical dry slope for the dry area	0.23
<i>struct</i>	-	switch for the non-erodible structure	none

In the morphology input parameters for the scaled runs, '*D50*' is taken as 0.40 mm that differs from the non-scaled runs. The scaled median sediment grain size is determined according to the recommendation of Sutherland et al. (2006). Here, it is suggested that an undistorted model and corresponding prototype should take the same Dean fall speed parameter in a suspension dominant environment. Definition of the Dean fall speed parameter, D_{ws} , is given as:

$$D_{ws} = \frac{H_s}{w_s T_p} \quad (4.2)$$

where H_s is the significant wave height, w_s is the fall speed of the median sediment and T_p is the spectral peak wave period.

The suspension dominance criterion is determined from Soulsby (1997) according to the following conditions:

if $\theta_{ws} < \theta_{cr}$, then bed is immobile (assume rippled)

if $\theta_{ws} < \theta_{cr} < 0.8$, then bed is mobile and rippled

if $\theta_{ws} > 0.8$, then bed is mobile and flat with sheet flow

if $u_{*ws} \leq w_s$, then no suspension

if $u_{*ws} > w_s$, then sediment is suspended.

where θ_{ws} is the Shields parameter, θ_{cr} is the threshold Shields parameter and u_{*ws} is the friction velocity. Here, since the main concern is whether the suspension is dominant or not, the last two conditionals are applicable in this study. Therefore, only the related parameters are defined below.

The friction velocity, u_{*ws} , is computed from:

$$u_{*ws} = \sqrt{\frac{\tau_w}{\rho}} \quad (4.3)$$

where τ_w is the skin bed shear stress and ρ is the density of water. According to Soulsby (1997), τ_w may be obtained from:

$$\tau_w = \frac{1}{2} \rho f_w U_w^2 \quad (4.4)$$

In Eq. 4.4, f_w is the wave friction factor and U_w is the bottom orbital velocity. U_w is calculated from the JONSWAP curve given in Soulsby (1997):

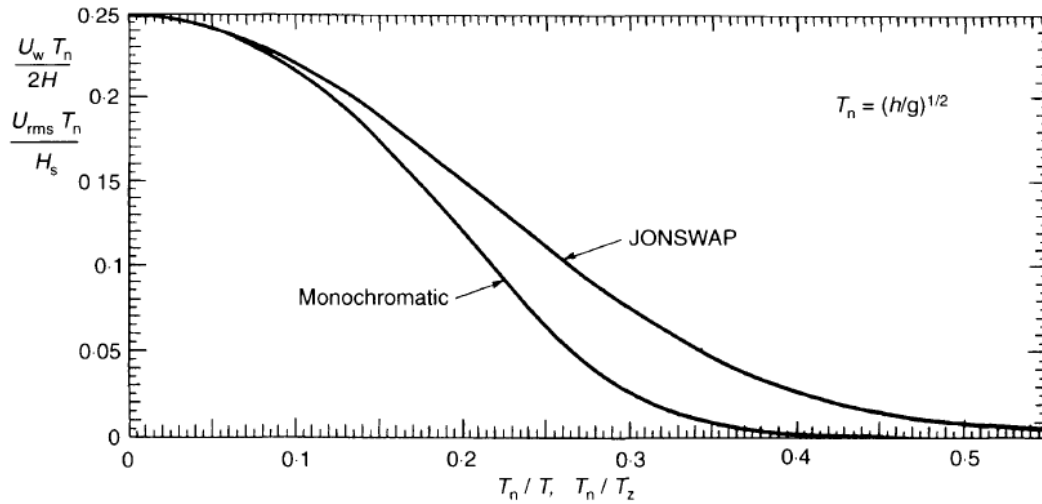


Figure 4.10 Bottom velocity for monochromatic $\left(\frac{T_n}{T}, \frac{U_w T_n}{2H}\right)$ and random $\left(\frac{T_n}{T_z}, \frac{U_{rms} T_n}{H_s}\right)$ waves (Soulsby, 1997).

Here, U_w and T_p are given as

$$U_w = \sqrt{2}U_{rms} \text{ and } T_p = 1.281T_z \quad (4.5)$$

where T_p is the peak wave period, T_n is already given in the upper right corner of the figure and T_z is the zero-upcrossing wave period.

The wave friction factor is also dependent on the wave Reynolds number, R_w , and the relative roughness, r :

$$R_w = \frac{U_w A}{\nu} \text{ and } r = \frac{A}{k_s} \quad (4.6)$$

where A is semi-orbital excursion and equals to $U_w T / 2\pi$, ν is the kinematic viscosity and k_s is the Nikuradse equivalent sand grain roughness, taken as, $k_s = 2.5 * d_{50}$. For rough turbulent flow friction factor, f_{wr} , is calculated following Soulsby (1997):

$$f_{wr} = 1.39 \left(\frac{A}{z_0} \right)^{-0.52} \text{ for all } r \text{ values} \quad (4.7)$$

For smooth turbulent flow friction factor, f_{ws} , is calculated from:

$$f_{ws} = BR_w^{-N} \quad (4.8)$$

where

$$B = 2, N = 5 \text{ for } R_w \leq 5 * 10^5$$

$$B = 0.0521, N = 0.187 \text{ for } R_w > 5 * 10^5$$

For the parameters f_{wr} and f_{ws} , the greatest of them is selected as f_w in Eq. 4.4.

Fall velocity, w_s , is calculated following Soulsby (1997):

$$w_s = \frac{\nu}{d_{50}} \left[(10.36^2 + 1.49D_*^3)^{1/2} - 10.36 \right] \text{ for all } D_* \quad (4.9)$$

In Eq. 4.9, ν is the kinematic viscosity taken as $1 * 10^{-6} \text{ m}^2/\text{s}$, d_{50} is the median sieve diameter of the grains and D_* is the dimensionless grain size obtained from:

$$D_* = \left[\frac{g(s-1)}{\nu^2} \right]^{1/3} d_{50} \quad (4.10)$$

where g is the gravitational acceleration, taken as 9.81 m/s^2 and s is the ratio of densities of grain and water, taken as 2.65.

Since the calibration case is BC1 as an equilibrium profile, fall velocities w_s and friction velocities u_{*ws} are computed for each cross-shore location of BC1 profile with the corresponding hydrodynamic parameters measured at each FOBS, such as significant and mean wave heights and peak wave periods.

It is seen that $u_{*ws} > w_s$ is true for each cross-shore location, therefore, the dominant sediment transport mode is determined to be *suspension*. Consequently, it is appropriate to use Dean fall parameter scaling in order to determine the corresponding prototype scale parameter.

As a result, with the Froude scale factor $n_d=25$, the median grain diameter increases from 0.15 mm to 0.40 mm in the scaled simulations.

'*facua*' parameter, as given in Section 4.3.2, is defined in the model as the wave asymmetry and skewness factor and recommended between values 0 and 1. However, in the non-scaled runs, the '*facua*' parameter is exaggerated in order to prevent excess erosion and promote more accretion. In the scaled runs, on the contrary, this parameter is decreased to 0.4 comparing to the non-scaled runs since the erosion-accretion scheme gives reasonable output values.

4.5 Comparison of Results

In this section, the output results of XBeach model and the LSTF data are compared for BC1, T1C1 and T3C1 according to two scenarios:

i) Non-scaled LSTF data

ii) Scaled LSTF data ($n_d=25$)

In non-scaled LSTF simulations, the laboratory dimensions are taken the same and the hydrodynamic and morphology parameters are taken as shown in Table 4.2 and Table 4.3.

In the scaled LSTF simulations, the laboratory dimensions are scaled up with respect to the Froude scale $n_d=25$. Also, the median grain size is scaled keeping Dean fall velocity parameter same both for model and prototype. Hydrodynamic and morphodynamic parameters are adjusted according to this scale as given in Table 4.4 and Table 4.5. After obtaining the simulation results from XBeach in scale of $n_d=25$, the values are rescaled down to the original dimensions according to Froude scaling factor once again and these scaled-down results are compared with the LSTF laboratory data.

In all simulations, one dimensional cross shore profile of BC1 and six cross-shore profiles for T1C1 and T3C1 (as shown in Figure 4.11) and measured LSTF data are compared to the XBeach outputs according to root mean square wave height, wave induced longshore velocity, mean water level values and the resulting bed profile. Moreover, the initial and final (computed as depth averaged) two-dimensional morphologies for both LSTF data and the XBeach outputs are compared in this section.

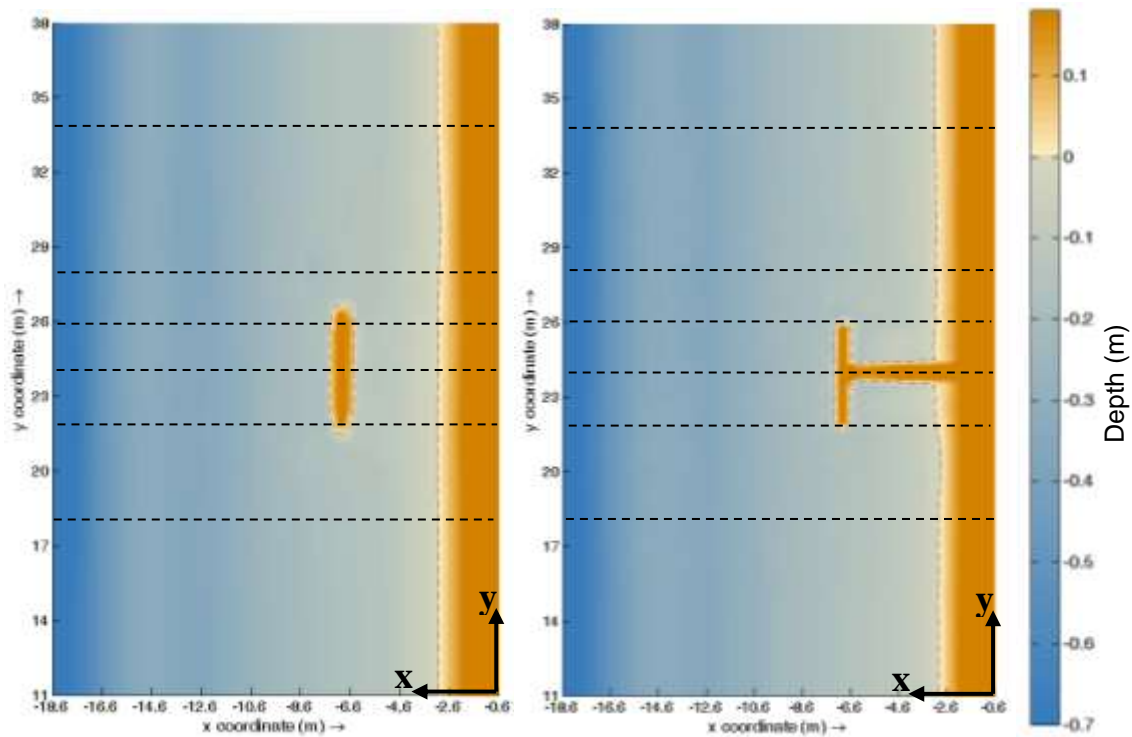


Figure 4.11 Modeled bathymetries and the cross sections for T1C1 and T3C1

4.5.1 Non-scaled LSTF Data

In this section, measured laboratory experiment data is compared with its corresponding case (BC1, T1C1 and T3C1) to XBeach output with the given parameters in Table 4.2 and 4.3. The duration of each run is 180 minutes.

4.5.1.1 Experiment Base Case 1 (BC1)

As explained before, BC1 is the adjusted LSTF configuration where the cross-shore profiles are same all over the domain. Therefore, for the sake of simplicity and to reduce the computational time, the model bathymetry is given as a one dimensional profile. BC1 experiment is performed in order to calibrate the bed profile and hydrodynamic conditions for the subsequent experiments. Initial bottom profile

given in BC1 experiment corresponds to an equilibrium profile which is obtained by generating the wave conditions for several hours till an equilibrium profile is reached for the given waves. Later, inserting the respective structures, this profile is also used in T1C1 and T3C1 experiments. Thus, the main purpose here is to obtain an unchanged (equilibrium) bed profile far from structures or in the absence of structures to emphasize the sedimentation behavior in the vicinity of a structure such as detached breakwater (T1C1) or T-Groin (T3C1).

The LSTF Experiment measurements and the XBeach model results are compared and discussed for the Base Case-1 (BC1) by the root mean square wave height (H_{rms}), the wave induced longshore velocity (v), the mean water level (η_{mean}) and the initial and final bed profiles in Figures 4.12, 4.13, 4.14 and 4.15.

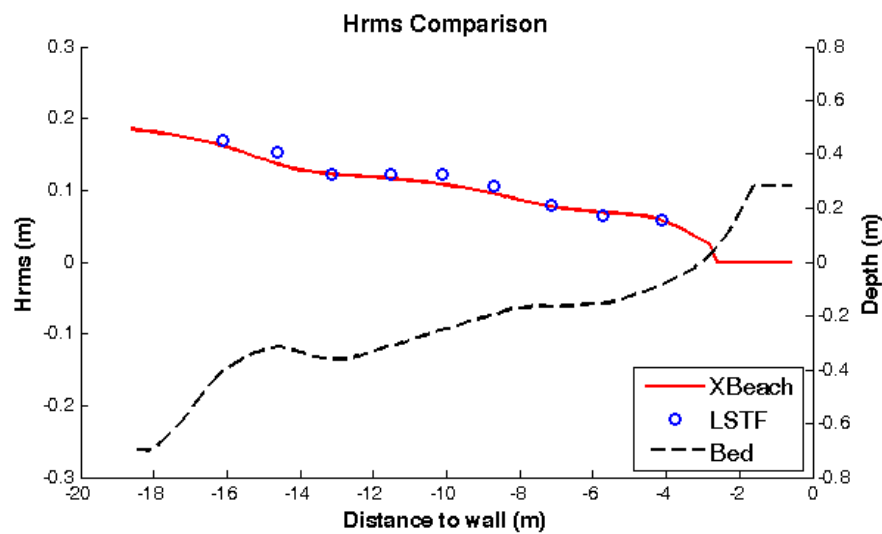


Figure 4.12 Root mean squared wave height comparison for BC1

It is seen from Figure 4.12 that the root mean squared wave heights are compared to the measured data fairly well. Moreover, the mean absolute error is obtained as 5.67 % indicating that the root mean squared wave heights are predicted in agreement with the measured values.

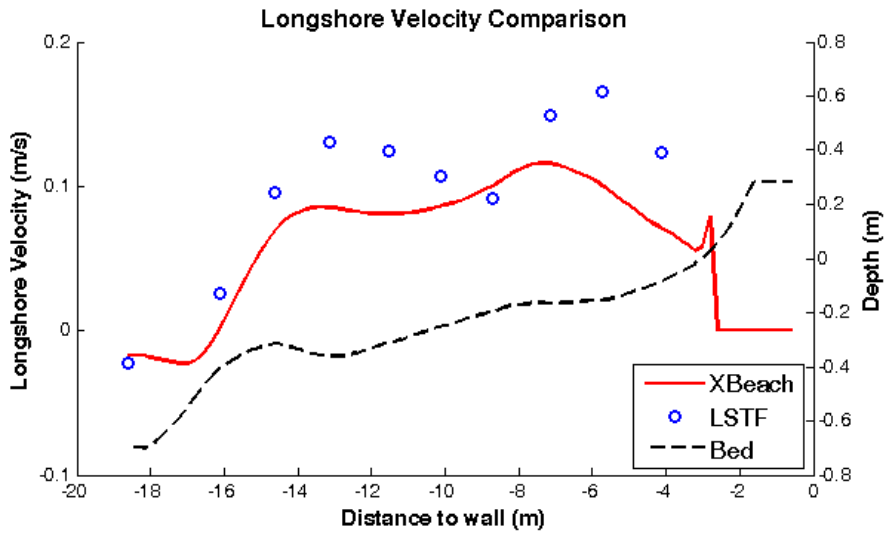


Figure 4.13 Wave induced longshore velocity comparison for BC1

XBeach model wave induced longshore velocity results compared to the measured data indicated some differences shown in Figure 4.13. It can be derived from the figure that the velocity profile is underestimated in general comparing to the measured ones although model output reveals a similar trend to the measured values. The mean absolute percentage error is obtained as 36.2% for the velocity comparison. The possible reason for the underestimation may be due to underestimation of radiation stress and roller effect components in the computations. Although, the lateral mixing viscosity enhancement factor parameter ($nuhv$) is lowered from the recommended value, the velocities could not reach the measured values. The peak longshore velocity value, which is the nearest to the shoreline, is not reached possibly due underestimation of the roller effects. Therefore, a detailed analysis and focus on the wave induced stresses in the momentum equations may be done for this study as a future work.

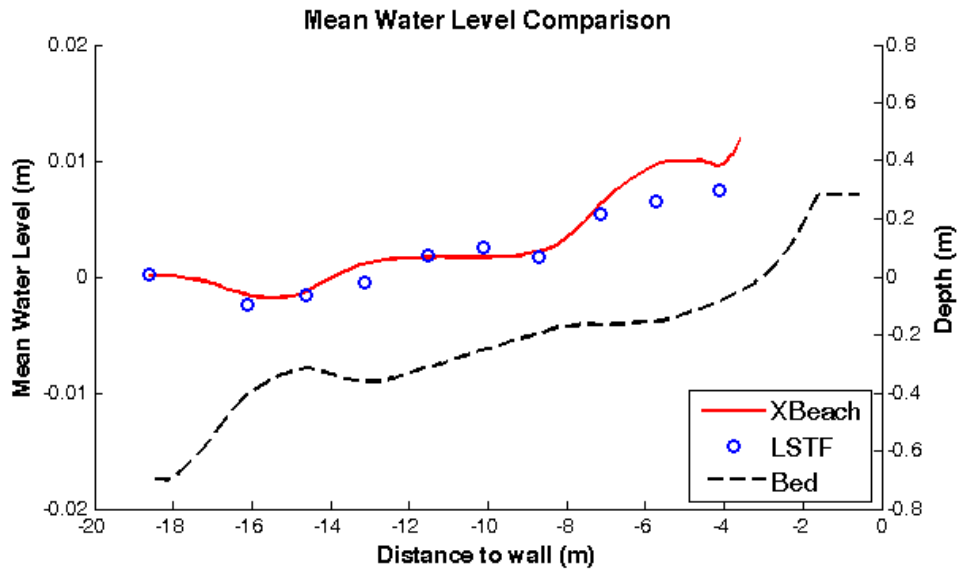


Figure 4.14 Mean water level comparison for BC1

Observed LSTF and XBeach model output mean water levels are compared in Figure 4.14 and it can be seen from the figure that model mean water levels have slightly higher values than observed. The mean absolute percentage error is between the measured and predicted data is 27.5 %. It is assumed to be a result of the wetting-drying algorithm used in the model, as XBeach is mainly developed and calibrated for dune erosion or overwash behavior near coastal regions, thus, the model may overestimate the wave setup amount contrary to the observed case. This issue should be further investigated in detail.

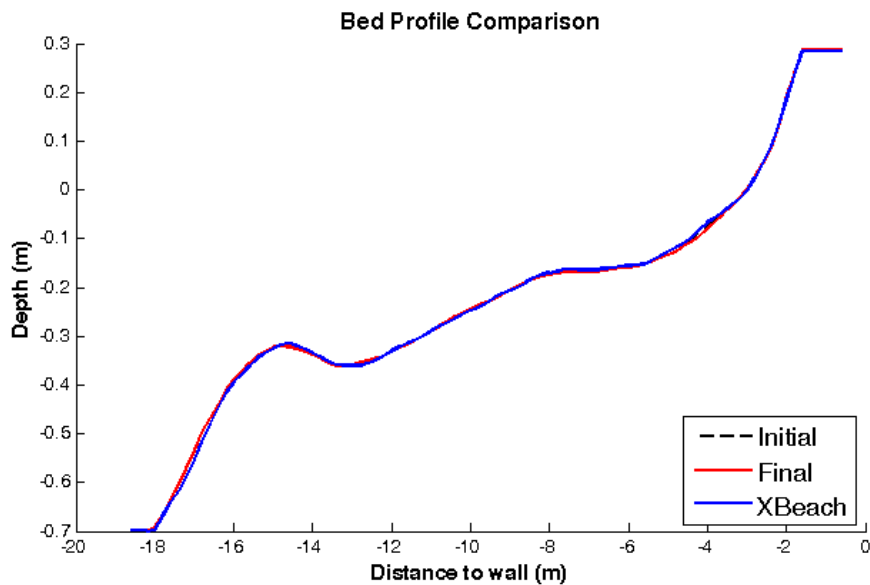


Figure 4.15 Measured initial bed level and computed and measured final bed level comparison for BC1

The initial bed, measured final bed and computed final bed profiles are shown in Figure 4.15. The measured initial and final bed profile remain unchanged with minor fluctuations. The mean absolute percentage error is 4.8% between the measured and predicted bed levels, which indicates a quite well estimation. Consequently, the computed final bed profile is calibrated to remain unchanged as much as possible by applying unreasonably high facua parameter, which is 5, and forcing the model not to erode near shoreline with the hydrodynamic and the morphology parameters given in Tables 4.2 and 4.3.

Nam et al. (2009) also modeled the LSTF BC1 experiment as mentioned in Section 2.3. It is also indicated that wave heights are well compared with the numerical model as in the case here. Moreover, the longshore current is improved with the roller model on with the roller parameter $\beta=0.1$ where the in the present study β is chosen further smaller. It is concluded in Nam et al. (2009) that the simulations show that the model reasonable predictions.

4.5.1.2 Experiment Test-1 Case-1 (T1C1)

The LSTF experiments named Test-1 are done in order to determine the hydrodynamic and morphologic behavior in the presence of the detached breakwater and the experiments started with the T1C1 run. The purpose in this laboratory-scaled experiment is to indicate the natural behavior of the wave breaking and the resulting flow velocities, thus sedimentation, near the headland structure. Here, the measurements and the non-scaled outputs of XBeach are compared and discussed in the root mean square wave height (H_{rms}), the wave induced longshore velocity (v), the mean water level (η_{mean}) and the initial and final bed levels from Figure 4.16 to Figure 4.25.

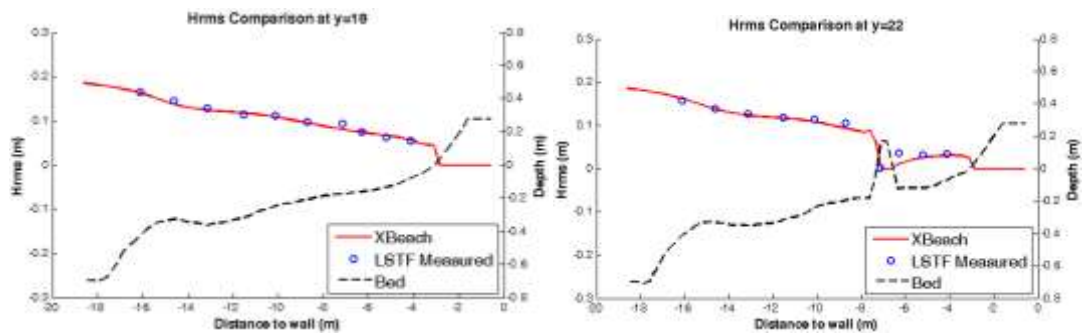


Figure 4.16 T1C1 Measured and computed H_{rms} values for $y=18$ m and $y=22$ m

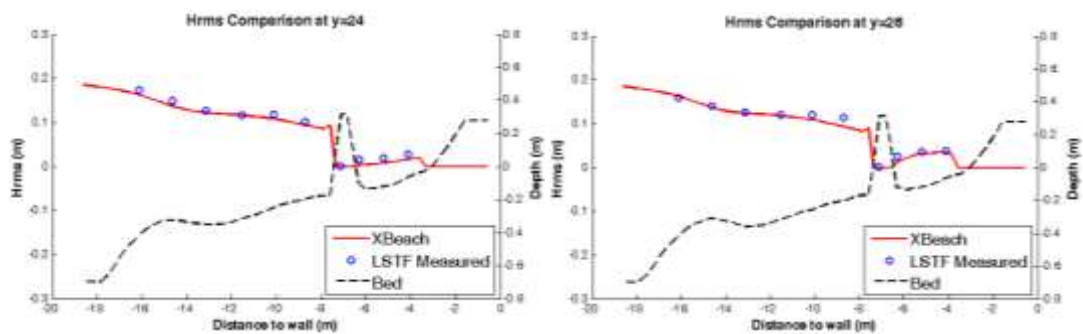


Figure 4.17 T1C1 Measured and computed H_{rms} values for $y=24$ m and $y=26$ m

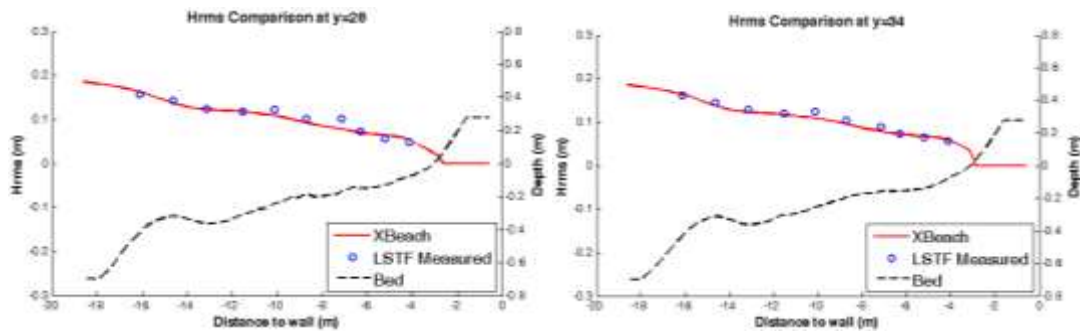


Figure 4.18 T1C1 Measured and computed H_{rms} values for $y=28$ m and $y=34$ m

In Figure 4.16, 4.17 and 4.18, it is seen that H_{rms} values are compared fairly well between the computed and the measured values. This is the fact that is expected to be true since the wave boundary conditions do not vary from the BC1 case. This is again a significant proof that the wave energy dissipation effects are modeled accurately. Especially, in Figure 4.17, the root mean squared wave heights behind the breakwater show that after interaction with an obstacle (in this case a detached breakwater) XBeach model works well in the lee of the breakwater, which implies the diffraction in the numerical model works properly.

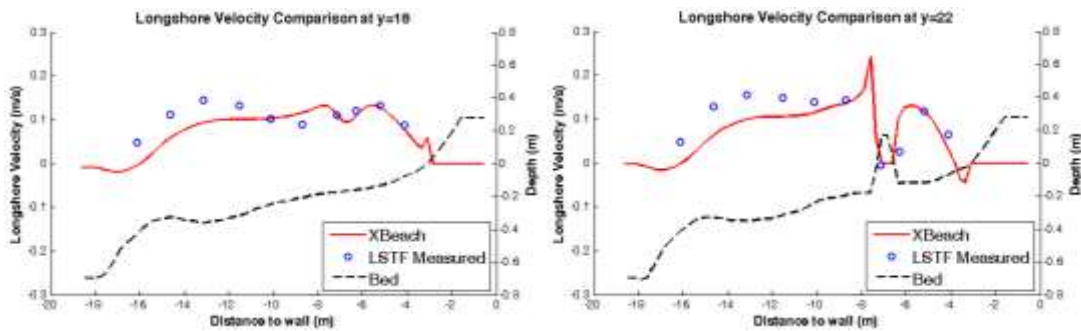


Figure 4.19 T1C1 Measured and computed ' v ' values for $y=18$ m and $y=22$ m

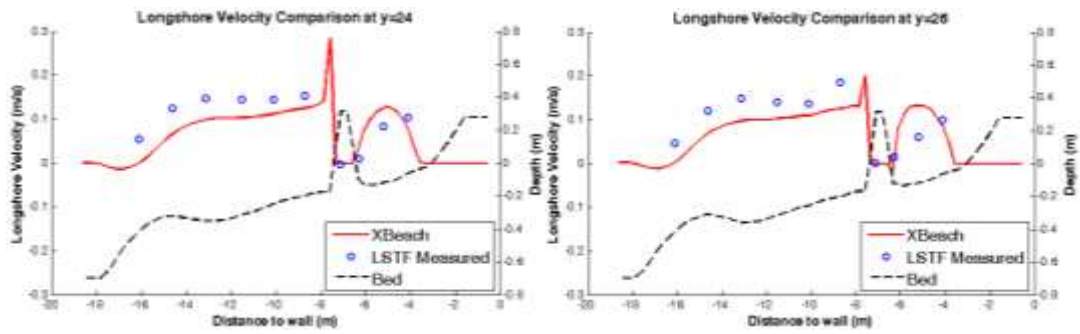


Figure 4.20 TIC1 Measured and computed ‘ v ’ values for $y=24\text{ m}$ and $y=26\text{ m}$

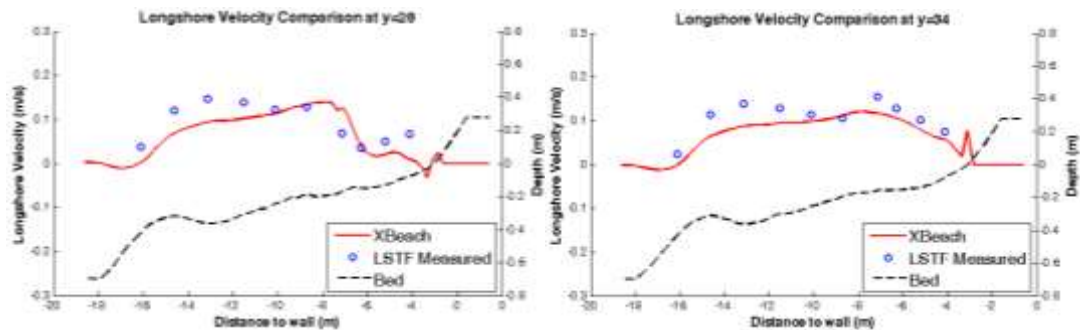


Figure 4.21 TIC1 Measured and computed ‘ v ’ values for $y=28\text{ m}$ and $y=34\text{ m}$

The wave induced longshore velocity comparison between the LSTF laboratory measurements and the computed longshore velocities are given in Figure 4.19, 4.20 and 4.21. It can easily be derived that the computed velocities are slightly underestimated comparing to the measured data and they follow the measured velocities’ trend in general. The computed longshore velocity indicated differences as explained in the BC1 run. Moreover, at the longshore stations $y=22\text{ m}$, $y=24\text{ m}$ and $y=28\text{ m}$, namely, where the structure is located, a velocity jump in front of the structure is observed. These peaks could be related to sharp changes in the wave heights around the structure and thus the increased gradients of radiation stresses.

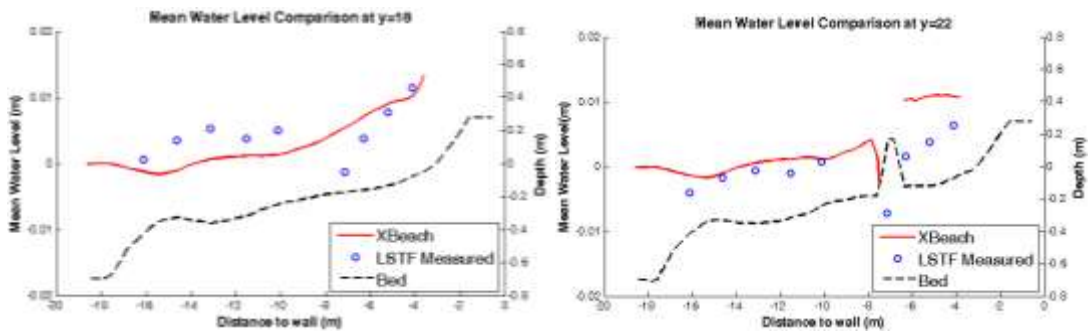


Figure 4.22 T1C1 Measured and computed ‘eta mean’ values for y=18m and y=22m

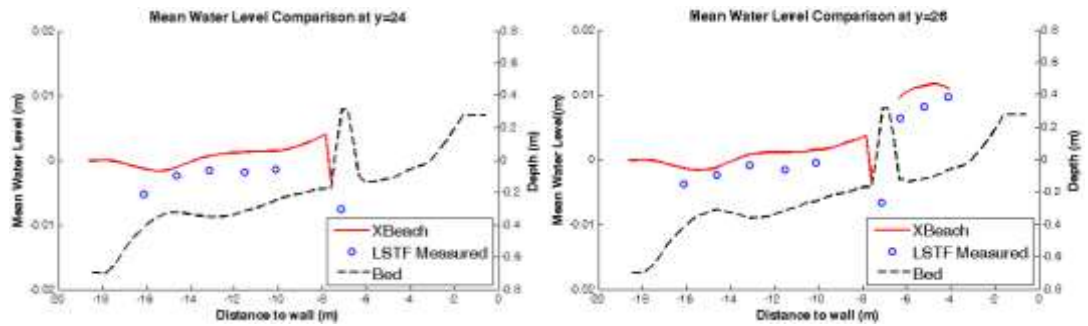


Figure 4.23 T1C1 Measured and computed ‘eta mean’ values for y=24m and y=26m

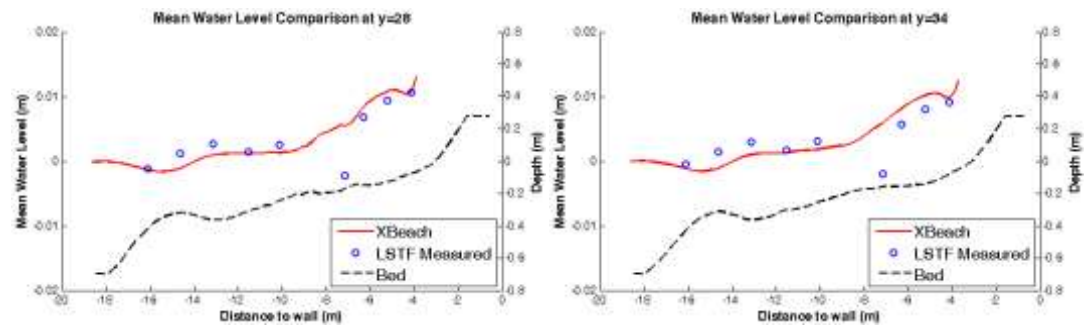


Figure 4.24 T1C1 Measured and computed ‘eta mean’ values for y=28m and y=34m

The comparisons of the six profiles of measured and computed mean water levels are given in Figure 4.22, 4.23 and 4.24. It is observed that the computed and measured mean water levels are compared well in the non-scaled T1C1 case. Around the

structure and at the shoreline, it differs from the measured data as observed in BC1 and this is explained in Section 4.5.1.1.

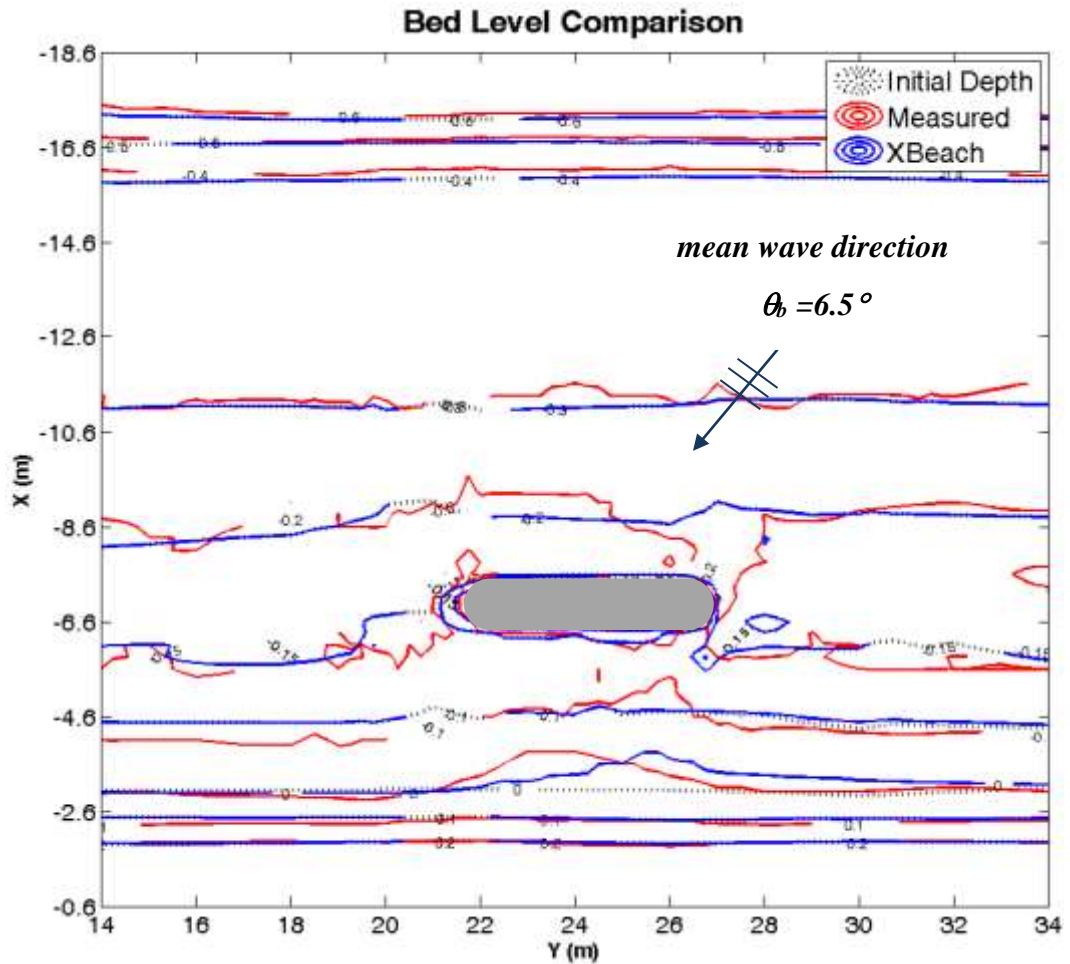


Figure 4.25 Measured initial and final bed and computed final bed level comparison for T1C1

The bed level comparison for the overall domain is shown in Figure 4.25. It can be concluded that the offshore bed level in the basin, ie. bed level lower than -0.3 m, shows no significant difference between the initial and final bed levels as well the bed level that is higher than the contour line 0.1 m. However, the shoreline is dramatically changed both in the measured and the computed bathymetry. The accumulation behind the detached breakwater at the final measured shoreline is

larger to the right as expected and the computed shoreline accreted slightly to the right compared to measured data in the lee of the breakwater, yet still in accordance with the expected shoreline movement. Moreover, the computed -0.1 m contour line indicates minor difference between the initial and final bed levels where the measured -0.1 m contour line shifted to the right and there is a major erosion comparing to the initial state. Also, there is significant erosion at both sides of the detached breakwater, namely, between $y= 18 \text{ m} - 22 \text{ m}$ and $y= 26 \text{ m} - 28 \text{ m}$. However, the computed erosion at the sides of the breakwater is limited. This is probably because of the selected unrealistically high asymmetry and skewness parameter, *facua*, reducing the capability to erode around the structure. Moreover, in front of the detached breakwater, wave reflection should also be present causing the wave heights to increase, thus the occurrence of erosion in front of the breakwater. Unlike to the measured case, XBeach model does not take the reflection into account, thus, underestimates the wave height and consequently erosion around structure. Another reason for not accurately computed the bed levels is the sediment concentration that is forced to the shoreline, thus the sediment volume conservation does not give expected results as Nam et al. (2010) indicated that the prediction of beach morphological change strongly depends on not only the output of the models for waves, nearshore currents, and sediment transport, but also on the numerical method for solving the sediment volume conservation equation.

Nam et al. (2010) used the numerical model in the same manner that is mentioned in Section 4.1.1 for the BC1 experiment and added morphological model as the sediment mass conservation equation in order to validate the overall model by using LSTF T1C1 data. It is indicated that the numerical model works in a good agreement for significant wave heights, longshore and cross-shore currents as well as the salient in the lee of the breakwater. However, similar to the case here, the observed data indicated an erosion between $y=26 \text{ m}$ and $y=28 \text{ m}$ near the breakwater where the computed bed level did not erode as the observed data.

Baykal (2012) also compared the similarities and differences between the developed numerical model and the measured values for BC1 and T1C1. The BC1 experiment comparisons between the numerical model and the measurements indicate well agreement and the accuracy increases with appropriate breaker index parameters. As mentioned at the beginning, Baykal (2012) compared the numerical model outputs and T1C1 case measurements and the results indicate that the morphology is in a good agreement such as the progress of shoreline towards the structure with a shift towards upstream and erosion of beach at downstream end. However, similar to the case in here and Nam et al.'s study (2009), the drastic scour at the upstream of the breakwater (between $y=26$ m and $y=28$) is not observed where the initiation of scour is indicated at the upstream end of the breakwater.

4.5.1.3 Experiment Test-3 Case-1 (T3C1)

The LSTF Test-3 experiments are done in order to determine the hydrodynamic and morphologic behavior in the presence of the T-Groin and they were started with the T3C1 experiment. The purpose in that laboratory-scaled experiment is to indicate the natural behavior of the wave breaking and the resulting flow velocities thus sedimentation in the presence of the T-Groin structure. Here, the LSTF measurements and the outputs of XBeach are compared and discussed in terms of the root mean squared wave height, the wave induced current, water levels and the final bed level.

The LSTF Experiment measurements and the XBeach model results are compared and discussed for the Test-3 Case-1 (T3C1) for the root mean square wave height (H_{rms}), the wave induced longshore velocity (v), the mean water level (η_{mean}) and the initial and final bed levels from Figure 4.26 to Figure 4.35. It should be noted that the measurements of x_4 (-4.125 m from the initial shoreline and -7.125 m from the wall shown in Figures 4.1, 4.2 and 4.3) are not taken into account in analyses since the gage here did not work properly (Nam et al., 2010).

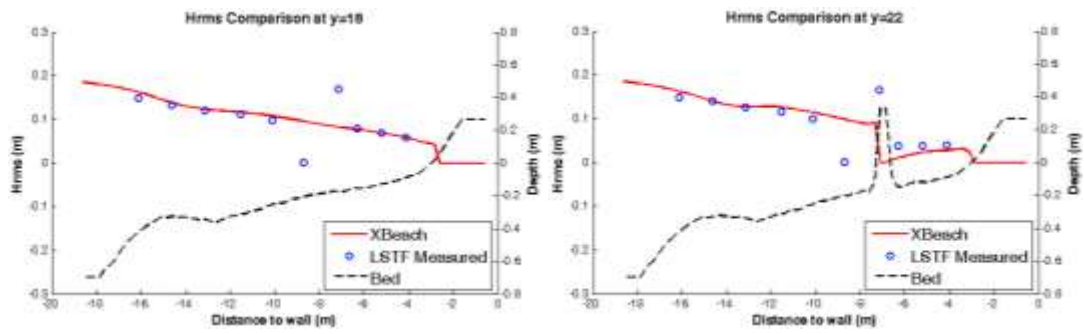


Figure 4.26 T3C1 Measured and computed H_{rms} values for $y=18$ m and $y=22$ m

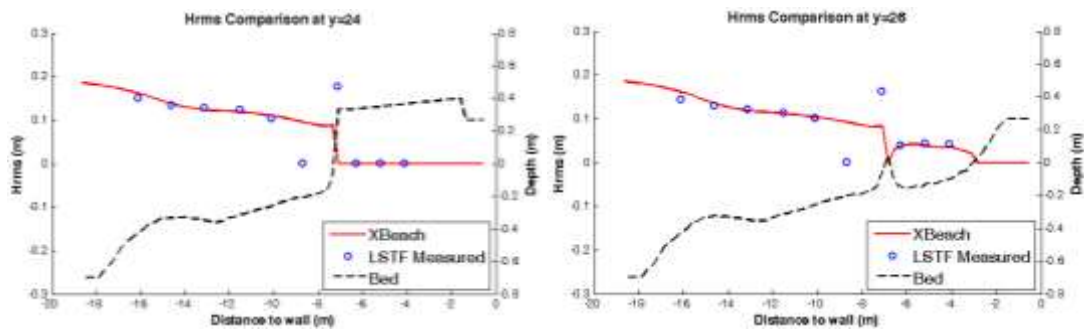


Figure 4.27 T3C1 Measured and computed H_{rms} values for $y=24$ m and $y=26$ m

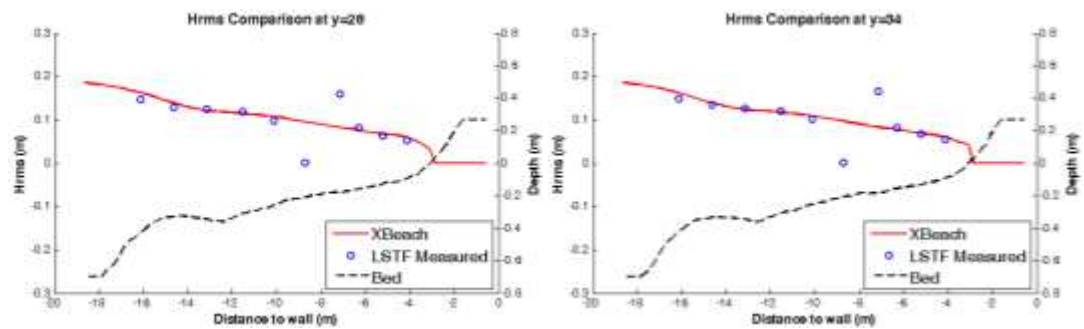


Figure 4.28 T3C1 Measured and computed H_{rms} values for $y=28$ m and $y=34$ m

In Figures 4.26, 4.27 and 4.28, it is indicated that H_{rms} values are in quite good agreement between the computed and the non-scaled measured values. As in the T1C1 case, it is expected to be true since the wave boundary conditions are calibrated with BC1 experiment. The implication of the comparison in Figure 4.26 shows that the root mean squared wave heights behind the breakwater after interaction with an obstacle (in this case a T-Groin) is computed quite in a similar trend and this reveals that an accurate diffraction behavior is observed behind the head of the T-Groin.

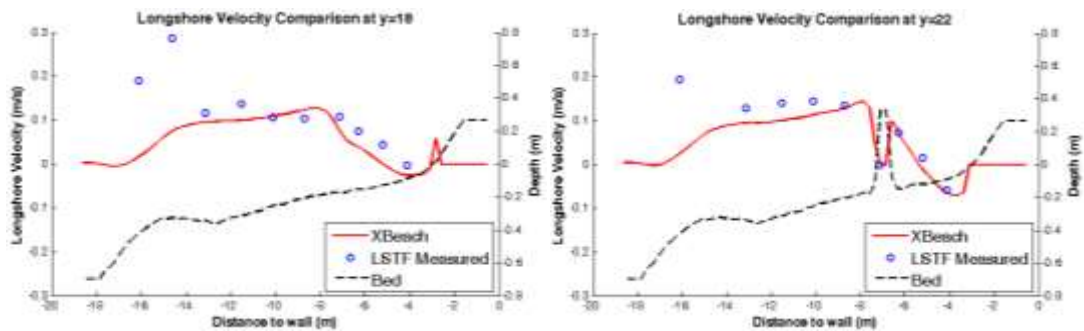


Figure 4.29 T3C1 Measured and computed v values for $y=18$ m and $y=22$ m

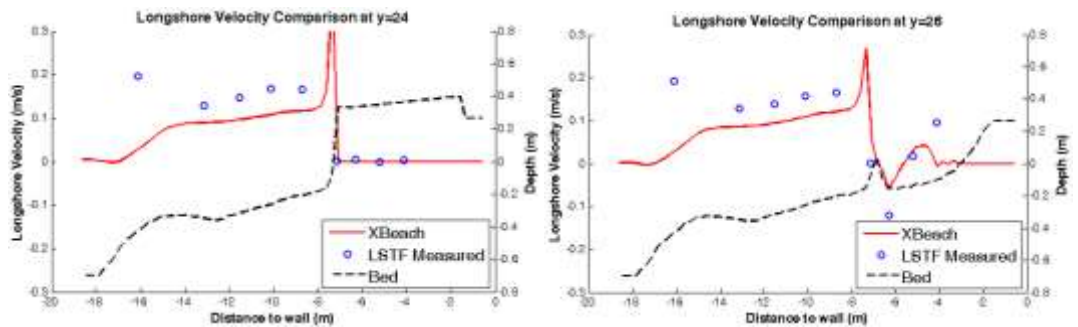


Figure 4.30 T3C1 Measured and computed v values for $y=24$ m and $y=26$ m

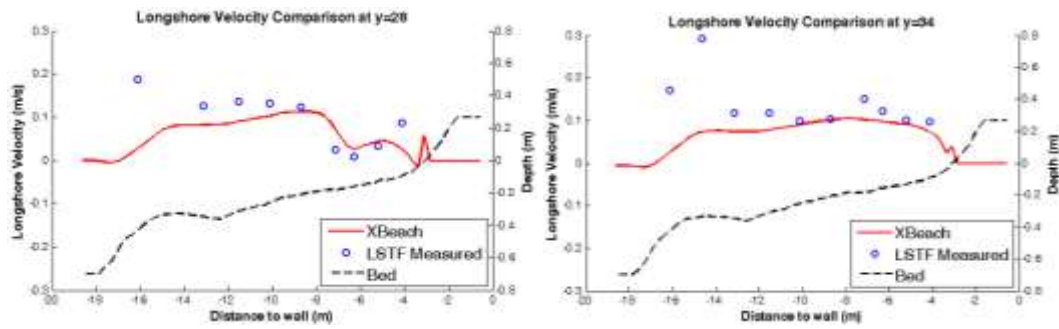


Figure 4.31 T3C1 Measured and computed v values for $y=28$ m and $y=34$ m

For T3C1 experiment, the wave induced longshore velocity comparison between laboratory measurements and computed longshore velocities are given in Figure 4.29, 4.30 and 4.31. It can easily be derived from the overall figures that the computed velocities are slightly underestimated comparing to the measured and they follow the measured velocities' trend as in T1C1 case. Moreover, at the longshore stations $y=24$ and $y=26$, a velocity jump in front of the structure is observed. These peaks could be related to sharp changes in the wave heights around the structure and thus the increased gradients of radiation stresses, as explained previously in T1C1 run. Also, the circulation cell velocity directions in the lee of the T-Groin indicate that the wave induced current velocity directions simulated fairly well to the measured values as can be seen from Figures 4.29 (right) and 4.30 (right).

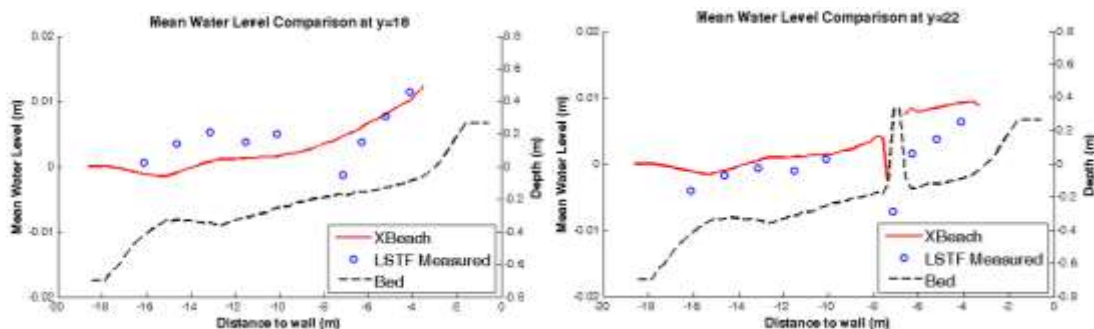


Figure 4.32 T3C1 Measured and computed ' η mean' values for $y=18$ m and $y=22$ m

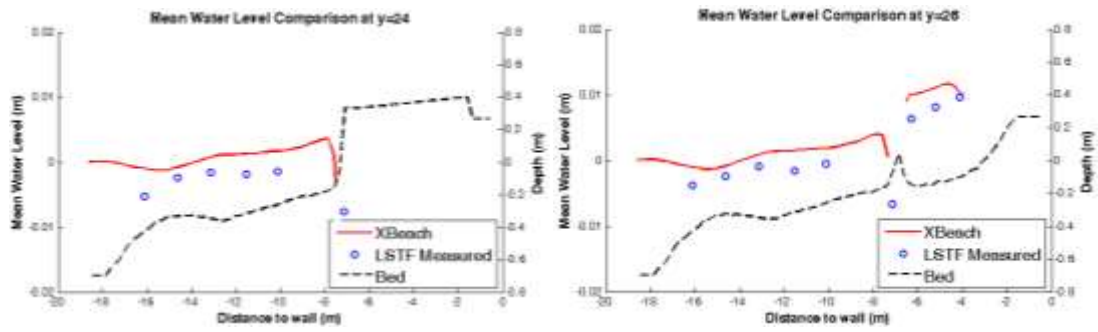


Figure 4.33 T3C1 Measured and computed ‘eta mean’ values for y=24m and y=26m

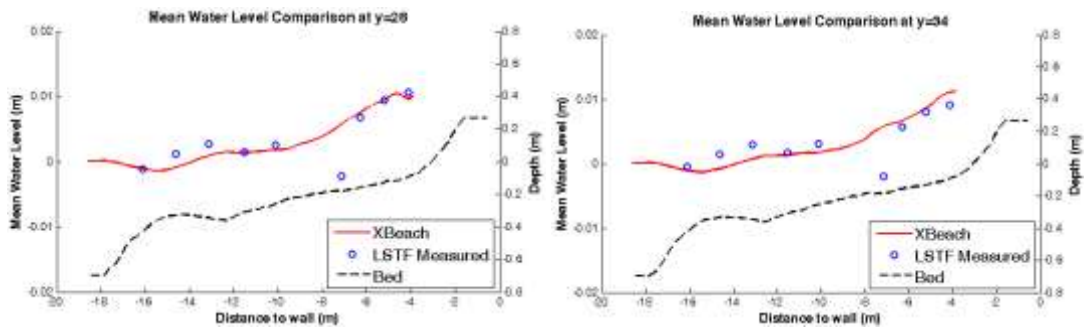


Figure 4.34 T3C1 Measured and computed ‘eta mean’ values for y=28m and y=34m

The comparisons of the measured and computed mean water levels are given in Figures 4.32, 4.33 and 4.34. It is observed that the computed and measured mean water levels are in agreement with minor differences in the non-scaled T3C1 run.

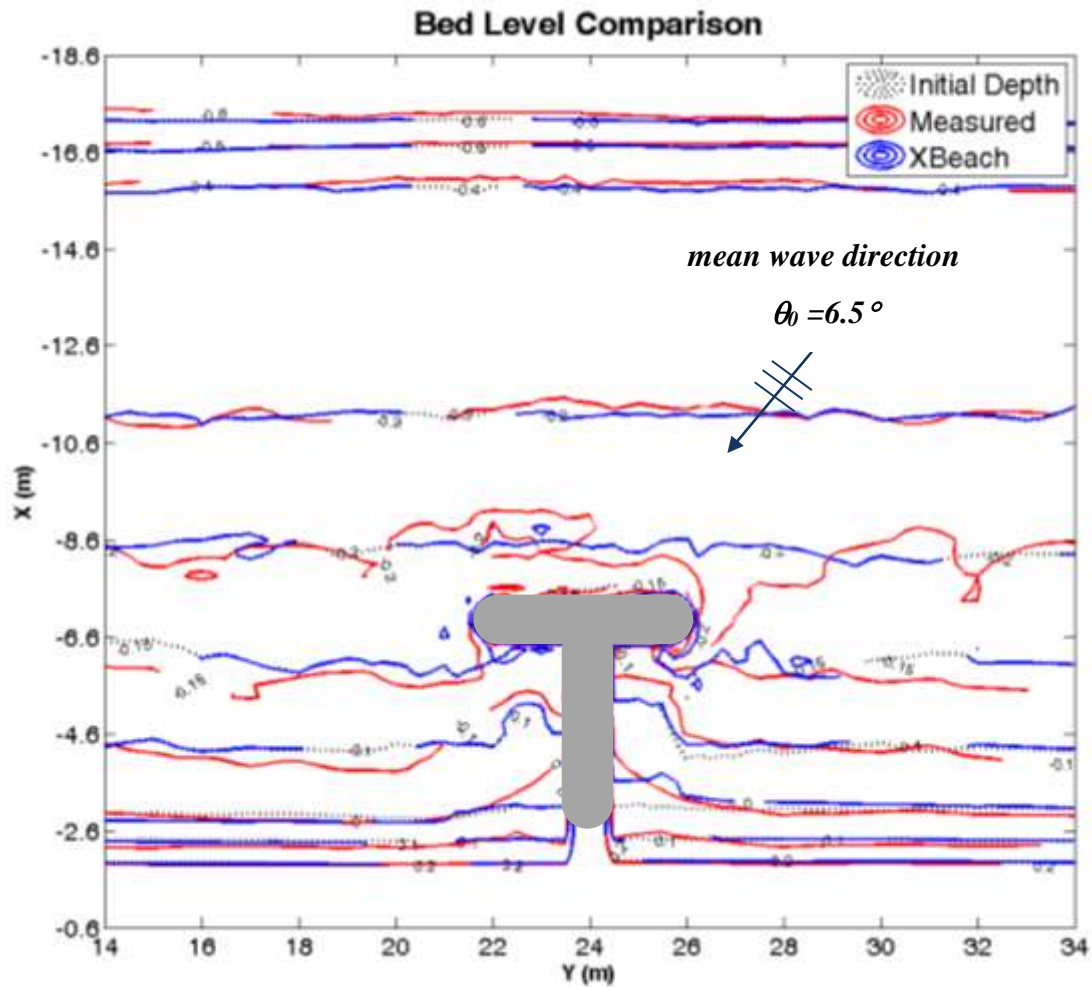


Figure 4.35 Measured initial and final bed and computed final bed level comparison for T3C1

The bed level comparison is shown in Figure 4.35. It can be concluded that the measured and computed offshore bed level in the experiment basin, i.e. bed level lower than -0.3 m, shows minor differences between the initial and final bed levels as well the bed level that is higher than the contour line 0.1 m. However, the shoreline is dramatically changed both in the measured and the computed bathymetry. The sediment accumulation in the lee of the T-Groin is observed to be produced symmetrically but the computed bed level shows sediment accumulation only at one side, between $y=24$ m and $y=26$ m, and the accretion at the left side of the T-Groin is

estimated insufficiently. Like the T1C1 case, the drastic erosion at the sides of the head could not be simulated and the bed levels near the T-Groin head remain the same after 180 minute simulation. Both in BC1 and T1C1 runs, it is estimated that the reason is the unrealistic value of *facua*, which is the outside of the indicated interval and it is assumed that the case is the same for T3C1 run. The higher the *facua* parameter is, the more sediment shoreward shift. Moreover, the wave reflection phenomenon is again ignored and it is assumed to be the case of the wave effect on erosion at the sides of the T-Groin head could not be computed.

Nam et al. (2010) carried out the computations of waves, wave-induced currents, sediment transport, and morphological evolution for T3C1 in the same manner as for T1C1 mentioned in Section 4.1.2. It is indicated that the numerical model works in a good agreement for significant wave heights, longshore and cross-shore currents as well as the salient in the lee of the T-Groin. However, similar to the T1C1 bed level case, the observed data indicated an erosion between $y=26$ m and $y=28$ m near the T-Groin head where the computed bed level did not show the same erosion tendency.

4.5.2 Scaled LSTF Data ($n_d=25$)

XBeach numerical model is mostly calibrated for the actual or prototype scales. Therefore, as explained in Section 4.3, laboratory scale has its restrictions in this numerical model, especially in the morphology computations since the model formulations are empirical (Brandenburg, 2010) and the corresponding calibration coefficients are dependent on the scales. In order to reduce such reverse effects, the laboratory scaled hydrodynamic and morphologic dimensions, such as wave heights, wave periods and the bed measurements, are assumed to be scaled-up by Froude scaling.

In this part, the measured LSTF dimensions and the hydrodynamic parameters such as root mean squared wave height and peak wave period are scaled up with the

Froude scale factor of $n_d=25$ and the parameters are introduced as the input parameters for XBeach. In the comparison and discussion part, the output values from the scaled up runs are scaled back down, thus the output values can be compared with the measured LSTF data. As in the non-scaled cases, these computations are compared and discussed in root mean squared wave height, wave induced longshore velocity, mean water levels and the final bed level points of view.

4.5.2.1 Experiment Base Case-1 (BC1) (Rescaled)

As explained before, BC1 is the adjusted LSTF configuration where the cross-shore profiles are same all over the domain and the same procedure is applied for the scaled inputs.

The LSTF Experiment measurements and observations and the XBeach model results are compared and discussed for the Base Case-1 (BC1) by the root mean square wave height (H_{rms}), the wave induced longshore velocity (v), the mean water level (η_{mean}) and the initial and final bed profiles in Figures 4.36, 4.37, 4.38 and 4.39.

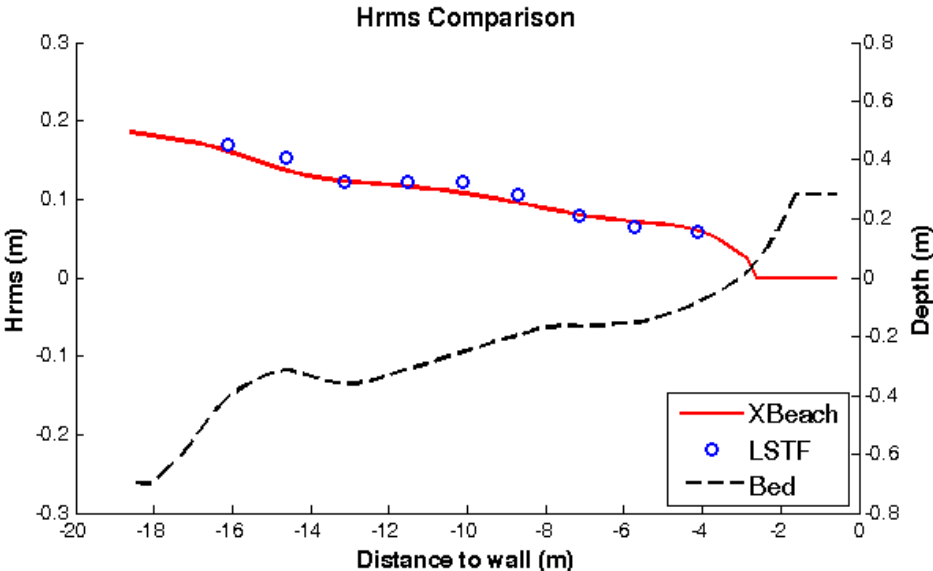


Figure 4.36 Root mean squared wave height comparison for BC1 (rescaled)

It is seen from Figure 4.36 that the root mean squared wave heights are compared to the measured ones fairly well. The mean absolute error is obtained as 6.0%.

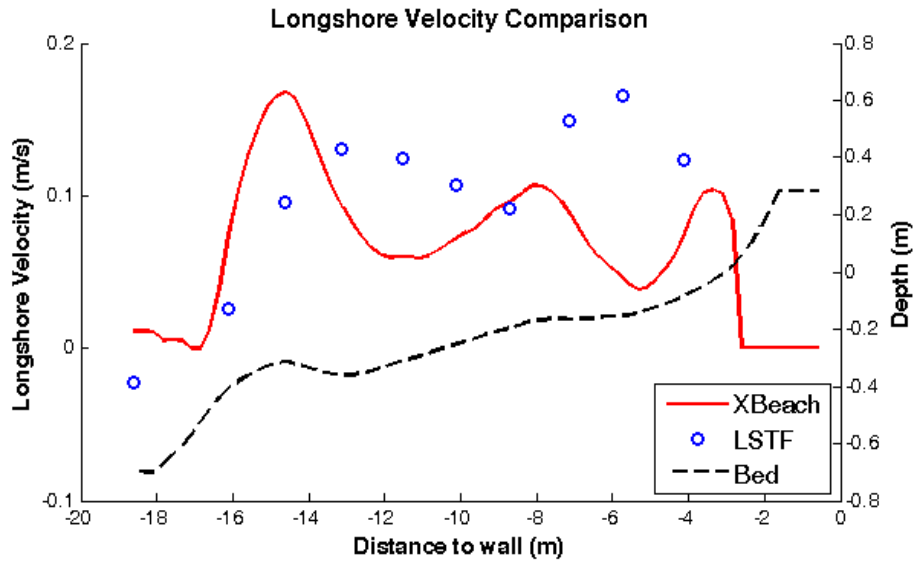


Figure 4.37 Longshore velocity comparison for BC1 (*rescaled*)

Rescaled XBeach model wave induced longshore velocity results compared to the measured data indicated some differences shown in Figure 4.37. It can be derived from the figure that the velocity profile is underestimated the cross-shore location from -13.125 m until the wall comparing to the measured ones. The mean absolute percentage error is obtained as 43.3% which is higher than the corresponding value of non-scaled BC-1

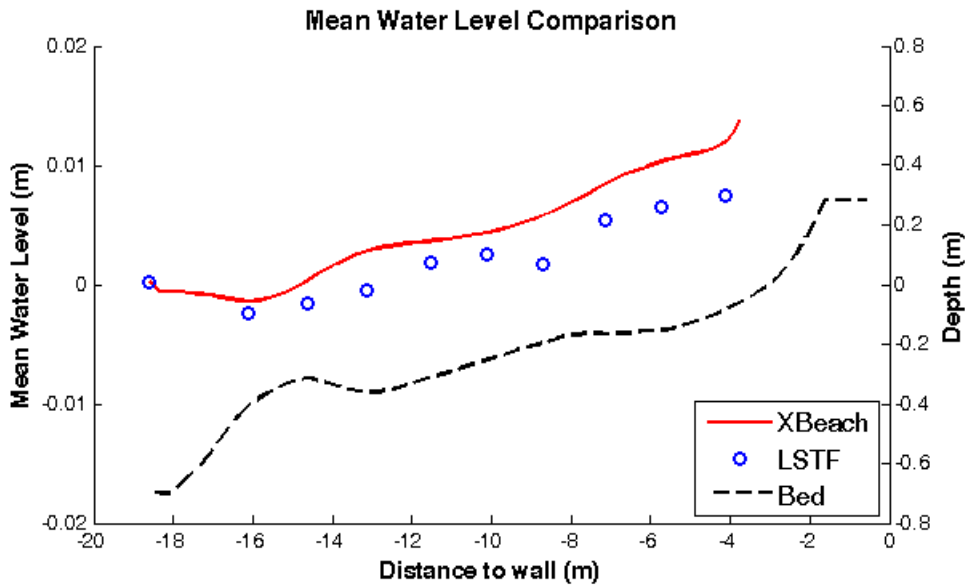


Figure 4.38 Mean water level comparison for BC1 (*rescaled*)

Observed LSTF and recalled XBeach model output mean water levels are compared in Figure 4.38 and it can be seen from the figure that model mean water levels have higher values than observed. The mean absolute percentage error is obtained as 93.3% which is higher than the corresponding non-scaled values. As in the non-scaled case, it is also assumed to be a result of the velocity profile difference between the observed and modeled. Moreover, again as given in the non-scaled case, XBeach is mainly developed and calibrated for dune erosion or overwash behavior near coastal regions, thus, the model may overestimate the wave setup amount contrary to the observed case. This issue should be further investigated in detail.

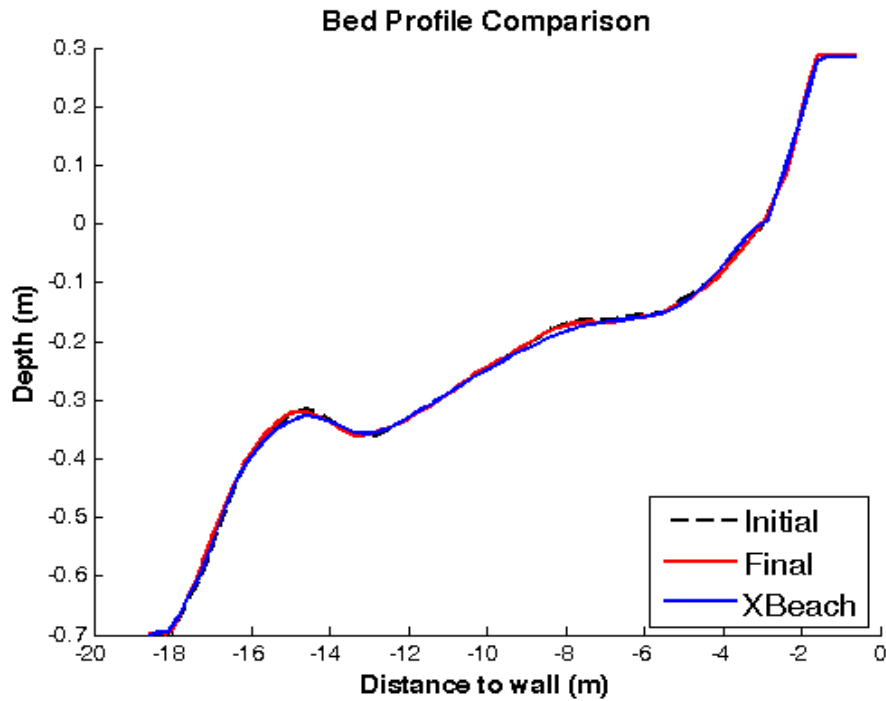


Figure 4.39 Measured initial bed level and computed and measured final bed level comparison for BC1 (*rescaled*)

The initial bed, measured final bed and computed and rescaled final bed profiles are shown in Figure 4.39. The measured initial and final bed profile remain unchanged with minor fluctuations. The mean absolute percentage error is 4.6% between the measured and the predicted value. Consequently, the computed final bed profile is calibrated to remain unchanged as much as possible by forcing the model not to erode near shoreline with the hydrodynamic and the morphology parameters given in Tables 4.5 and 4.6.

4.5.2.2 Experiment Test-1 Case-1 (T1C1) (*Rescaled*)

The scaled LSTF Experiment measurements and observations and the XBeach model results are compared and discussed for the Test-1 Case-1 (T1C1) for the root mean

square wave height (H_{rms}), the wave induced longshore velocity (v), the mean water level (η_{mean}) and the initial and final bed levels from Figure 4.40 to Figure 4.49.

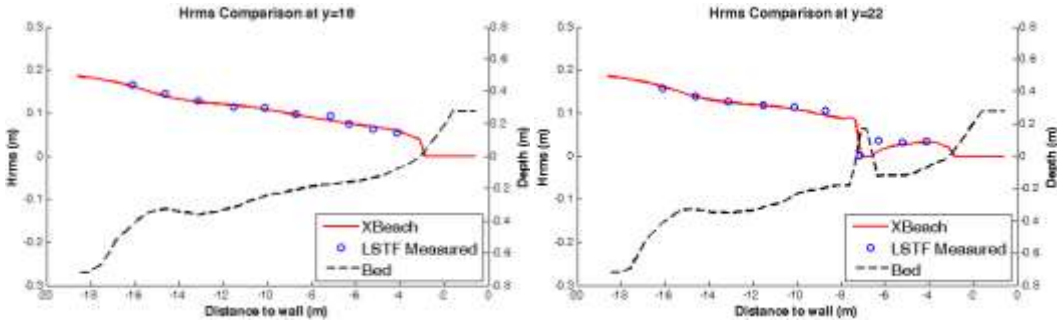


Figure 4.40 T1C1 Measured and computed H_{rms} values for $y=18\text{ m}$ and $y=22\text{ m}$ (rescaled)

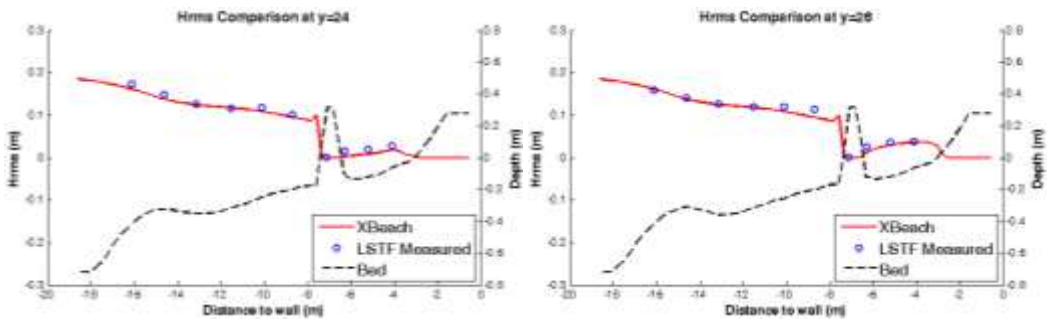


Figure 4.41 T1C1 Measured and computed H_{rms} values for $y=24\text{ m}$ and $y=26\text{ m}$ (rescaled)

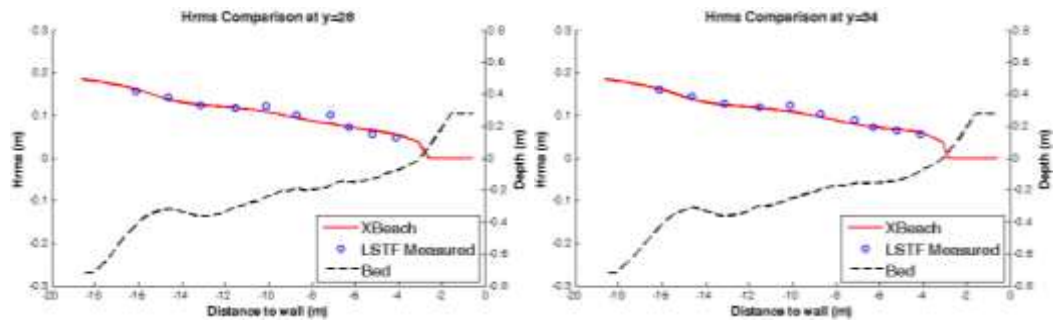


Figure 4.42 T1C1 Measured and Computed H_{rms} values for $y=28$ m and $y=34$ m
(rescaled)

In Figures 4.40, 4.41 and 4.42, it is seen that H_{rms} values are compared fairly well between the computed and the measured values. Since the hydrodynamic model in XBeach scales according to Froude (Brandenburg, 2010), there are no significant change in the wave height distribution when compared to non-scaled T1C1 case, given in Section 4.2.5.1.

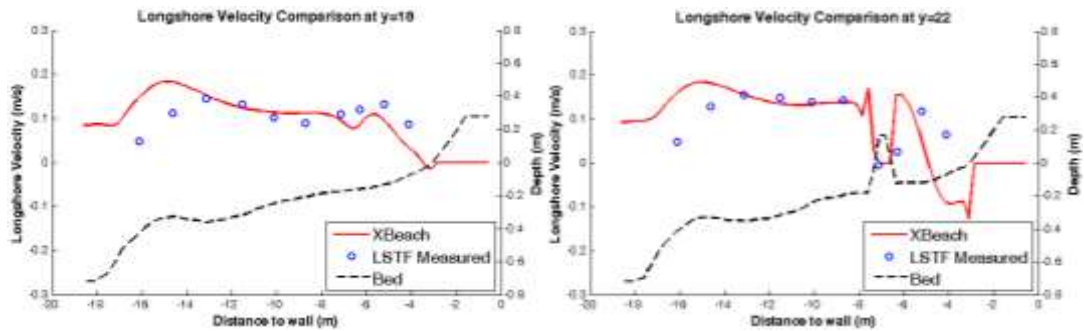


Figure 4.43 T1C1 Measured and computed v values for $y=18$ m and $y=22$ m
(rescaled)

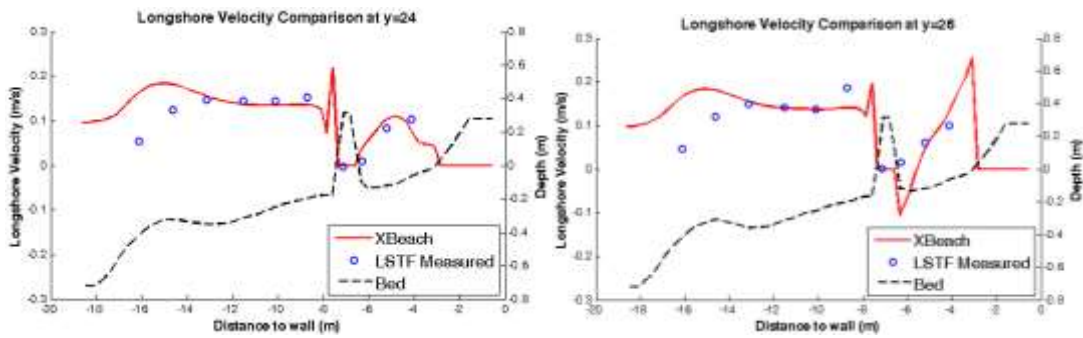


Figure 4.44 T1C1 Measured and computed v values for $y=24$ m and $y=26$ m
(rescaled)

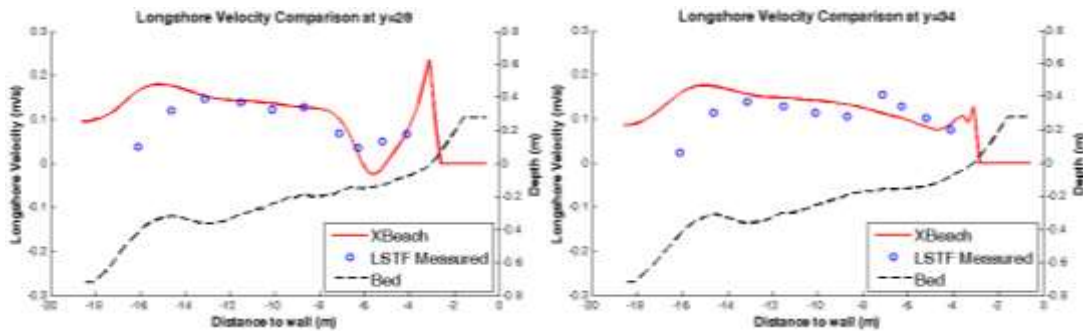


Figure 4.45 T1C1 Measured and computed v values for $y=28$ m and $y=34$ m
(rescaled)

The rescaled longshore velocity comparison between the laboratory measurements and the computed longshore velocities for six profiles are given in Figure 4.43, 4.44 and 4.45. It is obvious that the longshore velocities are compared much well than the non-scaled case of T1C1. Here, the flow circulation scheme behind the detached breakwater seems much better than the non-scaled case. Also, the velocity jump in front of the breakwater that is seen in the non-scaled T1C1 longshore velocity comparison is also seen in the scaled T1C1 computed outputs, too. Moreover, the wave induced current velocity distribution trends are in a good agreement with the LSTF measured values.

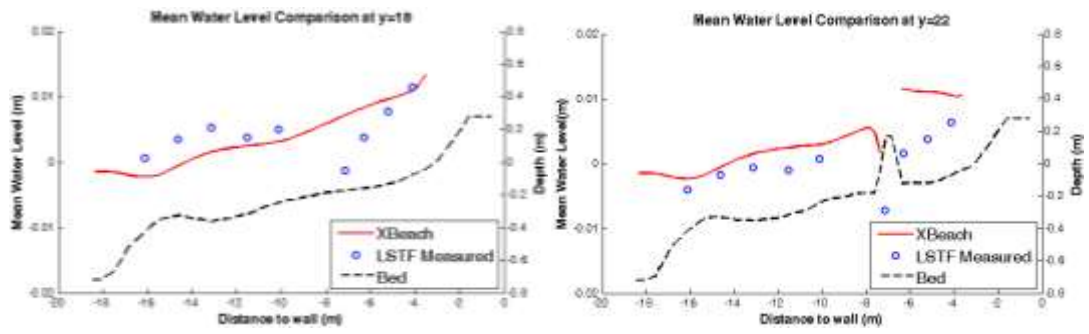


Figure 4.46 T1C1 Measured and Computed '*eta mean*' values for y=18m and y=22m (rescaled)

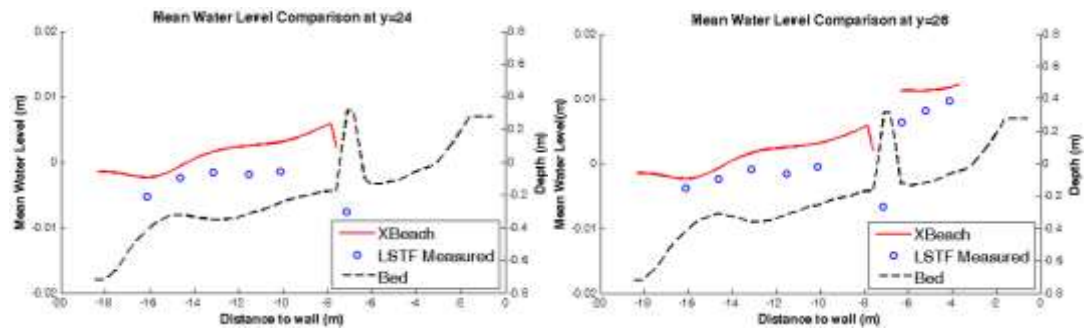


Figure 4.47 T1C1 Measured and Computed '*eta mean*' values for y=24m and y=26m (rescaled)

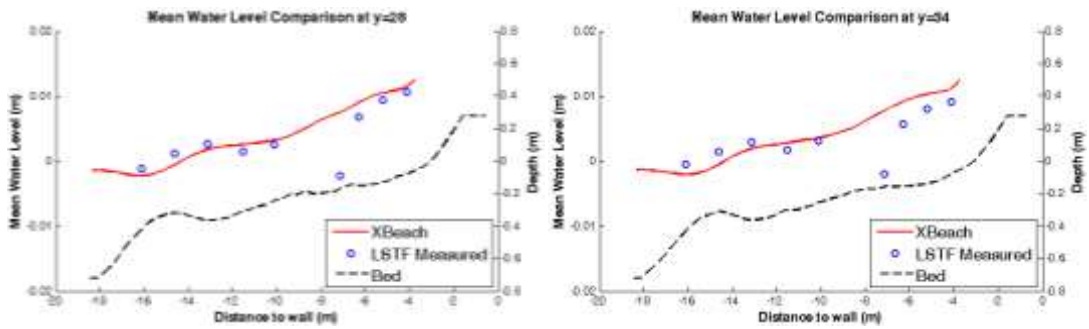


Figure 4.48 T1C1 Measured and Computed '*eta mean*' values for y=28m and y=34m (rescaled)

The comparisons of six profiles of the measured and computed mean water levels are given in Figure 4.46, 4.47 and 4.48. It is observed that the computed and measured mean water levels are compared well in the non-scaled T1C1 case.

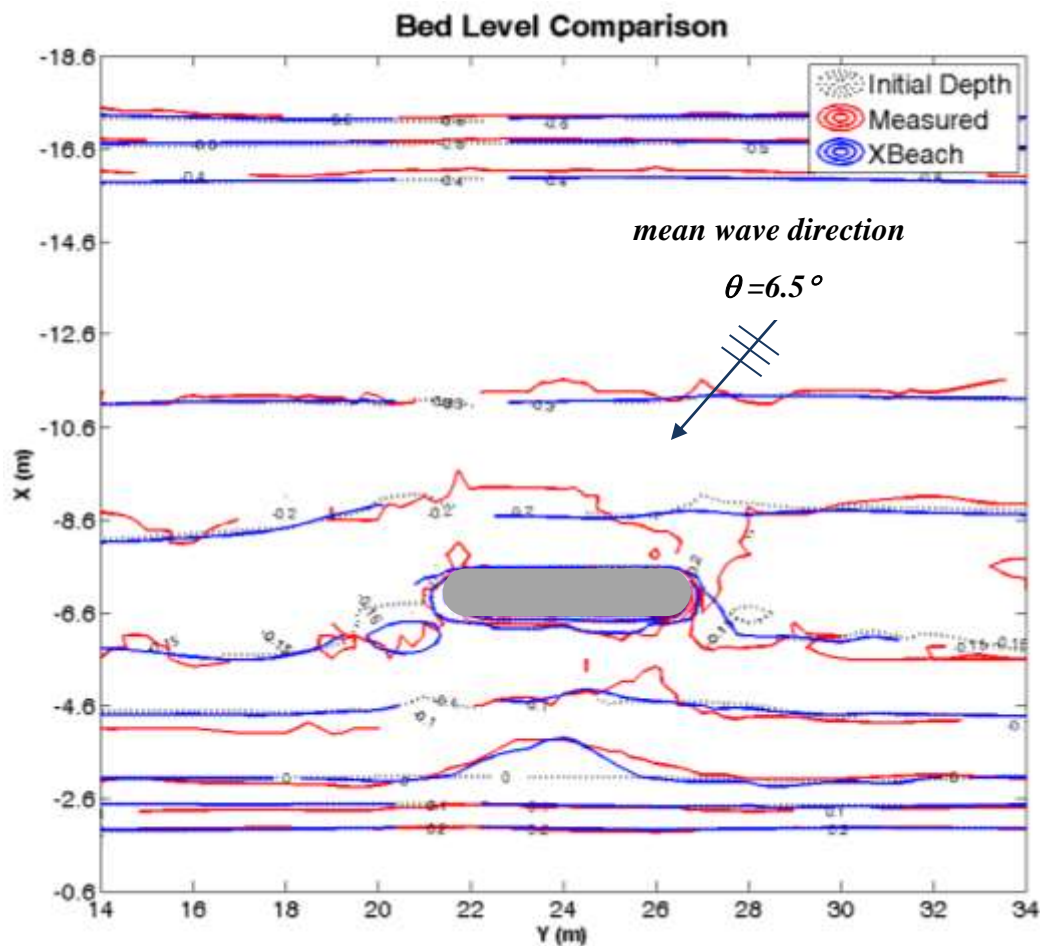


Figure 4.49 Measured initial and final bed and computed final bed level comparison for T1C1 (*rescaled*)

The bed level comparison for the whole domain is shown in Figure 4.49. It is seen from the figure that the offshore bed level in the basin, i.e. bed level lower than -0.3 m, shows no significant difference between the initial and final bed levels as well the bed level that is higher than the contour line 0.1 m like in the non-scaled T1C1 case.

However, the main difference of the morphologies between non-scaled and scaled model output, is the salient at the lee of the breakwater. In the non-scaled T1C1 case, shoreline at the lee was shifted to the right where the scaled run output give higher accuracy with the measured bed level. This difference between the non-scaled and scaled runs is assumed to be due to the velocity profile differences behind the breakwater. However, the -0.1 m and -0.2 m contour lines indicate some discrepancies at both sides of the breakwater. Erosion between $y=26$ and $y=28$ at the right side of the breakwater could not be modeled the reason is assumed to be similar with the corresponding non-scaled case. As an advantage of the vanishing the laboratory scale effects and since the input parameters are much likely to be a prototype scale, it is not needed to modify the '*facua*' parameter to an unreasonable value. In fact, the value is used between the limits that are defined as 0 and 1 in the XBeach User Manual (Roelvink et al, 2015).

4.5.2.3 Experiment Test-3 Case-1 (T3C1) (*Rescaled*)

The scaled LSTF Experiment observations and measurements and the XBeach model results are compared and discussed for the Test-3 Case-1 (T3C1) for the root mean square wave height (H_{rms}), the wave induced longshore velocity (v), the mean water level (η_{mean}) and the initial and final bed levels from Figure 4.50 to Figure 4.58. As mentioned previously in Section 4.5.1.3, the measurements of x_4 (-4.125 m from the initial shoreline and -7.125 from the wall shown in Figures 4.1, 4.2 and 4.3) are not taken into account in analyses since the gage here did not work properly (Nam et al., 2010).

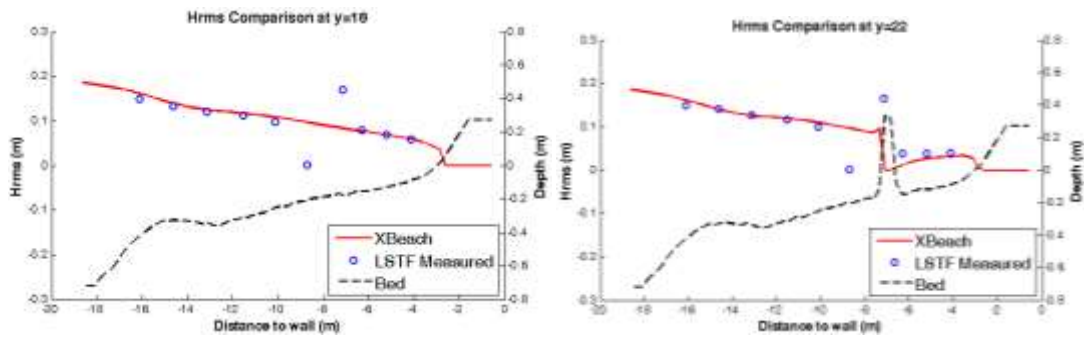


Figure 4.50 T3C1 Measured and computed H_{rms} values for $y=18$ m and $y=22$ m
(rescaled)

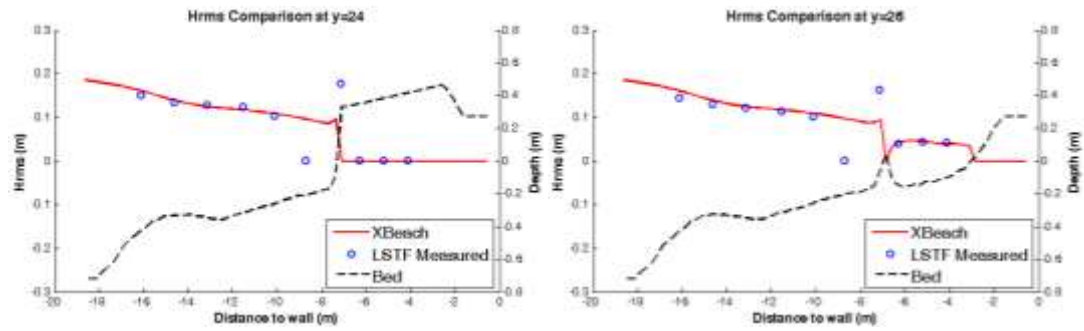


Figure 4.51 T3C1 Measured and computed H_{rms} values for $y=24$ m and $y=26$ m
(rescaled)

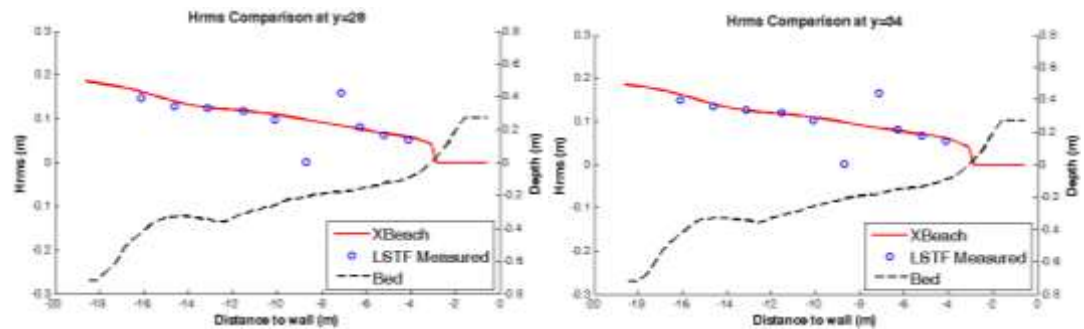


Figure 4.52 T3C1 Measured and computed H_{rms} values for $y=28$ m and $y=34$ m
(rescaled)

In Figures 4.50, 4.51 and 4.52, it is seen that H_{rms} values are compared fairly well between the computed and the measured values. Since the hydrodynamic model in XBeach scales according to Froude (Brandenburg, 2010), there are no significant change in the wave height distribution when compared to non-scaled T3C1 case, given in Section 4.5.1.3.

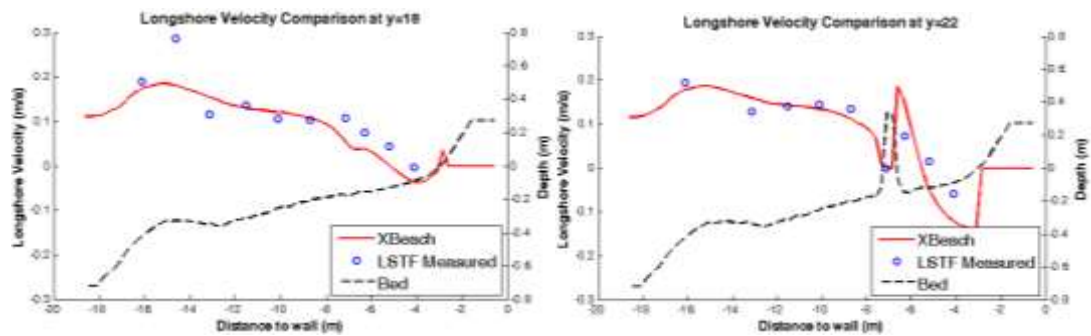


Figure 4.53 T3C1 Measured and computed v values for $y=18$ m and $y=22$ m
(rescaled)

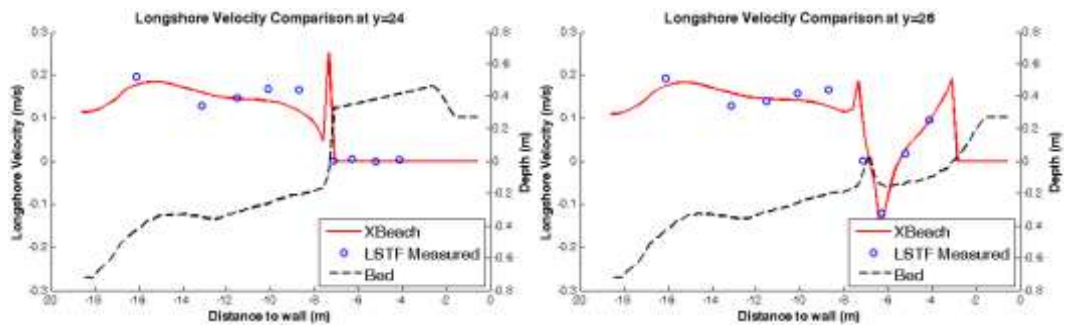


Figure 4.54 T3C1 Measured and computed v values for $y=24$ m and $y=26$ m
(rescaled)

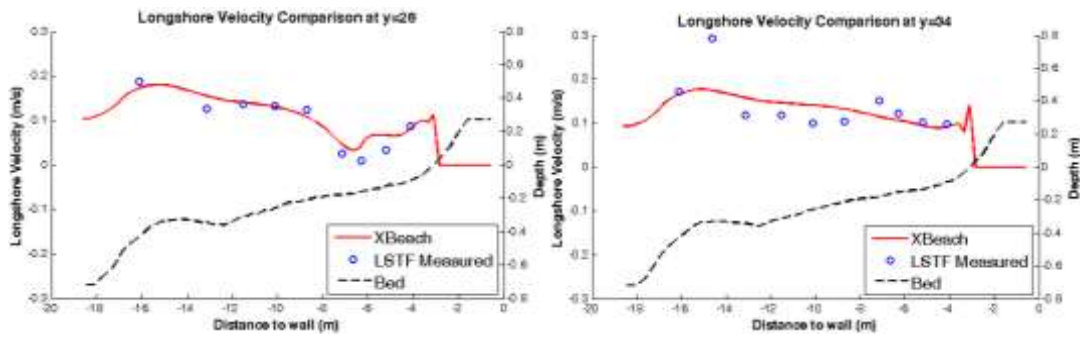


Figure 4.55 T3C1 Measured and computed v values for $y=28$ m and $y=34$ m
(rescaled)

The scaled longshore velocity comparison between scaled laboratory measurements and the computed longshore velocities are given in Figures 4.53, 4.54 and 4.55. The wave induced longshore velocities are in quite well agreement with the measured values. Moreover, as in scaled T1C1 run, the flow circulation scheme in the lee of the T-Groin indicates as good agreement as the non-scaled T3C1 comparison. As the previous comparisons of longshore current velocities, the velocity jump especially in front of the head of the T-Groin is also seen here. Moreover, the wave induced current velocity distribution trends are in a good agreement with the LSTF measured values.

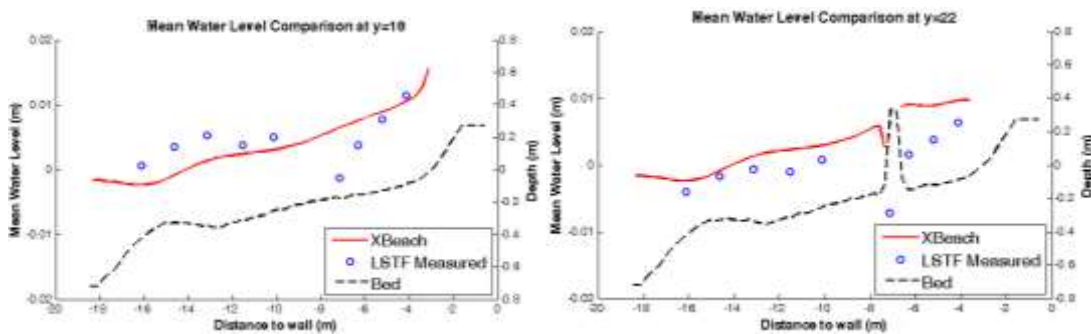


Figure 4.56 T3C1 Measured and Computed ‘eta mean’ values for $y=18$ m and $y=22$ m
(rescaled)

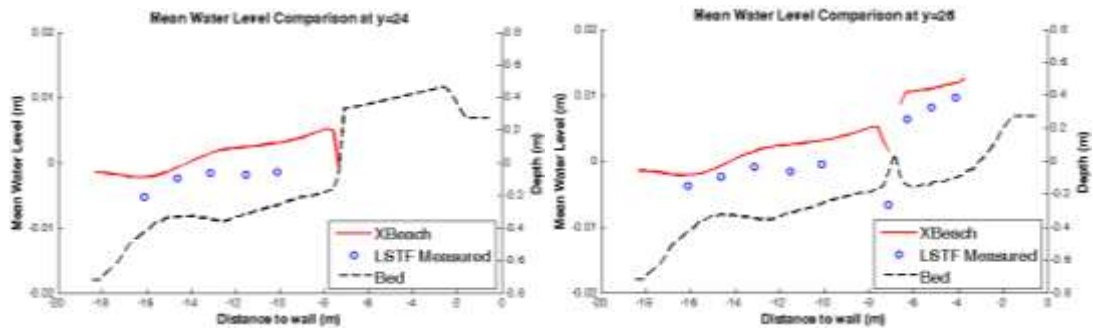


Figure 4.57 T3C1 Measured and computed '*eta mean*' values for y=24 m and y=26m (rescaled)

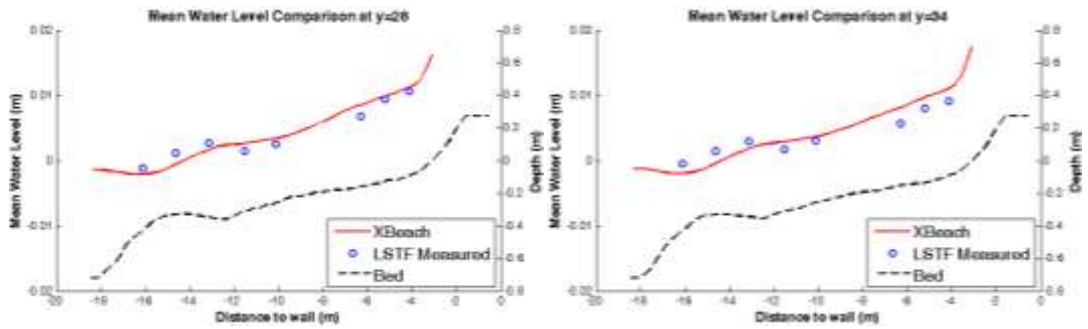


Figure 4.58 T3C1 Measured and computed '*eta mean*' values for y=28 m and y=34m (rescaled)

The comparisons of the measured and computed mean water levels are given in Figures 4.56, 4.57 and 4.58. It is observed that the computed and measured mean water levels are compared well as in the non-scaled T3C1 case.

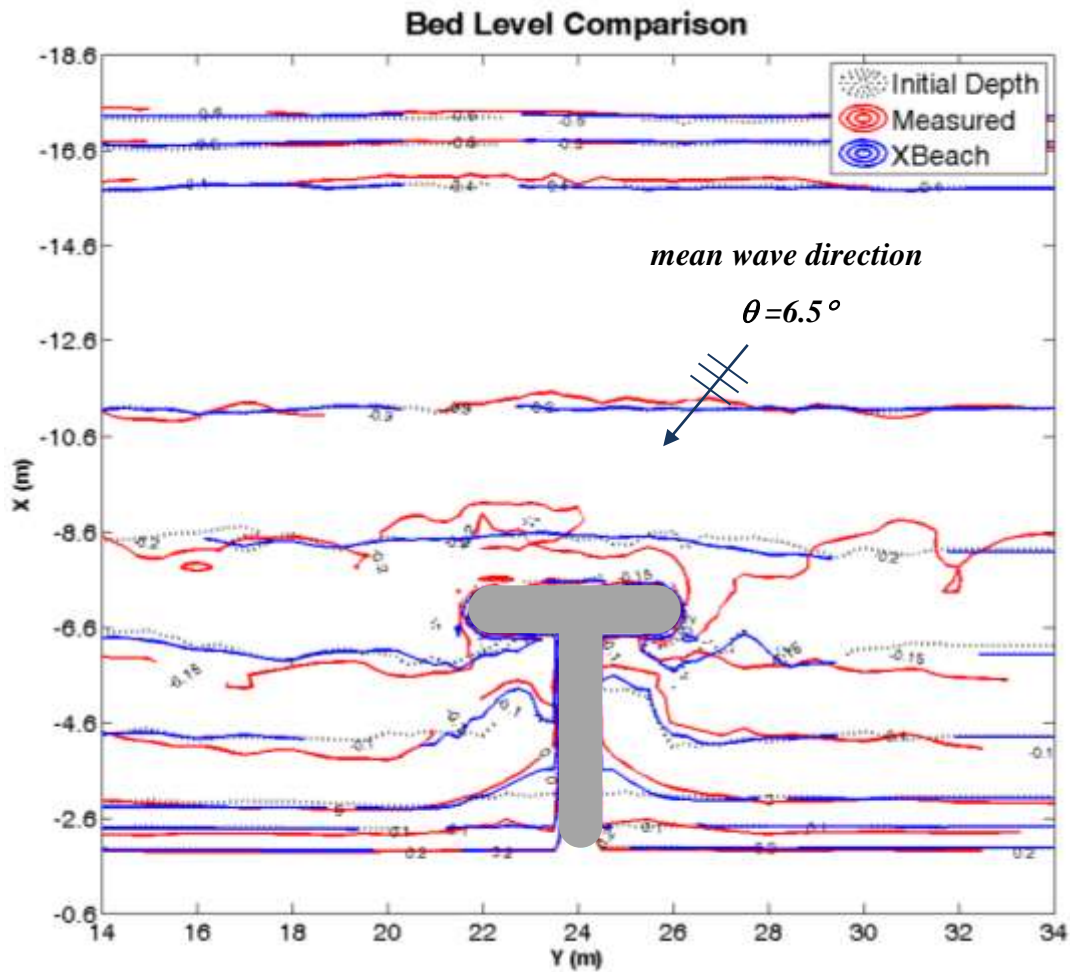


Figure 4.59 Measured initial and final bed and computed final bed level for T3C1
(rescaled)

The bed level comparison for scaled T3C1 is shown in Figure 4.59. It is seen from the figure that the offshore bed level in the basin, ie. bed level lower than -0.3 m, shows no significant difference between the initial and final bed levels as well the bed level that is higher than the contour line 0.1 m like in the non-scaled T3C1 case. However, the main difference of the morphologies between non-scaled and scaled model outputs, is the salient at the lee of the head of the T-Groin. In the non-scaled T3C1 case, the accumulated sediment was merely on the right side of the groin where in the scaled part the accumulation is on the both sides. Moreover the final computed -0.1 contour of the bed level indicates a good agreement with the

measured contour. Likewise, there is a tendency to resemble the erosion that took part at the right side of the T-Groin head, which is the -0.2 m contour. Again, the morphology parameters are used more in a convenient way as discussed in the scaled TIC1 comparisons.

CHAPTER 5

A CASE STUDY: MODELING MANAVGAT RIVER MOUTH WITH XBEACH

Coastal areas where the river meets with the large water bodies are highly complex and vulnerable areas where various physical processes come into picture. Natural hazards including storm surges, flooding due to inland precipitation and climate change-related hazards such as mean sea level rise may result in more disastrous consequences near such regions. Developing mitigation strategies and exposure outputs in vulnerability analyses for the occurrences of these natural events require an in-depth understanding of governing physical processes, investigating the interactions between these events and the effects of these interactions on coastal systems such as estuaries, lagoons or deltas, and detailed site investigations and modeling studies.

Located in Antalya Turkey, Manavgat River Mouth is modeled with XBeach in this study in order to investigate the hydrodynamic and morphologic conditions and variations between December 4th and 15th, 1998. Based on the available very limited bathymetric data and the fluvial dominated combined river-discharge and storm event between the above mentioned dates, the main purpose of this part is to carry out a preliminary study on testing XBeach numerical model in a fluvial dominated river mouth bathymetry and the behavior of the nearby coastal region.

5.1 Study Area

Antalya is a coastal city located in the southern Turkey and the city has its coasts by the Mediterranean Sea. The study area, Manavgat region, which is one of the most

populated province within the borders of Antalya has shoreline length of almost 46 km. The Manavgat River, giving the name of the province, passes through the center of the Manavgat province where most of the population is located and the river flows into the Mediterranean Sea 6.8 km after passing through the Manavgat town. Figure 5.1 and Figure 5.2 shows the location of the study area in Turkey.



Figure 5.1 Manavgat province and Manavgat river mouth location in Turkey



Figure 5.2 The most recent Google Earth Image for the study area, Manavgat river mouth

Manavgat River is mostly known for the ‘Manavgat Fall’ located at nearly 14.2 m upstream of the river mouth. The nearby site is visited by number of tourists every year and the nearby coastal region is a home for highly demanding touristic activities such as camp tourism and recreational boats which navigates between Manavgat town and the Mediterranean Sea. Also, there are several berthing places and fishing facilities nearby the mouth. Consequently, this coastal part of the Manavgat region requires high attention regarding to both the human activities and the natural occurrences.

Although Manavgat River Mouth consists of a sand bar that is used as beach especially in summer season and a demanding touristic area, the mouth part is observed to be highly unstable throughout the years till the jetties were constructed

and it is thought to be like that due to strong alongshore sediment transport and high river floods (Guler et al., 2003). The river mouth behavior that is measured in several years are obtained from Guler et al. (2003).

On Manavgat River, there are two dams named Oymapınar and Manavgat Dams from upstream to downstream, respectively (Figure 5.3). Oymapınar Dam was put into operation in 1987 and similarly, Manavgat Dam has been operating since 1984. The river discharge amount downstream is directly related to and dependent on especially Manavgat Dam tailwater and spillway discharge amount.

Additionally, from the river sediment transport point of view, at the upstream part, the sediment is accumulated and deposited in the dams' catchment areas resulting in the decrease in the amount of sediment carried by the river to the sea thus disrupting the natural balance of the river mouth. Consequently, sediment carried by the river is very limited at the downstream of the river. This condition is assumed to make the river mouth vulnerable to extreme or unexpected occurrences leading to instability of the small sand accumulations and sand bar near the river mouth.

In order to reduce the adverse effects of storm waves and unstable sedimentation near the mouth, two jetties have been constructed between the years 1996-1999, as 'east' and 'west' jetties by General Directorate of Railways, Harbors and Airports Construction (DLH).

Storm between 4th and 15th December, 1998 and its effects to the mouth

During the construction stages of the jetties, there are several bathymetric maps obtained throughout the mouth, river and the sea bed. While the east jetty construction was going on, between 4th and 15th of December 1998, a significant river discharge has been observed which has flooded the Manavgat town according to General Directorate of State Hydraulic Works (DSI). For that duration, the daily

average river discharge data has been obtained from DSI Manavgat-Şelale discharge gaging station located at the downstream of the Manavgat Dam and 1 km upstream of the Manavgat Fall (Figure 5.4).



Figure 5.3 Oymapınar and Manavgat Dams and the river gage station locations on Manavgat River

Between the above mentioned dates, and as can be seen from Table 5.1, the maximum daily averaged river discharge was recorded as 780 m³/s for which the river bed was not sufficient to carry at some river sections.

Table 5.1 Discharge data between 4th and 15th December, 1998

Day (December, 1998)	Daily Average Discharge (m³/s)
4	99
5	186
6	262
7	439
8	425
9	534
10	780
11	618
12	446
13	337
14	280
15	362

A bathymetric map was taken on 4th of December, 1998, by DLH. Guler et al. (2003) have emphasized that sediment accumulation, that is blocking the mouth, interrupted the river flow throughout the outlet. The recorded flood and the wave action during that flood together with the tidal fluctuations, wind setup, and barometric effects are estimated to be the main causes of that washed away sediment accretion at the river mouth. On 15th of December, 1998, another bathymetric map was taken by DLH in order to reveal the morphological differences after the flood. Guler et al. (2003) has given the bathymetric maps before and after the flood as in Figure 5.4 and Figure 5.5. It should be noted that the construction of the west jetty is not shown in these figures (Figure 5.4 and 5.5) but it is shown in the following digitized bathymetries.

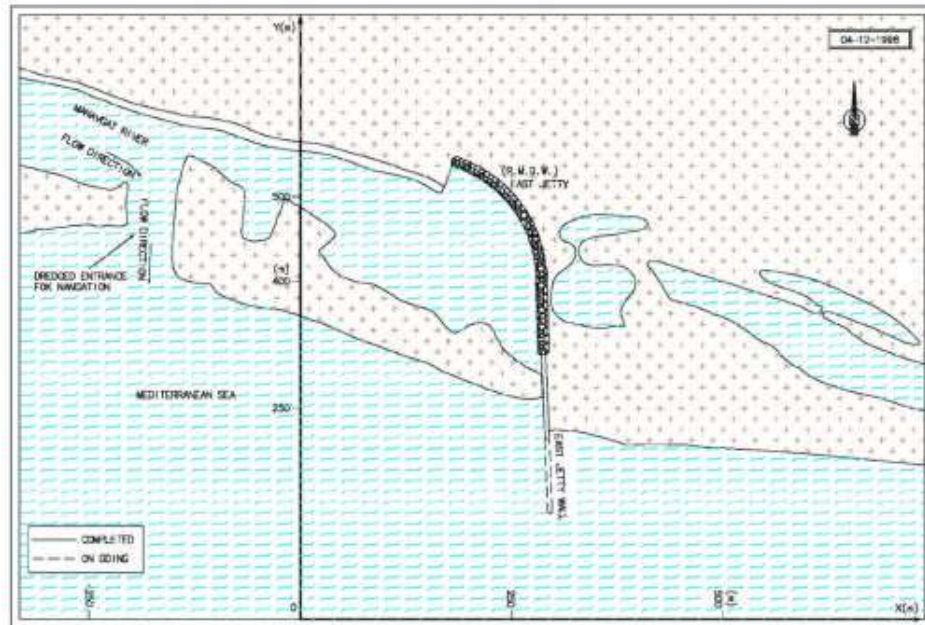


Figure 5.4 Shoreline measurement of Manavgat river mouth on December 4th, 1998
(Guler et al., 2003).

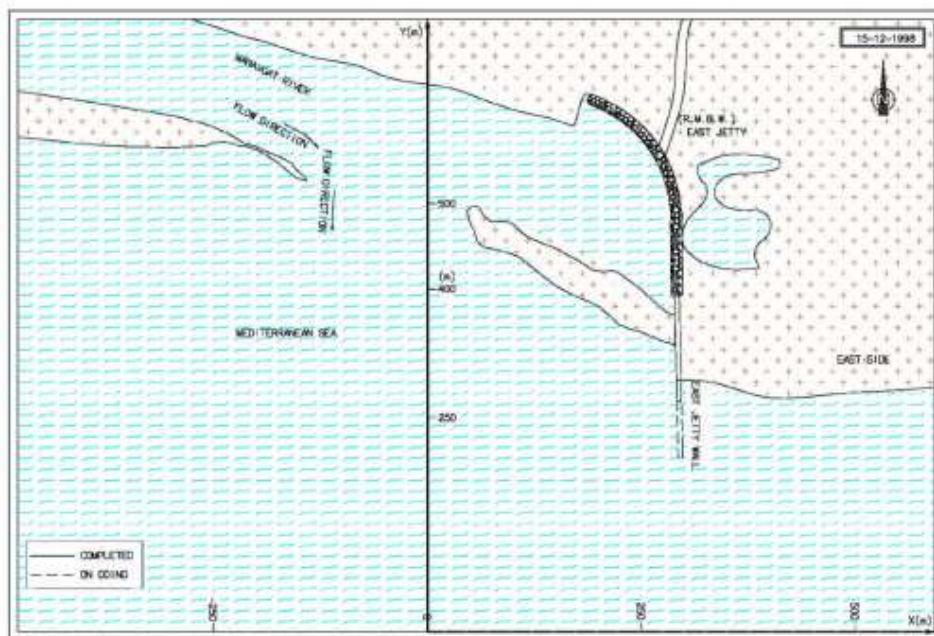


Figure 5.5 Shoreline measurement of Manavgat river mouth on December 15th, 1998
(Guler et al., 2003).

In this study, the comparison between the nearshore bathymetric measurements of 4th and 15th December 1998 is carried out by modeling the morphological changes at the river mouth under river discharge and wave conditions with XBeach numerical model.

5.2 Model Setup

The model setup is done by the existing bathymetric measurements of the study area for the given duration, between 4th and 15th December, 1998. As the input bathymetry, domain is selected and produced as 3.3km x 4.2km consisting of 20m x 20m grids. The nearshore region is obtained from the DLH bathymetric maps where the offshore part of the selected domain is taken from navigation charts of Office of Navigation, Hydrography and Oceanography (SHODB). Initial bathymetry is shown in Figure 5.6 and a closer look to the river mouth bathymetry is given in Figure 5.7.

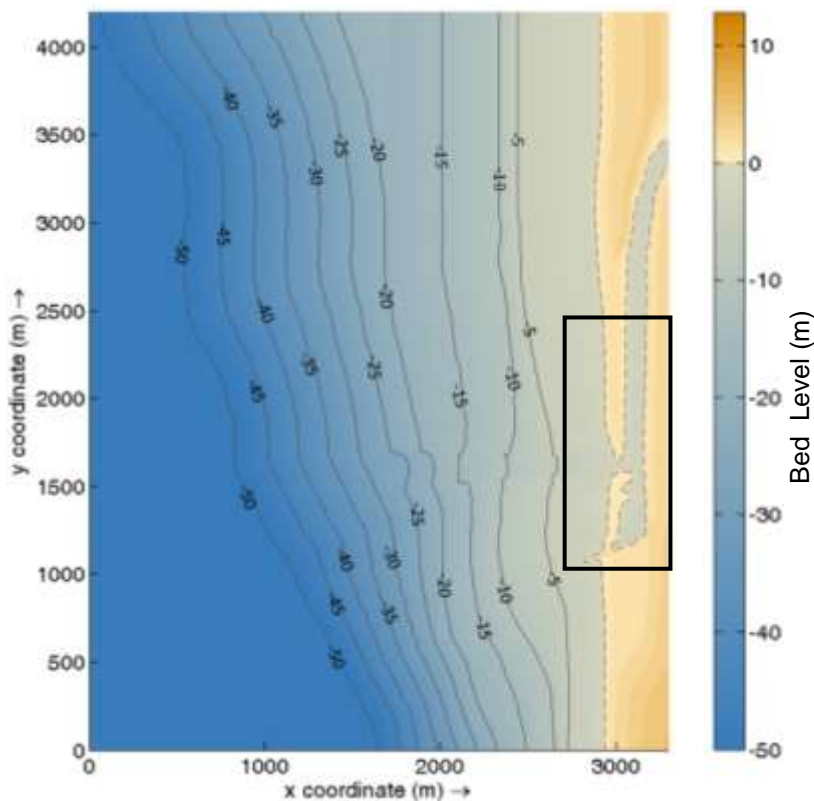


Figure 5.6 Initial bathymetry according to the measurements of DLH for date 4.12.1998.

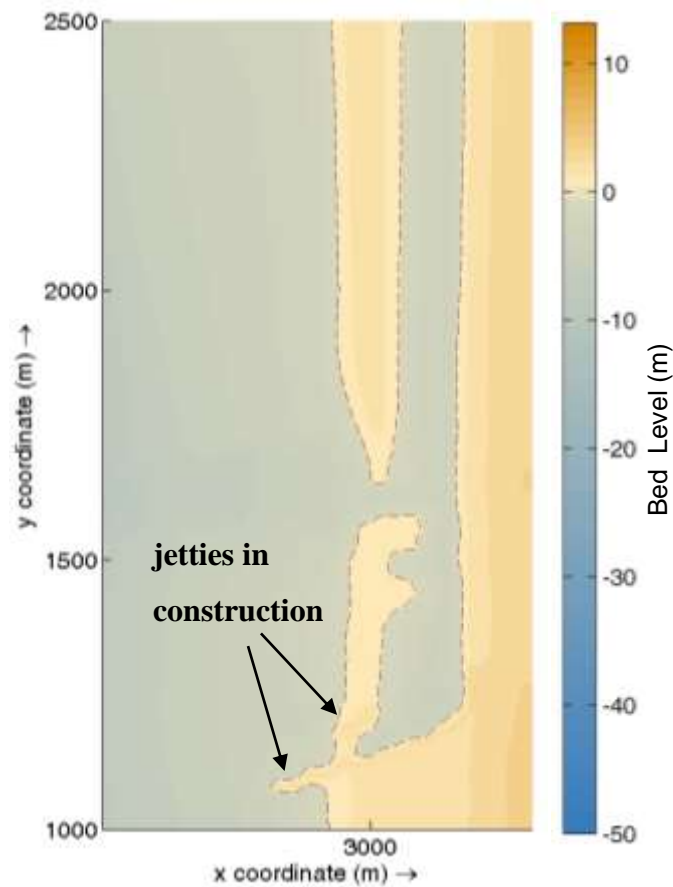


Figure 5.7 A closer look to the bathymetry between $x= 2500 \text{ m} - 3300 \text{ m}$ and $y= 1000 \text{ m} - 2500 \text{ m}$.

The model duration is taken as 12 days in order to be able to compare the before and after nearshore morphology conditions and the bottom contours that are taken between 4th and 15th December, 1998 since there is a drastic change at the river mouth as it is clearly indicated in Figures 5.4 and 5.5.

For that duration, the daily average river discharge data obtained from DSI (Table 5.1) has been taken as the river discharge input for XBeach numerical model.

In order to determine the seaward effect at the river mouth, the storm conditions and the wave climate are investigated and the correspondent nearshore wave properties

are determined with W61 that is a deep water wave-hindcasting numerical model developed by Middle East Technical University, Ocean Engineering Research Center (METU-OERC). The wave-hincasting model uses the hourly average wind data and the effective fetch lengths computed for the selected representative point which is chosen as 36.60 N and 31.40 E, for this case study (Figure 5.7).

The effective fetch length is found by dividing each 22.5 degree interval by 7.5 degree and it is found by the following equation:

$$F_{eff} = \frac{\sum F_i \cos^2 \alpha_i}{\sum \cos \alpha_i} \tag{5.1}$$

In Eq. 5.1, F_{eff} is the effective fetch length for the 22.5 degree interval, F_i is the fetch lengths obtained by each 7.5 degree and α_i is the angle of the fetch segment.

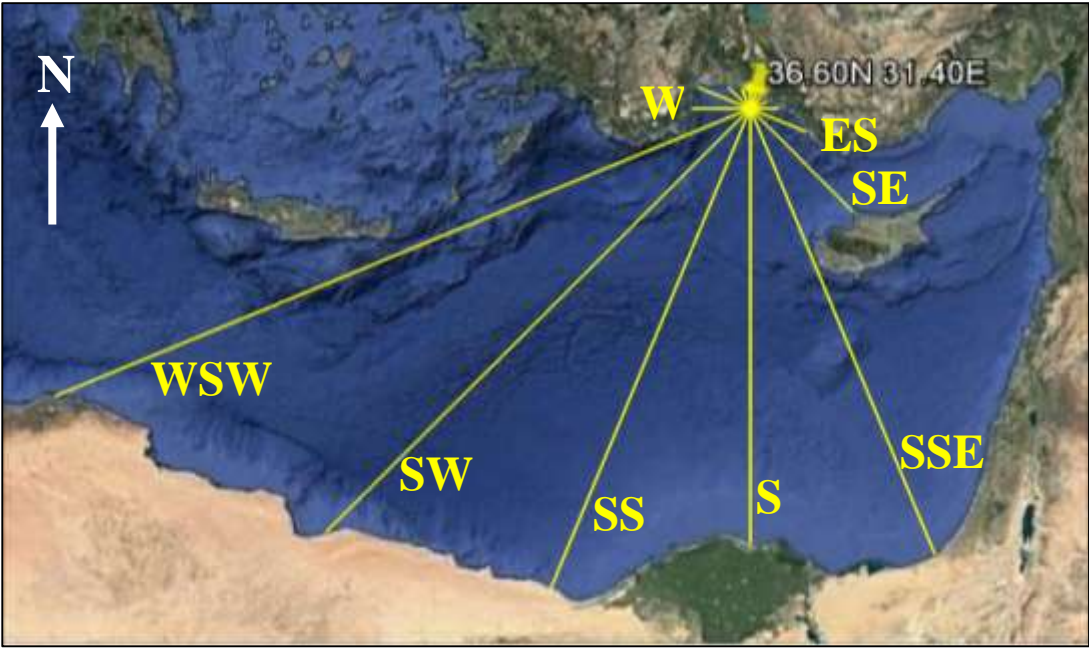


Figure 5.8 Determination of the effective fetch lengths (Google Earth, 2016).

Wind data is taken from European Center of Medium-range Weather Forecasting (ECMWF) for the point, 36.60N, 31.40 E. Wind velocities adopted from ECMWF dataset are applied to the hindcast model, W61, for one month as December 1998, in order to clearly determine the exact duration of the storms happened between 4th and 15th of December, 1998.

In the given duration, three significant storms occurred, with the storm average significant deep water wave heights, H_s , 0.47 m, 1.08 m and 1.27 m, respectively, according to the resulting wave-hindcast model outputs calculated with W61.

The next step is to apply the wave boundary conditions to XBeach. The final W61 wave outputs which are the storms mentioned above occurred within the 12-day duration, the deep water significant wave heights and the significant wave periods are used as stationary wave boundary conditions in XBeach numerical model input and these corresponding storm and wave parameters are given in Table 5.3.

Table 5.2 Wave Climate Properties for the given duration (4th-15th December 1998)

Storm Number	Start Date	Duration (hours)	H_{s0} (m)	H_{rms} (m)	T_{s0} (s)	Direction (°)
Storm #1	05/12/1998	53	0.47	0.33	2.78	SE
Storm #2	09/12/1998	20	1.08	0.76	4.20	S
Storm #3	10/12/1998	14	1.27	0.90	4.42	W

In order to clearly determine the discharge and wave effects near Manavgat River Mouth, a summary graph for the concurrent river discharge and storm wave data is given in Figure 5.8 indicating the starting dates of storms and the corresponding daily mean river discharge data. From the figure, it is seen that the output wave height is proportional to the river discharge data for that duration.

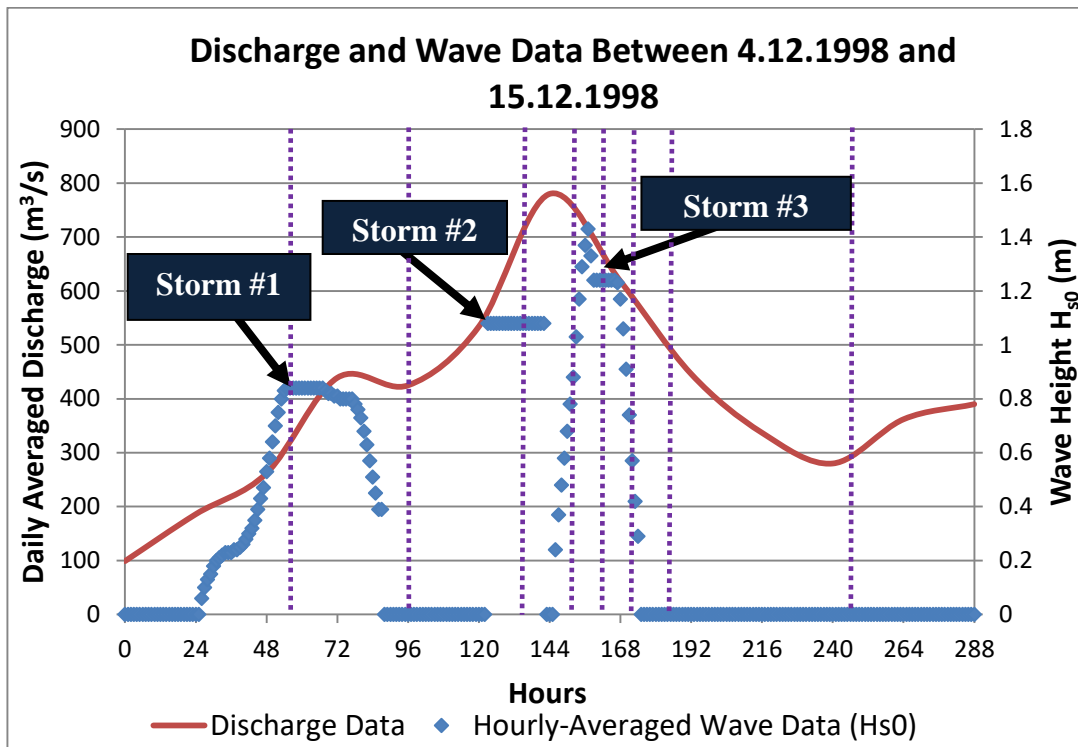


Figure 5.9 Daily Mean River Discharge Data (red line), concurrent hourly averaged deep water significant wave heights (large blue dots) and the time steps at which the hydrodynamic and morphologic conditions are presented (purple small dots) between December 4th and 15th, 1998.

5.3 Determination of the Model Parameters

In this section, the parameters that are used as XBeach inputs are discussed for the numerical modeling of hydrodynamic and morphological conditions between December 4th and 15th, 1998 at Manavgat river mouth. The input parameters are analyzed in two steps which are i) Hydrodynamic and ii) Morphology parameters.

5.3.1 Hydrodynamic Parameters

Simulation of the river mouth and its near shore morphology requires accurate hydrodynamic conditions as a first step. However, other than the bathymetric maps given by DLH, there is not any data reached regarding wave height or current measurements at the river mouth, or water levels reached by the sea and river around the river mouth during the flood event, the vegetation and the sediment sizes at various locations of the river mouth at the time of selected event. Therefore, determination of model parameters is mainly based on the recommended values of the numerical model in this preliminary study. As a future study, more detailed sensitivity analyses of the most effective parameters may be done for the study area. The parameters that are related to the hydrodynamic conditions, the definitions of these parameters and the corresponding discharge and wave data information are given in Table 5.3.

Table 5.3 Hydrodynamic parameters applied in model for Manavgat river mouth

PARAMETER	UNITS	DEFINITION	MODEL VALUES
<i>instat</i>		seaward boundary condition	stat_table
<i>bcfile</i>		wave boundary conditions	Time Series file
<i>break</i>	-	wave breaker type	Baldock
<i>gamma</i>	-	breaker index	0.78
<i>eps</i>	m	threshold water depth above which are considered wet	0.01
<i>hmin</i>	m	threshold water depth above which Stokes drift is included	0.1
<i>zs0</i>	m	initial water level	0.20
<i>tideloc</i>	-	Number of corner points on which a tide time series is specified	1
<i>bedfriccoef</i>	-	bed friction coefficient	default

(Table 5.3 continued)

PARAMETER	UNITS	DEFINITION	MODEL VALUES
<i>nuhv</i>	-	longshore viscosity enhancement factor	0.05
<i>roller</i>	-	switch to enable roller model	1
<i>beta</i>	-	breaker slope coefficient in roller model	0.1
<i>morfac</i>	-	morphological acceleration factor	10
<i>disch_loc_file</i>		name of discharge locations file	Location File
<i>disch_timeseries_file</i>		name of discharge time series file	Time Series File

'*instat*' parameter is used to define the wave boundary conditions, i.e. stationary or instationary. Since there are three storms happened between the selected dates, it is defined as '*stat_table*' which is a stationary time varying type of wave boundary condition. By applying this wave boundary condition option, the model applies the corresponding wave conditions for given each duration time step. This parameter requires a file called '*bcfile*' consisting of H_{m0} , as significant wave height, T_p , as peak wave period, θ , main angle in degrees, s , as spreading parameter and duration for each storm and these wave boundary condition parameters are given in Table 5.3.

The wave breaking type and the breaker index (*break* and *gamma* parameters, respectively) are chosen as the Baldock's approach (1998) that is explained in Section 3.2.2. The breaker index for this formulation is applied as 0.78 unlike the scaled LSTF input parameters given in Table 4.2. The main reason for this the computed waves are not as steep as the LSTF case, therefore the breaker index is selected lower than the LSTF breaker index value for Manavgat river mouth runs.

As explained previously, the parameter that is defined as the threshold water depth above which is considered wet is '*eps*'. The value is selected as 0.01 m as it is seen that value worked well within the longshore velocity point of view in the prototype (scaled) LSTF input parameters considered in the scope of Section 4.4.

'*hmin*' parameter is the threshold water depth that is the limiter for the flow depth and this value is selected as 0.1 m, since this value has given reasonable results when applied within the prototype LSTF input parameters, as in '*eps*' parameter case.

The initial water level is defined as the keyword '*zs0*' and it is applied as 0.10 m as a result of the sea water level calculations consisting of wind setup, barometric and coriolis effects which are assumed to have higher impacts for a rather short term duration. Here, the wind setup is determined as the following Eq. 5.2 adopted from OCDI (2002):

$$\eta_0 = 4.8 * 10^{-2} \frac{F}{h_{mean}} U_{ave,10}^2 \quad (5.2)$$

Here, η_0 is the wind setup, F is the effective fetch length, h_{mean} is the average water depth across the dominant fetch and $U_{ave,10}$ is the average wind speed.

Barometric and coriolis force effects on mean sea level are assumed as 10% of the sum of wave and wind setups (Walton and Dean, 2009). Each wind setup quantity was calculated according to Eq. 5.2. Wave set-up, in fact, is computed in XBeach at each time-step. However, for the sake of simplicity, wave setup is taken as %20 of the deep water significant wave heights for the barometric and coriolis effects computation. Therefore, the assumption for the initial water level, 0.20 m, is applicable considering these effects.

The tidal variations are applied with the keyword '*tideloc*' in XBeach numerical model. According to Alpar et al. (2000) Eastern Mediterranean Sea tide oscillations are mainly semidiurnal. Likely, the western part of the Mediterranean Sea is mixed but mainly semidiurnal. Moreover, Yüce and Alpar (1994) indicated that in the Gulf of Antalya the tidal regime is mixed but mainly semidiurnal in the nature. According to Erdemli tide gauge located in the eastern part of the Mediterranean Sea, the monthly average for tidal amplitude for December is measured as 34.8 cm

(ERDEMLI, n.d.) and considering that the tide amplitude decreases westwards in the Mediterranean Sea (Alpar et al., 2000). Based on the information given previously, taking tide amplitude as 0.20 m is reasonable since there is no measured data neither in Erdemli nor in Antalya gauge records between 4th and 15th December, 1998. Consequently, at this stage, tide amplitude input is introduced as 0.20 m to the model as time series with semidiurnal time steps for the given duration for the sake of simplicity.

Bed friction is to be remained by the recommended value which is the Chézy friction coefficient and this parameter is predetermined as $C=55 \text{ m}^{1/2}/\text{s}$.

'*nuhv*' parameter is the longshore viscosity enhancement factor and this parameter is explained in detail in Section 4.3.1. This is chosen as 0.05 which gives the most appropriate solution for this case.

The parameters which are '*roller*' and '*beta*' within input file are to determine the roller behavior. The 'surface roller' formulation is activated and switched on with the value '*1*' and the '*beta*' is the breaker slope coefficient in the roller model given in Section 3.3.1. The smaller the '*beta*' parameter, the more shoreward shift in wave induced setup, return flow and the alongshore current (Roelvink et al., 2015). According to this definition, '*beta*' is remained by predetermined value as '*0.1*' since it is usually considered as a reliable value in literature.

'*morfac*' parameter is defined in XBeach as the morphological acceleration factor used to readjust the hydrodynamic and morphological time scales. This parameter is used for the cases where morphology response is slower than the hydrodynamic time scale. In order to shorten the length of simulation time, the morphology is accelerated by that defined factor. Therefore, in the Manavgat river mouth simulations, '*morfac*' parameter is chosen as 10 since the simulation time corresponds rather to medium-term morphological changes.

In order to, apply the river discharge to the domain, two files are needed to be defined, namely, ‘*disch_loc_file*’ and ‘*disch_timeseries_file*’. The former parameter file consists of the location of the river discharging points in the model domain and the latter is used to define discharge amount with its corresponding model time. Here, since the river discharge values are daily average as given in Table 5.4, it is assumed that the river discharge is constant value for the given day and taken as average river discharge.

5.3.2 Morphology Parameters

In this part, selection and calibration of the morphology parameters which are used as XBeach input are going to be discussed for Manavgat River Mouth. Morphology parameters include the sediment transport and bed update schemes and these parameters are given in Table 5.6. Morphology parameters other than discussed here are taken as the recommended values.

Table 5.4 Morphology Parameters applied in model for Manavgat river mouth

PARAMETER	UNITS	DEFINITION	MODEL VALUES
<i>D50</i>	m	median grain size	0.001
<i>form</i>	-	equilibrium sediment transport formulation	vanthiel_van rijn
<i>lws</i>		switch to enable long wave stirring	0
<i>facua</i>	-	factor for setting wave asymmetry and skewness together	0.1
<i>wetslp</i>	-	critical wet slope for the wet area	0.3
<i>dryslp</i>	-	critical dry slope for the dry area	1.0
<i>struct</i>	-	switch for the non-erodible structure	1

The median grain size parameter ' D_{50} ' is given as 0.001 m which is adopted from Guler (1997). Therefore, the median sand size is taken as 0.001 m in model input parameters.

The sediment transport equilibrium formulations are selected as '*vanthiel_vanrijn*'. The formulations used in '*vanthiel_vanrijn*' parameter are the Van Thiel and Van Rijn Approach (Van Rijn, 2007a,b,c; Van Thiel de Vries, 2009) given in Section 3.5.2.2.

Long wave stirring option accounts for the keyword '*lws*' in XBeach. Since effects of small wave induced long waves promote higher erosion rates than expected, these effects are neglected in the present study, and thus, this switch is turned off.

The '*facua*' parameter is the alias depending on the wave skewness and asymmetry and the parameter is the correspondent of the ' u_a ' in Eq. (3.49) and this parameter is explained in Section 4.3.2 in detail. This parameter is considered to be one of the most important parameters from the morphological change point of view as mentioned previously. Here, '*facua*' parameter is chosen as 0.1 which is the recommended value for this parameter.

The switches for short wave turbulence and long wave stirring parameters, namely, '*turb*' and '*lws*' are switched off due to high turbulence values, thus, erosion rates when switched on. Further sensitivity analyses may be done with different combinations of these switches.

The parameters '*wetslp*' and '*dryslp*', defined as critical wet and dry slopes, are applied as 0.3 and 1.0, respectively. These parameters are directly related with the avalanching process which is the main morphology behavior for the Manavgat River Mouth case since the sand dune is completely washed away. The selection of these parameters is done by trial and error until the bed profile resembles the resulting

measured morphology. It should be noted that these values are also recommended by Roelvink et al. (2015).

The ‘east’ and ‘west’ jetties are defined as ‘non-erodible layers’ in XBeach input file. The distinction between erodible and non-erodible structures is introduced with a different bathymetry-like input format. The switch to introduce these structures on model bathymetry is ‘*struct*’ and it is switched on during the numerical computation.

5.4 Results and Discussions

In this part, the output results of XBeach are discussed in wave heights, resultant GLM velocities, and the final bed levels points of view at the critical time steps within the bathymetric range of $x= 2500 \text{ m} - 3300 \text{ m}$ and $y= 1000 \text{ m} - 2500 \text{ m}$. It should be noted that the H_{rms} values lower than 0.2 m are not taken into account in the wave distribution figures.

The critical time steps are determined according to the river discharge and storm intensity and the model time steps that are considered in this section was previously given in Figure 5.9. For initial and final bed levels, the comparison between the numerical model and the measured output values is given and possible indicators of differences between observations and model results are discussed. The initial bathymetry taken on 4th December, 1998, was previously given in Figure 5.5.

Waves and Depth Averaged velocities at $t=55h$

Computed root mean squared wave height after 55 morphologic hours of simulation is given in Figure 5.10.

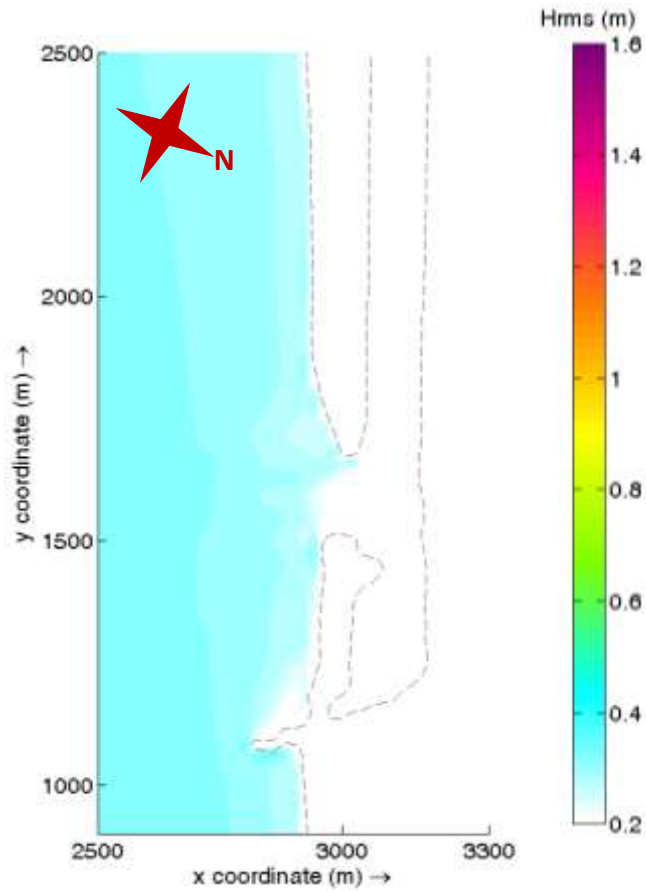


Figure 5.10 Root Mean Squared Wave Height Distribution after 55 hours of simulation

In Figure 5.10, simulated H_{rms} wave height distribution is given. Here, the hourly averaged deep water significant wave height is given as 0.84 m which approximately equals to 0.59 m root mean squared wave height value. The figure indicates that, the waves reach up to the river mouth inlet but they are not able to penetrate into the river due to strong river discharge around $300 \text{ m}^3/\text{s}$.

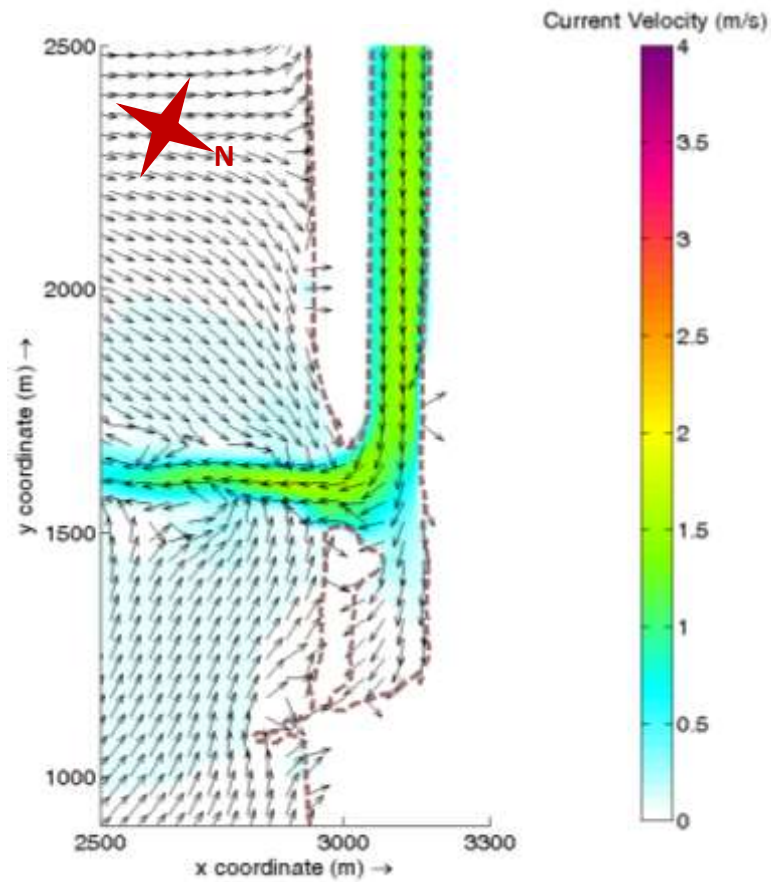


Figure 5.11 Depth Averaged Flow Velocity Field after 55 hours of simulation

In Figure 5.11, depth averaged velocity distribution is given for Manavgat river mouth nearshore region. Here, the river discharge is interpolated at this time step as $314 \text{ m}^3/\text{s}$. At the inlet of the river mouth, the velocities increase approximately up to 1.5 m/s .

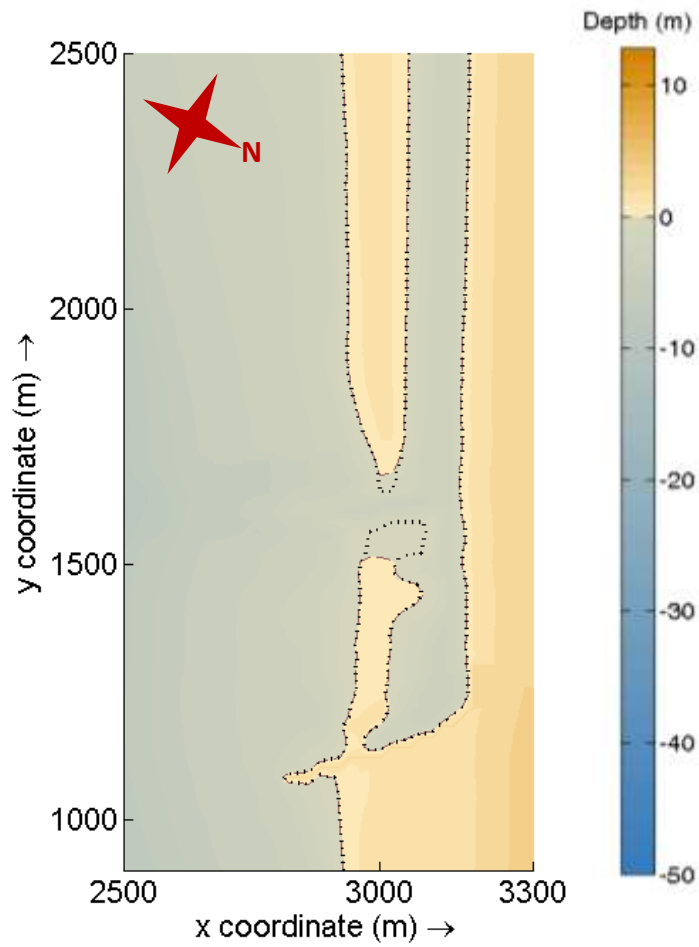


Figure 5.12 Initial shoreline (black dotted line), computed bed levels and shoreline (brown dashed line) after 55 hours of simulation

In Figure 5.12, the computed bed level after 55 hours of morphologic time is given. Here, it is clearly shown that the head of the small sand bar is eroded significantly.

Depth Averaged velocities at t=95h

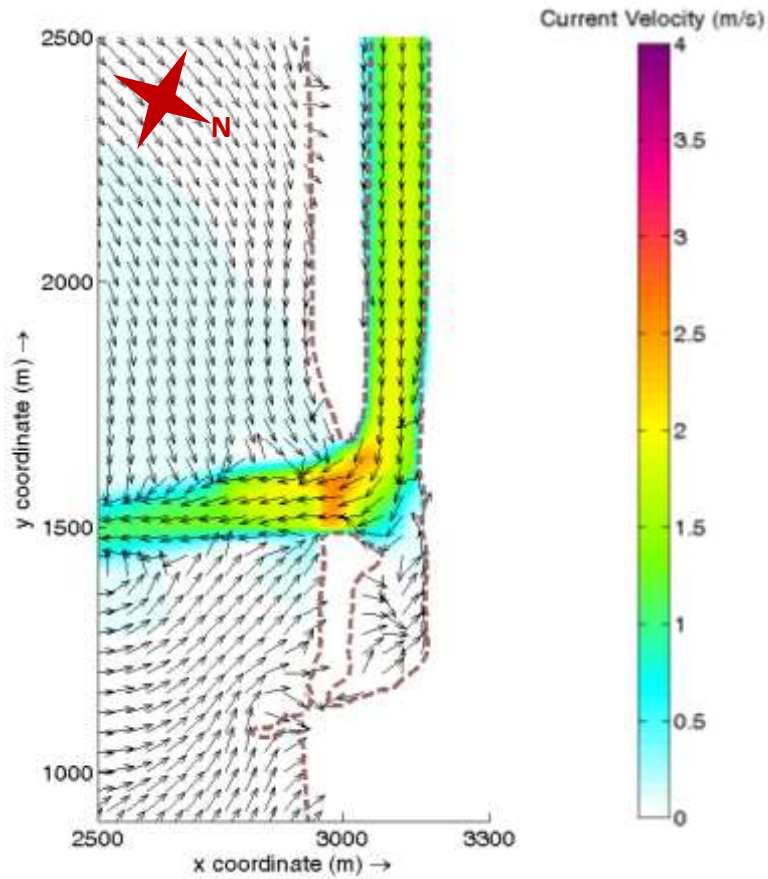


Figure 5.13 Depth Averaged Flow Velocity Field after 95 hours of simulation

In Figure 5.13, depth averaged velocity distribution is given for Manavgat river mouth nearshore region. It should be noted that at this time step, there is no wave action computed. Here, the river discharge is interpolated at this time step as 426 m^3/s . At the inlet of the river mouth, the velocities further increase approximately up to 2.0 m/s although the inlet is enlarged by erosion due to the further increased river discharge.

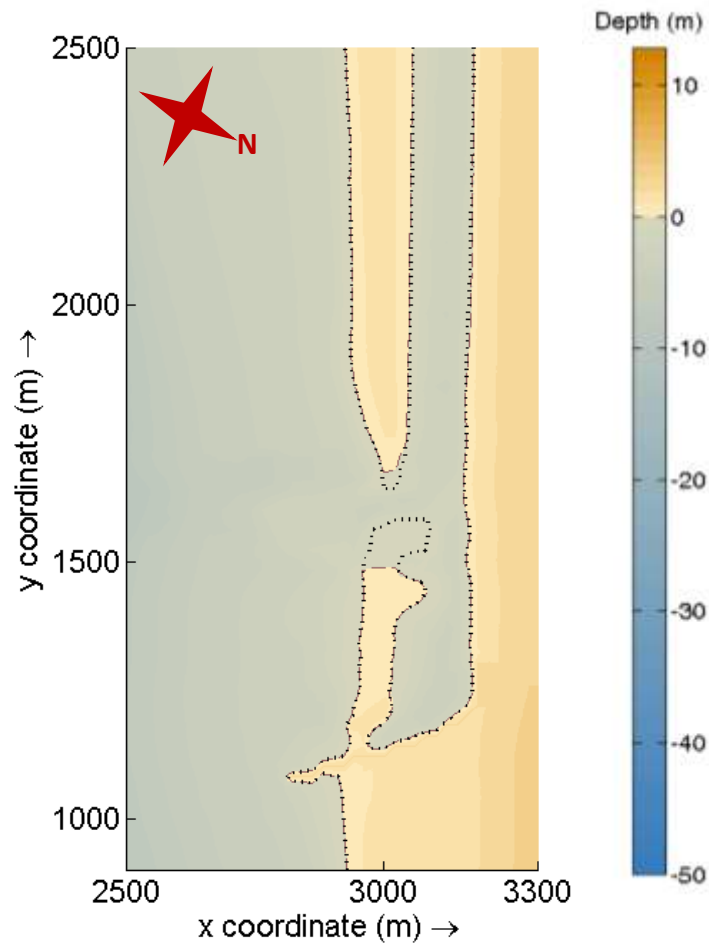


Figure 5.14 Initial shoreline (black dotted line), computed bed levels and shoreline (brown dashed line) after 95 hours of simulation

In Figure 5.14, the computed bed level after 95 hours of morphologic time is given. Here, it is clearly shown that the head of the small sand bar is further eroded comparing to the previous case.

Waves and Depth Averaged velocities at t=126h

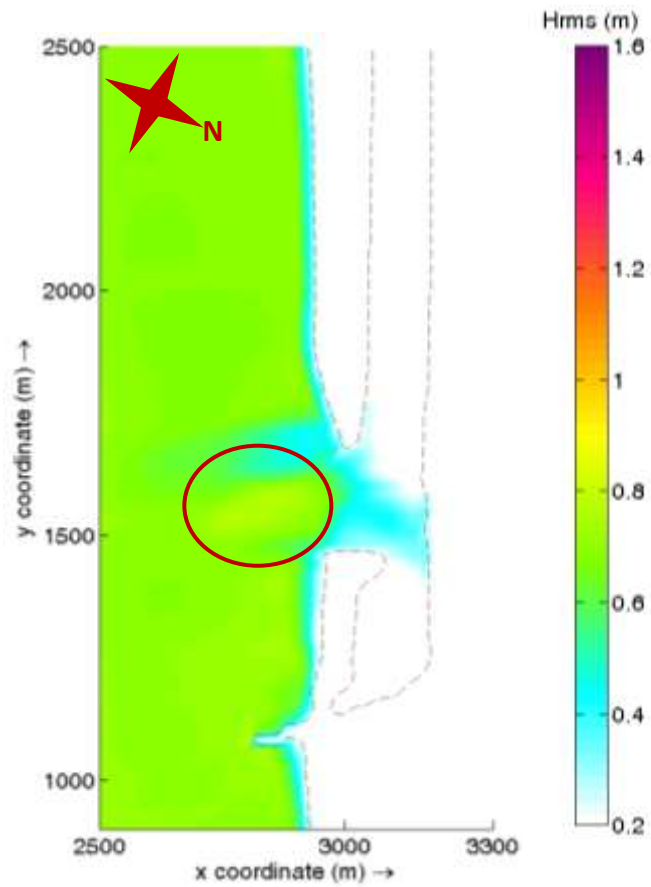


Figure 5.15 Root Mean Squared Wave Height Distribution after 126 hours of simulation

In Figure 5.15, simulated H_{rms} wave height distribution is given. Here, the hourly averaged deep water significant wave height is given as 1.08 m which is approximately equal to 0.76 m root mean squared wave height value. The figure indicates that, the waves enter through the river mouth directed towards rather south with the effect of river discharge of around $595 \text{ m}^3/\text{s}$. It is also seen that at the river mouth wave heights are rather amplified at the river mouth (red circle in Figure 5.15) which is due to accumulated sand at the river mouth and the river discharge running against them.

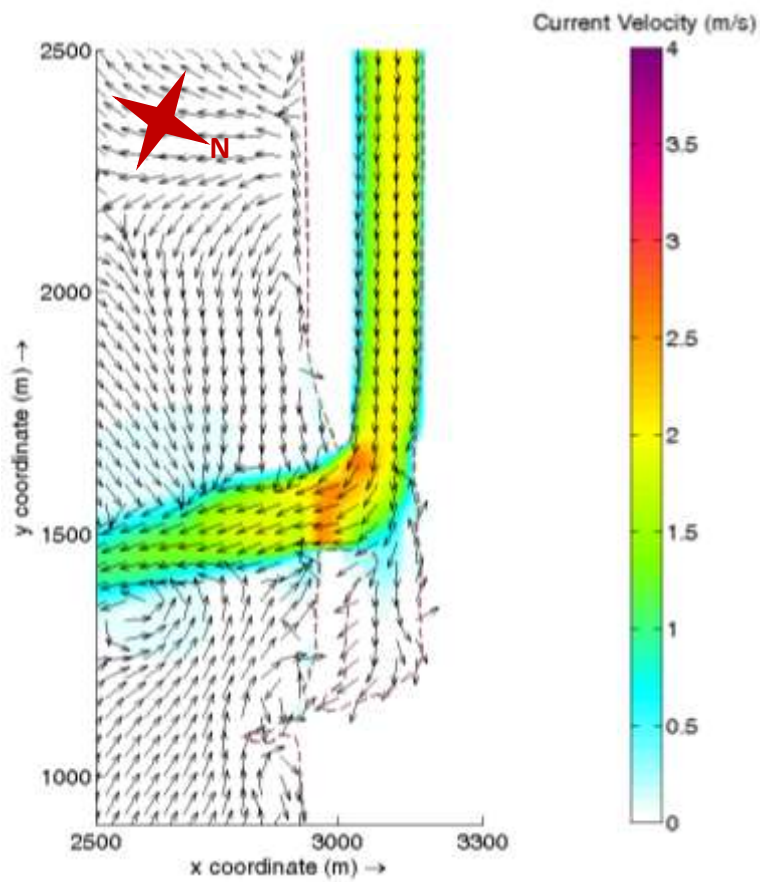


Figure 5.16 Depth Averaged Flow Velocity Field after 126 hours of simulation

In Figure 5.16, depth averaged GLM velocity distribution is given for Manavgat River Mouth nearshore region after 126 hours of morphologic simulation. Here, the river discharge is interpolated at this time step as $595 \text{ m}^3/\text{s}$. At the inlet of the river mouth, the velocities range between 1.5 to 2 m/s.

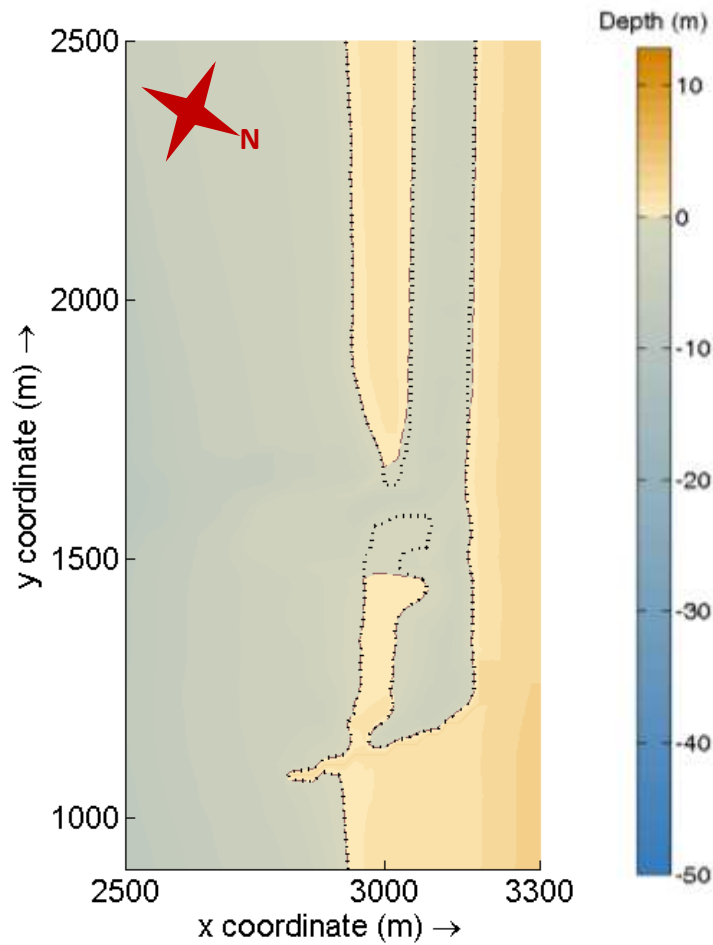


Figure 5.17 Initial shoreline (black dotted line), computed bed levels and shoreline (brown dashed line) after 126 hours of simulation

In Figure 5.17, the computed bed level after 126 hours of morphologic time is given. Here, it is clearly shown that the initiation of erosion at the larger sand bar is observed. Moreover, minor indications of the river bed erosion due to high velocity at the mouth inlet can be derived from the figure.

Depth averaged velocities and bed levels at t=143h

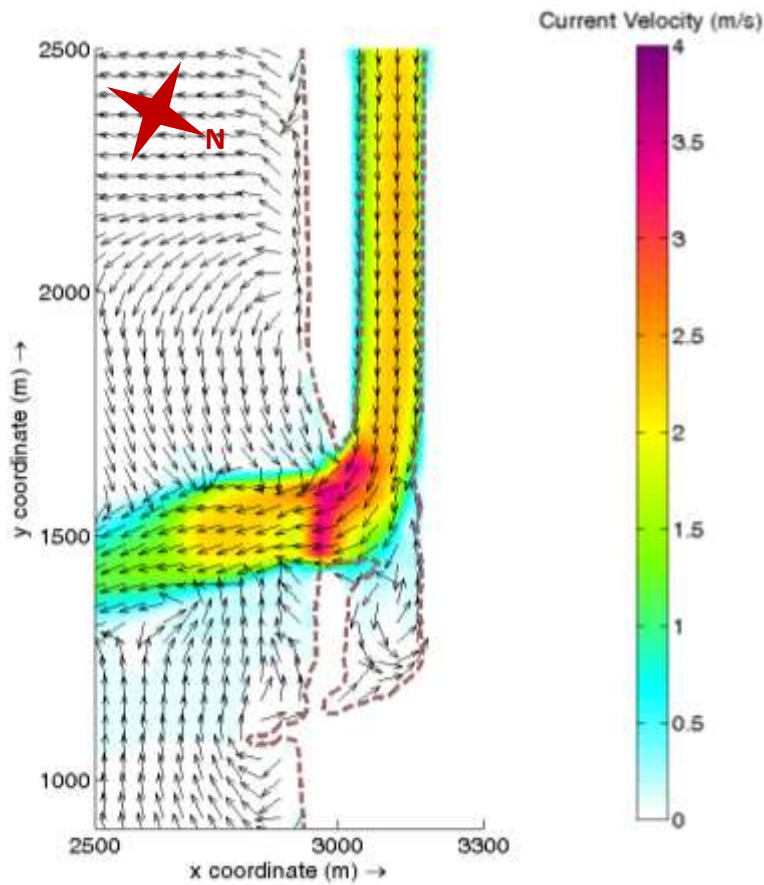


Figure 5.18 Depth Averaged Flow Velocity Field after 143 hours of simulation

In Figure 5.18, depth averaged GLM velocity distribution is given for Manavgat river mouth nearshore region. It should be noted that at this time step, there is no wave action computed. Here, the river discharge is interpolated at this time step as $770 \text{ m}^3/\text{s}$. At the inlet of the river mouth, the velocities reach nearly up to 3 m/s due to the further increased river discharge comparing with previous case.

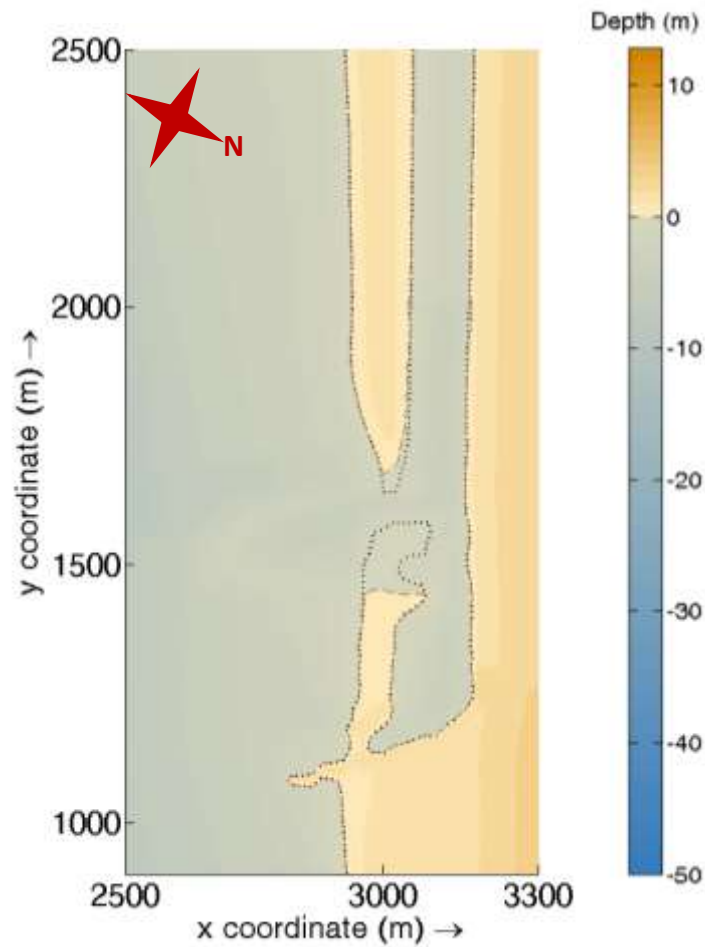


Figure 5.19 Initial shoreline (black dotted line), computed bed levels and shoreline (brown dashed line) after 143 hours of simulation

In Figure 5.19, the computed bed level after 143 hours of morphologic time is given. Here, minor indications of the river bed erosion due to high velocity at the mouth inlet can be seen from the figure.

Waves, depth averaged velocities and bed levels at t=157h

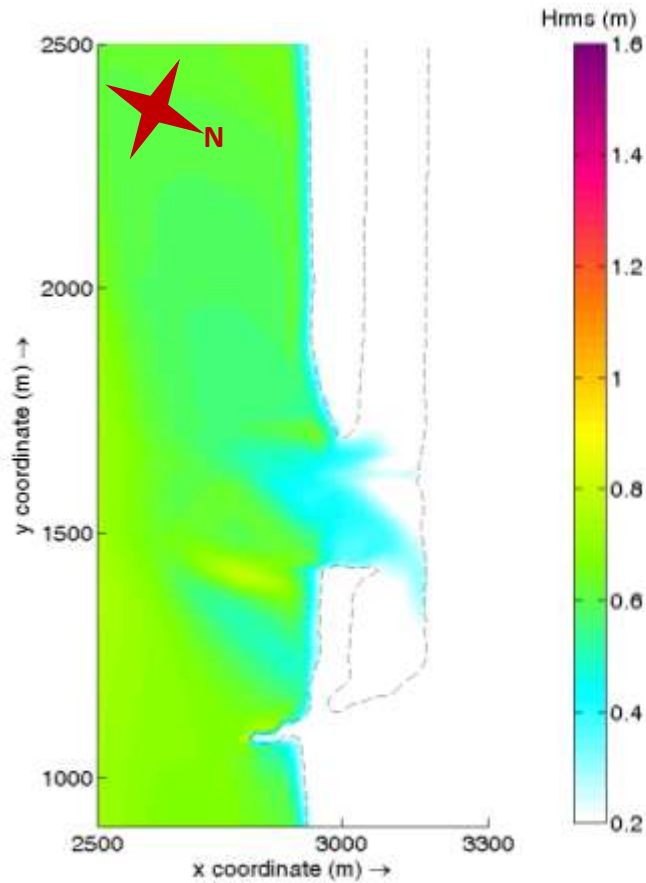


Figure 5.20 Root Mean Squared Wave Height Distribution after 157 hours of simulation

In Figure 5.20, simulated H_{rms} wave height distribution is given. Here, the hourly averaged deep water significant wave height is given as 1.43 m which is approximately equal to 1.01 m root mean squared wave height value. The figure indicates that, the waves enter through the river mouth.

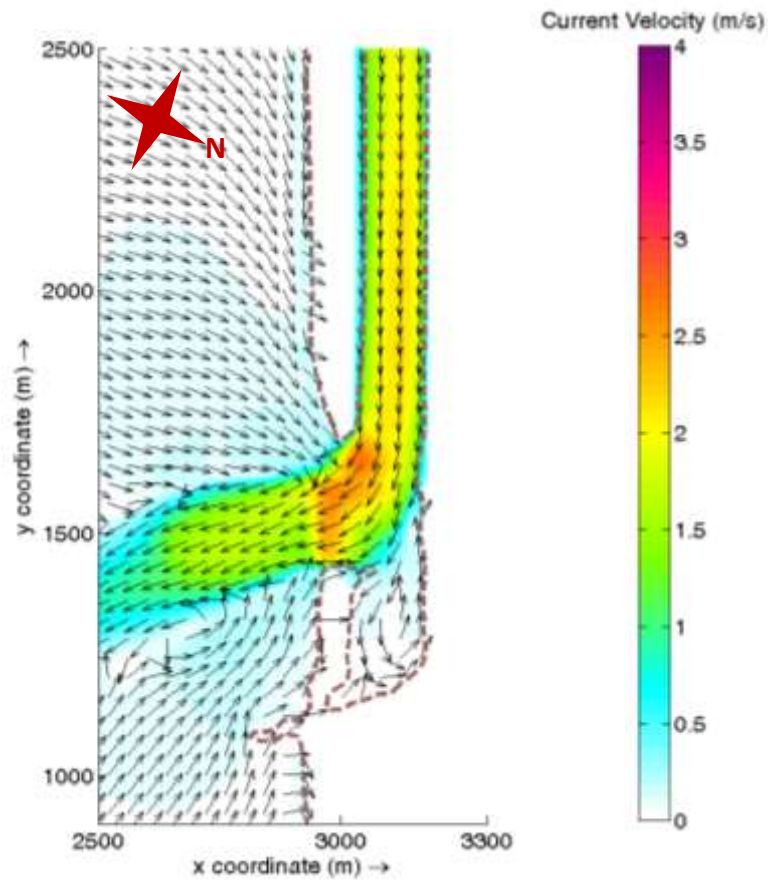


Figure 5.21 Depth Averaged Flow Velocity Field after 157 hours of simulation

In Figure 5.21, depth averaged GLM velocity distribution is given for Manavgat river mouth nearshore region after 157 hours of morphologic simulation. Here, the river discharge is interpolated at this time step as $692 \text{ m}^3/\text{s}$. At the inlet of the river mouth, the velocities range between 1.5 to 2 m/s.

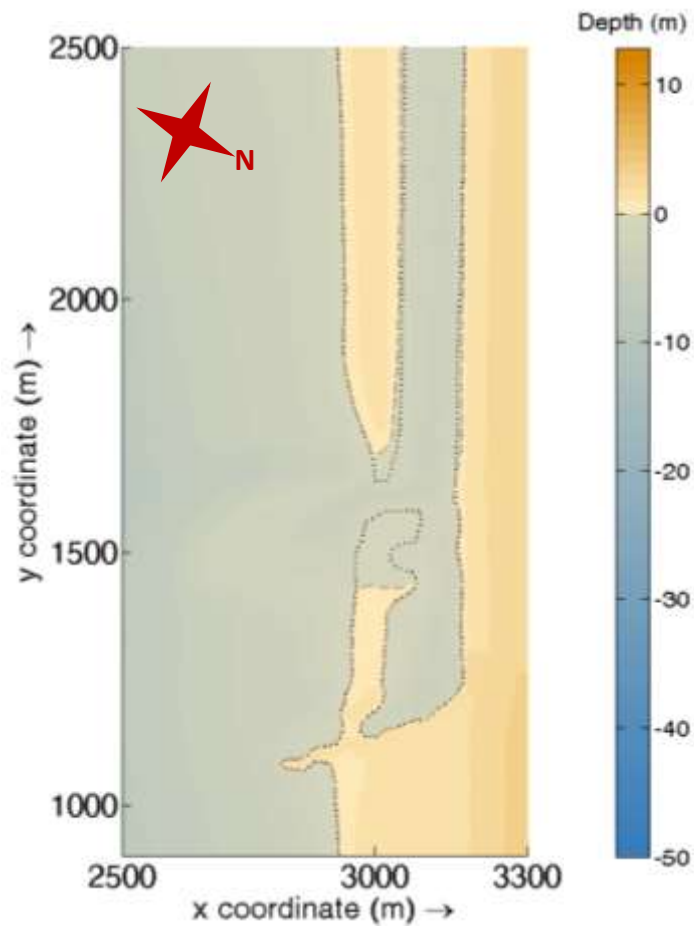


Figure 5.22 Initial shoreline (black dotted line), computed bed levels and shoreline (brown dashed line) after 157 hours of simulation

In Figure 5.22, the computed bed level after 157 hours of morphologic time is given. Here, minor indications of the river bed erosion due to high velocity at the mouth inlet can be seen from the figure.

Depth averaged velocities and bed levels at t=175h

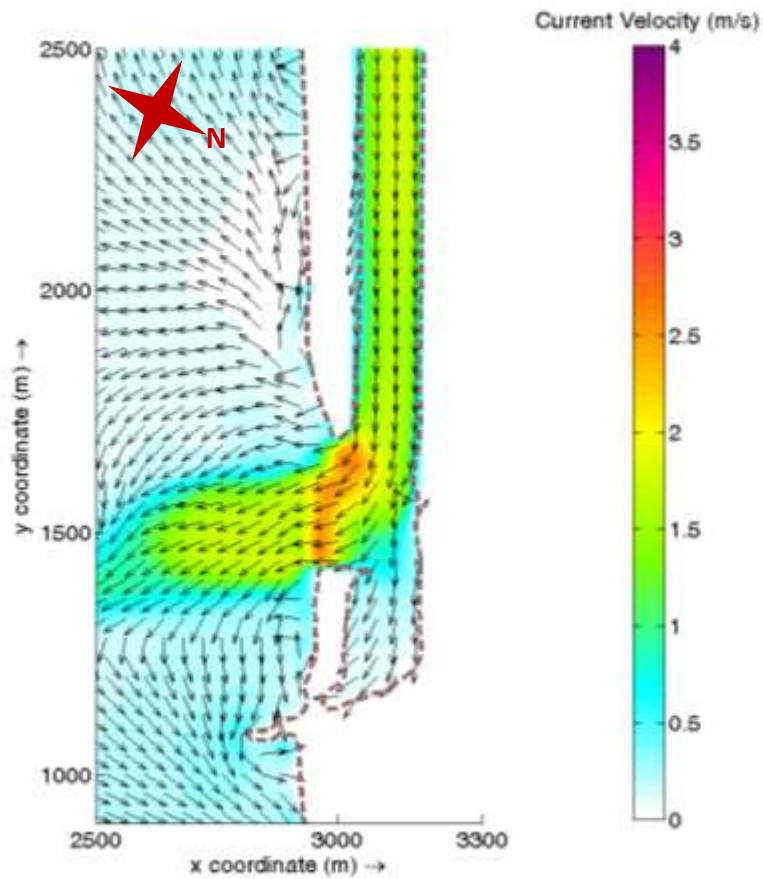


Figure 5.23 Depth Averaged Flow Velocity Field after 175 hours of simulation

In Figure 5.23, depth averaged GLM velocity distribution is given for Manavgat river mouth nearshore region. It should be noted that at this time step, there is no wave action computed. Here, the river discharge is interpolated at this time step as $568 \text{ m}^3/\text{s}$. At the inlet of the river mouth, the velocities nearly stayed the same as the previous time step.

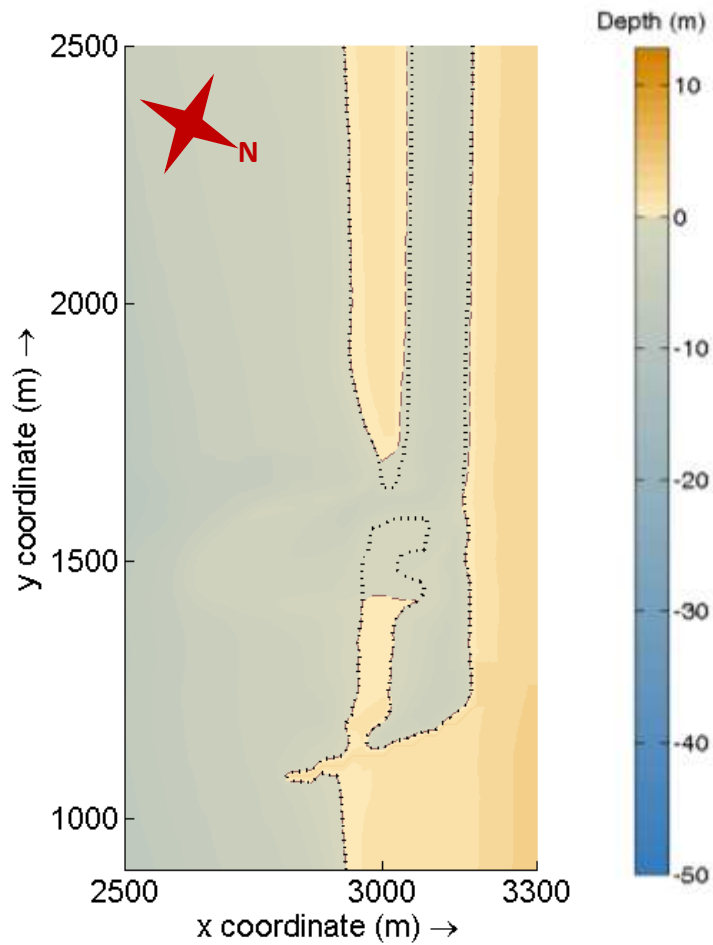


Figure 5.24 Initial shoreline (black dotted line), computed bed levels and shoreline (brown dashed line) after 175 hours of simulation

In Figure 5.24, the computed bed level after 175 hours of morphologic time is given. Here, minor indications of the river bed erosion due to high velocity at the mouth inlet can be seen from the figure.

Depth averaged velocities and bed levels at t=239 h

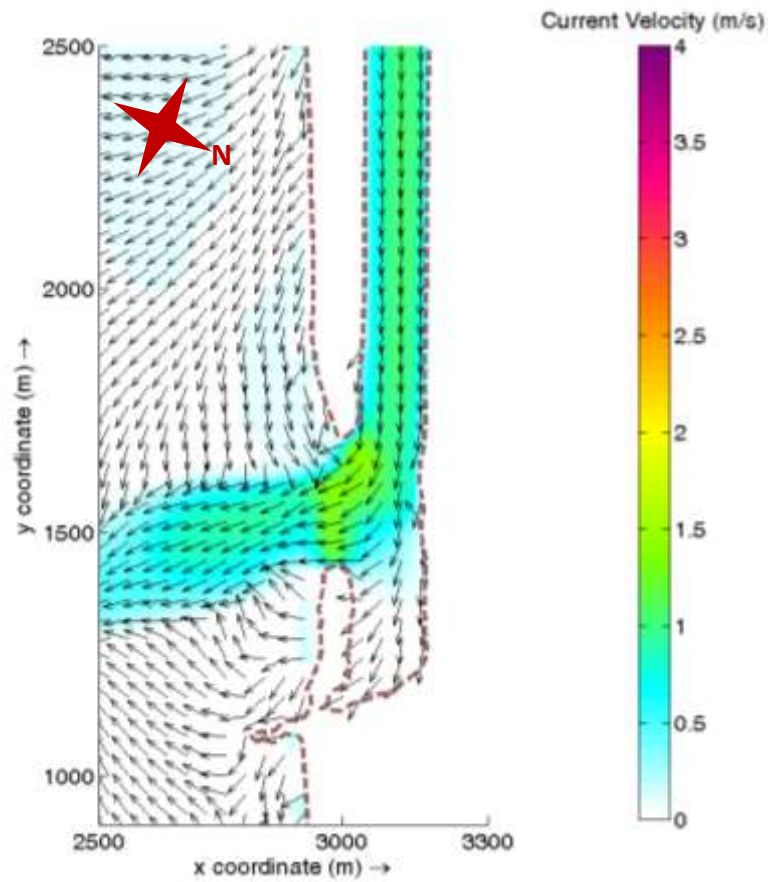


Figure 5.25 Depth Averaged Flow Velocity Field after 239 hours of simulation

In Figure 5.25, depth averaged GLM velocity distribution is given for Manavgat river mouth nearshore region. It should be noted that at this time step, there is no wave action computed. Here, the river discharge is interpolated at this time step as $282 \text{ m}^3/\text{s}$. At the inlet of the river mouth, the velocities decreased down to 1.5 m/s comparing to previous time step.

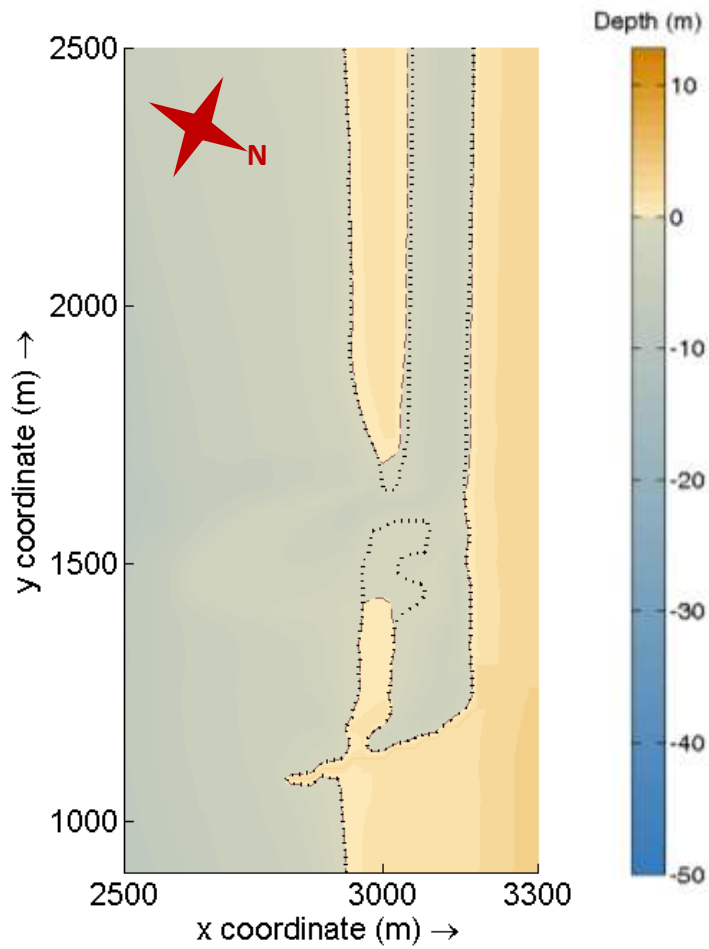


Figure 5.26 Initial shoreline (black dotted line), computed bed levels and shoreline (brown dashed line) after 239 hours of simulation

In Figure 5.26, the computed bed level after 239 hours of morphologic time is given. Here, bed level comparing to the previous time step does not change significantly.

Cumulative Sediment Accretion/Erosion Quantities at the River Mouth

After 288 morphologic hours of the simulation, the accretion/erosion scheme around the mouth is given in Figure 5.27.

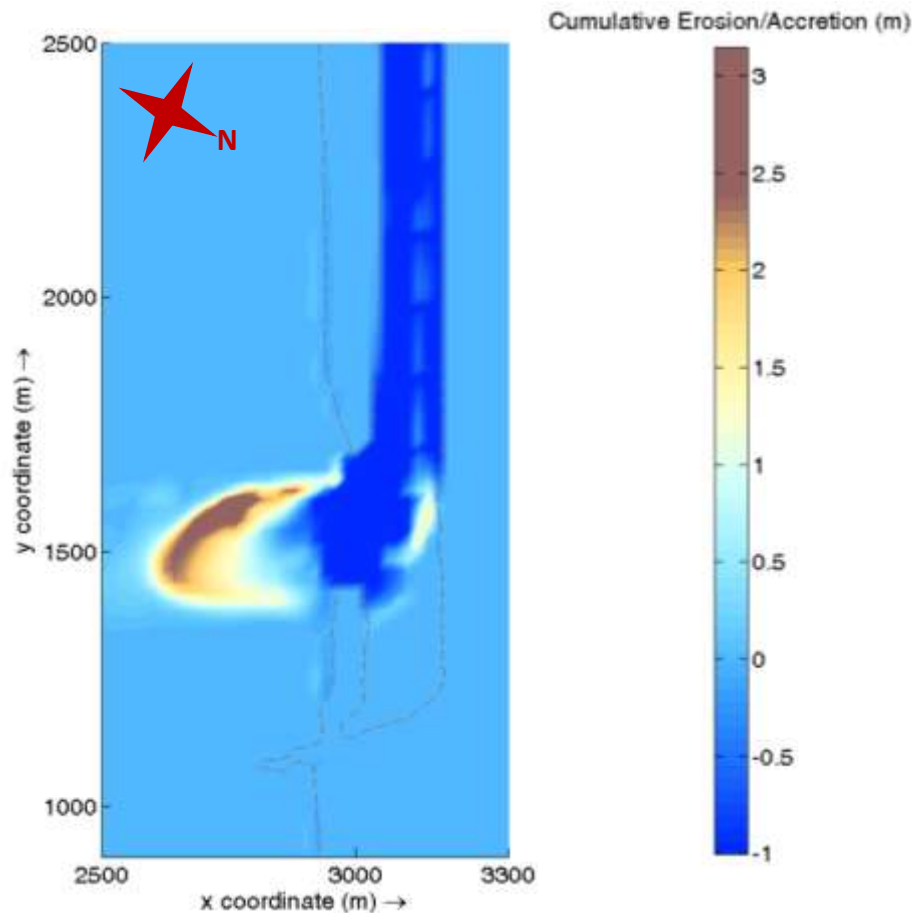


Figure 5.27 Cumulative sediment accretion/erosion scheme at the end of the simulation

According to the resulting output of the numerical model (Figure 5.28), it is observed that the eroded material is accreted in front of the river mouth, forming a submerged sand bar mainly towards to the south. Moreover, at the river meandering part, there is a small sand accumulation that can also be seen from the above figure. This is

probably due to a flow circulation scheme at that part of the river due to increasing river discharge seen in Figures 5.13, 5.16, 5.18 and 5.21.

Shoreline Comparison Between Final Measured and Predicted Bed Levels

The initial, measured final and computed final shorelines are given in Figure 5.27.

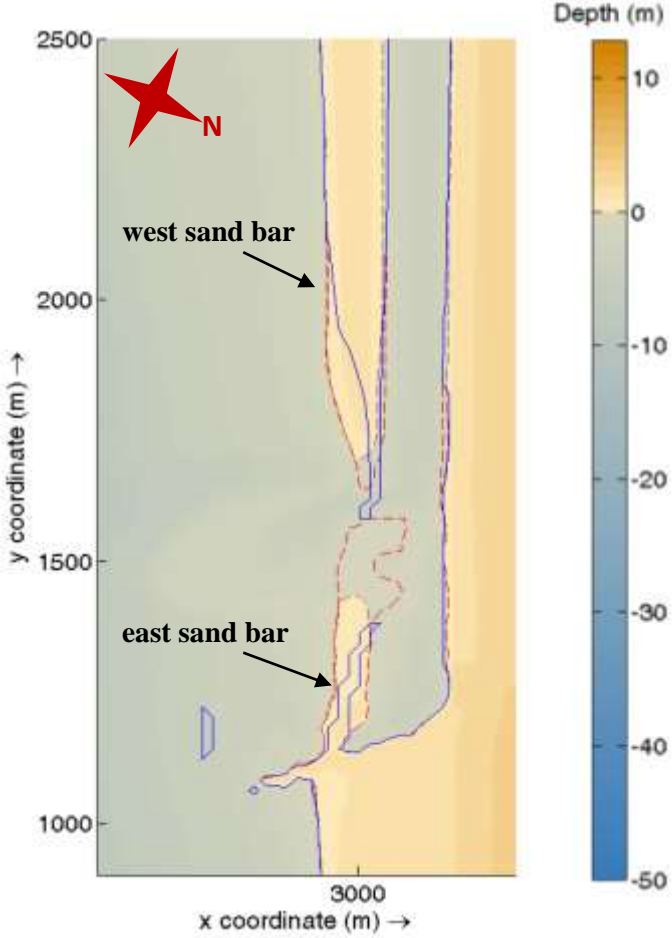


Figure 5.28 Initial (red dashed line) resulting measured (blue line), and final computed (brown dashed line, main color map in the figure) after 288 hours of simulation

In Figure 5.27, initial shoreline indicated by the blue dashed line, final computed shoreline indicated by the brown dashed line and the final measured bathymetry indicated by the red line are given. As can be seen from the figure, the smaller sand island (east sand bar) around the river mouth is completely washed away. This is assumed to be due to both the extreme discharge schemes of the river flow and storm occurred between 4th and 15th of December, 1998. Moreover, the mean sea level fluctuations in combination with the stormy wave climate also led the river mouth a complete reshape.

There are some resemblances and differences between the computed shoreline and the measured one after 12 days. The lower seaward side of the west sand is observed to be eroded more than the computed shoreline. A possible reason for this underestimation of erosion is the wave action, which might actually happened more intense than the computed waves. Another possible reason for the difference is the selected parameters as well as switched off parameters such as '*turb*' and '*lws*' given in Table 5.5. A detailed sensitivity analyses for these parameters are needed for this area as a further study. Moreover, wave-current interaction parameter is also switched off due to computational instability for the given bathymetry. However, this phenomenon should be taken into account in further studies. In the meanwhile, the computed upper seaward side of the west sand bar is not eroded as the measured case. Similarly, in both measured and computed cases, the fork-like structure at the head of the east sand bar is completely washed away. Again, the seaward side of the computed shoreline at east sand bar indicates underestimation of the erosion. The possible reason is assumed to be the same with the west sand bar case. Moreover, the differences between the computed and measured shorelines are also likely to be due to grid size, model assumptions, input assumptions, lack of data especially of the land elevations, lack of wave data to compare with the computed results or combinations of two or more of them.

CHAPTER 6

CONCLUSION

In this study, the applicability of XBeach numerical model to both laboratory and field data is tested and the model results are compared with the measured data in two different applications:

- i. Modeling the laboratory data including wave, current and bed level measurements in the vicinity of coastal structures as detached breakwater and T-groin and comparing the relevant model outputs
- ii. Modeling Manavgat river mouth morphology changes in a fluvial dominant coastal flooding occurrence consisting of the measured bathymetries between dates 4th and 15th December, 1998 and the simulated the bed level changes focusing on the shoreline variation.

In the first part of the study (see Chapter 4), laboratory data that is obtained from the Large-Scale Sediment Transport Facility (LSTF) (Gravens and Wang, 2007) is compared to the XBeach model results of root mean squared wave heights, depth averaged wave induced longshore currents, mean water levels and the final bed levels in three cases, i) Experiment Base Case-1 (BC1) which is the calibration experiment to reveal that the bed is in stability under the given wave conditions, ii) Experiment Test-1 Case-1 (T1C1) in which the detached breakwater is placed and iii) Experiment Test-3 Case-1 (T3C1) in which the T-groin is placed.

In the calibration process of the hydrodynamic properties of BC1, it is seen that with lower values of '*hmin*' and '*eps*', especially the velocity computations did not reach

to a steady state. Therefore, '*hmin*' and '*eps*' parameters are increased to values which are not compatible with the laboratory dimensions. Also, it is observed that the longshore velocity distribution is very sensitive to '*nuhv*' parameter, that is, longshore viscosity enhancement factor. For the lower values of this parameter, viscosity in the lateral direction decreases, therefore, the velocity distribution resembles to the ones in the laboratory conditions.

After the hydrodynamic parameters are determined, performances of morphology parameters are tested in order to designate the morphology input parameters. The calibration criterion is to remain the equilibrium bed profile of BC1 under the given wave conditions. It is observed that recommended value range, for '*facua*' parameter, which is the alias for the wave asymmetry and skewness having great effect on a stronger onshore sediment transport, is not sufficient for this case. Within this recommended range, between zero and unity, the bed level eroded until the simulation stopped and the equilibrium bed level state is diminished. Therefore, '*facua*' parameter is increased up to '5', until the bed level does not change compared to the equilibrium level. It is also seen that for other experiments, T1C1 and T3C1, the erosion/accretion scheme on two dimensional experiments does not give satisfying results within the recommended values of '*facua*'. However, the predicted bed morphology results in the vicinity of detached breakwater and T-groin with the calibrated '*facua*' value, which is '5' as previously mentioned, indicate a good agreement with some underestimation of morphology changes, especially in front of the detached breakwater and T-groin.

The second attempt to compare the model output values to the LSTF measured data is to scale the laboratory experiment parameters according to Froude scaling rules to the prototype dimensions. Within this scope, the basin dimensions, wave heights and wave periods are scaled up, the model is run with the scaled dimensions and related parameters, and the results are rescaled back down to original dimensions to effectively compare with the measurements. By this way, the scale dependency noted by Brandenburg (2010) of the numerical model is tried to be eliminated. In the

calibration process of the scaled dimensions, again, BC1 experiment as the base in the determination of input hydrodynamic and morphologic parameters. The parameters '*hmin*' and '*eps*' are remained the same, which are compatible with the scaled experiment parameters. Moreover, '*facua*' parameter is selected within the recommended range, as '0.4'. For the experiments in the vicinity of the detached breakwater and T-groin structures, namely, T1C1 and T3C1, the bottom contours improved and the accretion schemes in the lee of the detached breakwater and behind the head of the T-Groin show better agreement than the previous non-scaled cases. However, similar to the non-scaled case, there are also some underestimations of the morphology change, especially in front of the breakwater and T-groin. The most prominent fact between the comparison of original and scaled data is that the more accurate bed morphology is obtained with morphology parameters within the range of the recommended values given for prototype dimensions. Therefore, it can be concluded that the model is successful in predicting the wave heights and longshore currents where the morphology is very dependent on the scale of the case.

In the second part of the study (see Chapter 5), Manavgat river mouth morphology is modeled for a fluvial dominated coastal flooding between 4th and 15th of December, 1998. The initial bathymetry is digitized and introduced into the XBeach numerical model with the flow parameters as well as wave related hydrodynamic and morphology input parameters. At critical time steps which are coincident with observed higher or lower discharge quantities as wave heights increases or decreases, output values of the model is investigated in the following points of view: root mean squared wave heights, flow velocities (both river flow and wave induced current velocities) and the resulting morphology as well as the final computed cumulative sediment accretion/erosion scheme. Here, it is observed that the fork-like part of the east sand bar is completely washed away, which shows great resemblance between both measured and computed bathymetries. Consequently, the river mouth is enlarged in both cases, predicted and measured. The shoreline between east jetty and the final river mouth is well agreed with the measured final shoreline. Moreover, although there are no indications in the measured bathymetry, a submerged sand bar

is generated in front of the river mouth, which is a consequent of the accumulation of eroded material. Seaward side of the sand east sand bar is eroded in the measured bathymetry more than the computed one. One possible reason for that is the hindcasted wave data. In this study, as previously mentioned, the wind data adopted from ECMWF is applied into the wave-hindcasting numerical model, W61, and the resulting storm conditions are introduced into XBeach as wave related input parameters. However, according to Raschle and Ardhuin (2012), ECMWF wind speed analyses are systematically underestimated comparing to Climate Forecast System Reanalysis (CFSR) wind data.

Future recommendations are listed as the following for this study:

For the comparison between LSTF experiment measurements and the XBeach model outputs,

- It may be further investigated to implement different sediment transport formulations to the model source code that is less dependent on the scaling effects.

For the Manavgat river mouth modeling case,

- It may be further investigated to use CFSR wind data and to compare other third generation wave hindcasting models such as SWAN and WAVEWATCH.
- Water surface fluctuations, which were mainly based on the assumptions and calculations in this study, may be adopted from the CFSR database.
- Selected turbulence and long wave stirring parameters, 'turb' and 'lws', respectively, require a more detailed sensitivity analyses with different combinations of these parameters.

- Wave-current interaction option is switched off during the simulations due to computational instability for the given bathymetry. This phenomenon is of great importance in the presence of high current speeds especially near river mouths. Thus, as a future study, wave-current interaction should be taken into account with an appropriate bathymetry.

REFERENCES

Alpar, B., Dogan, E., Yuce, H., & Altioek, H. (2000). Sea level changes along the Turkish coasts of the Black Sea, the Aegean Sea and the Eastern Mediterranean. *Mediterranean Marine Science*, 1(1), 141-156.

Bakker, W. T. (1968). A mathematical theory about sand waves and its application on the Dutch Wadden Isle of Vlieland. *Shore and Beach*, Vol 36, No 2, P 5-14, Oct 1968. 10 P, 12 Fig, 1 Tab, 6 Ref.

Baldock, T. E., Holmes, P., Bunker, S., & Van Weert, P. (1998). Cross-shore hydrodynamics within an unsaturated surf zone. *Coastal Engineering*, 34(3), 173-196.

Battjes, J. A. (1974). *Computation of set-up, longshore currents, run-up and overtopping due to wind-generated waves* (Doctoral dissertation, TU Delft, Delft University of Technology).

Baykal, C. (2012). *Two-dimensional depth-averaged beach evolution modeling* (Doctoral dissertation, Ph. D. Thesis, Middle East Technical University, Ankara, Turkey).

Baykal, C. (2014). Development of a numerical 2-dimensional beach evolution model. *Turkish Journal of Earth Sciences*, 23(2), 215-231.

Baykal, C., Ergin, A., & Güler, I. (2013). Two-Dimensional Depth-Averaged Beach Evolution Modeling: Case Study of the Kızılırmak River Mouth, Turkey. *Journal of Waterway, Port, Coastal, and Ocean Engineering*, 140(3), 05014001.

Bayram, A., Larson, M., and Hanson, H. (2007). "A new formula for the total longshore sediment transport rate." *Coastal Eng.* 54, pp.700-710.

Bolle, A., Mercelis, P., Roelvink, D., Haerens, P., & Trouw, K. (2011). Application and validation of XBeach for three different field sites. *Coastal Engineering Proceedings*, 1(32), 40.

Brandenburg, P. G. (2010). Scale dependency of dune erosion models: performance assessment of the DUROS and XBeach model for various experiment scales.

Briand, M.H.G., and Kamphuis, J.W. (1993). Sediment transport in the surf zone: A quasi 3-D numerical model. *Coastal Eng.*, Vol.20, pp.135-156.

Bruun, P., (1954), "Coast Erosion and the Development of Beach Profiles", Beach Erosion Board Technical Memorandum No.44, U.S. Army Engineer Waterways Experiment Station, Vicksburg, MS.

Buttolph, A. M.; Reed, C. W.; Kraus, N. C; Ono, N.; Larson, M.; Camenen, B.; Hanson, H.; Wamsley, T. and Zundel, A. K. (2006). Two-Dimensional Depth-Averaged Circulation Model CMS-M2D: Version 3.0, Report 2, Sediment Transport and Morphology Change. ERDC/CHL-TR-06-7. Vicksburg, Mississippi, US Army Engineer Research and Development Center, 156 p.

Camenen, B., Larson, M. (2005). A general formula for non-cohesive bed load sediment transport. *Estuarine, Coastal and Shelf Science* 63, 249–260.

Camenen, B., Larson, M. (2007). A unified sediment transport formulation for coastal inlet application. Technical report ERDC/CHL CR-07-1, US Army Engineer Research and Development Center, Vicksburg, MS.

Camenen, B., Larson, M. (2008). A general formula for noncohesive suspended sediment transport. *Journal of Coastal Research* 24 (3), 615–627.

Capobianco, M., Hanson, H., Larson, M., Steetzel, H., Stive, M. J. F., Chatelus, Y., ... & Karambas, T. (2002). Nourishment design and evaluation: applicability of model concepts. *Coastal Engineering*, 47(2), 113-135.

CEM. (2003). "Coastal Engineering Manual," U.S. Army Corps of Engineers, Coastal Eng. Research Center, U.S. Government Printing Office.

CIRIA, CUR, CETMEF (2007). *The Rock Manual. The use of rock in hydraulic engineering (2nd edition)*. C683, CIRIA, London.

CIRIA. (1996). "Beach Management Manual," CIRIA Report 153, CIRIA, London.

Cities and Coastal Areas. (n.d.). Retrieved July/August, 2016, from http://www.unep.org/urban_environment/issues/coastal_zones.asp

Colbo, K. (2006). Lateral Reynolds stress and eddy viscosity in a coastal strait. *Journal of physical oceanography*, 36(5), 770-783.

Dabees, M., and Kamphuis, J. W. (1998). ONELINE, a numerical model for shoreline change. *Coastal Engineering Proceedings*, 1(26).

Dally, W. R., & Osiecki, D. A. (1994). The Role of Rollers in the Surf Zone Currents. *Coastal Engineering Proceedings*, 1(24).

Dally, W.R., Brown, C.A. (1995). A modeling investigation of the breaking wave roller with application to cross-shore currents. *Journal of Geophysical Research*, 100 (C12), 24873–24883.

Daly, C., Roelvink, J. A., van Dongeren, A. R., & McCall, R. T. (2010). Short wave breaking effects on low frequency waves. *Proceedings 30th International Conference on Coastal Engineering*, San Diego, 1–13.

Dean, R. G. (1977). *Equilibrium beach profiles: US Atlantic and Gulf coasts*. Department of Civil Engineering and College of Marine Studies, University of Delaware.

Dean, R. G. (1987). Coastal sediment processes: Toward engineering solutions. In *Coastal Sediments* (p. 24). ASCE.

Dean, R. G., (1991), "Equilibrium Beach Profiles: Characteristics and Applications", *Journal of Coastal Research*, Vol.7, No.1 pp.53-84.

Del Valle, R., Medina, R., & Losada, M. A. (1993). Dependence of coefficient K on grain size. *Journal of waterway, port, coastal, and ocean engineering*, 119(5), 568-574.

ERDEMLI. (n.d.). Retrieved June 22, 2016, from <http://www.psmsl.org/data/obtaining/stations/2009.php>

Fagherazzi, S., & Overeem, I. (2007). Models of deltaic and inner continental shelf landform evolution. *Annu. Rev. Earth Planet. Sci.*, 35, 685-715.

Fleming, C.A., Hunt, J.N., 1976. Application of a sediment transport model. *Proc. 15th Coastal Engineering Conference*, ASCE, 1184– 1202.

Frostick, L. E., McLelland, S. J., & Mercer, T. G. (Eds.). (2011). *Users guide to physical modelling and experimentation: Experience of the HYDRALAB network*. CRC Press.

Galappatti, R., & Vreugdenhill, C. B. (1985). A depth integrated model for suspended transport. *Journal for Hydraulic Research*, 23(4), 359–377.

Goda, Y. (2010). "Random Seas and Design of Maritime Structures." 3rd Edition. World Scientific Publishing. ISBN-13: 978-981-4282-40-6., 708pp.

Gravens, M. B., & Wang, P. (2007). *Data report: Laboratory testing of longshore sand transport by waves and currents; morphology change behind headland structures* (No. ERDC/CHL-TR-07-8). Engineer Research and Development Center Vicksburg, MS, Coastal and Hydraulics Lab.

Güler, I. (1997). Investigation on protection of Manavgat River mouth. *Yüksel Proje International Co. Inc., Reserach Project Report*.

Güler, I., Ergin, A. Yalçiner, A. C. (2003). Monitoring Sediment Transport Processes at Manavgat River Mouth, Antalya Turkey. *Proceedings COPEDEC VI, Colombo, Sri Lanka*. Paper No 139.

Hamilton, D. G., B. A. Ebersole, E. R. Smith, and P. Wang. (2001). Development of a largescale laboratory facility for sediment transport research. (No. ERDC/CHL-TR-01-22). Engineer Research and Development Center Vicksburg, MS. Coastal and Hydraulics Lab.

Hanson, H., and Kraus, N. C. (1989). *GENESIS: Generalized Model for Simulating Shoreline Change. Report 1. Technical Reference* (No. CERC-TR-89-19-1). Coastal Engineering Research Center Vicksburg MS.

Hanson, H., M. Larson, and N. C. Kraus. (2001). A new approach to represent tidal currents and bathymetric features in the one-line model concept. *Proceedings Coastal Dynamics '01*, ASCE, 172-181.

Hanson, H., M. Larson, N. C. Kraus, M. B. Gravens. (2006). Shoreline response to detached breakwaters and tidal current: Comparison of numerical and physical models. *Proceedings 30th International Conference on Coastal Engineering*, ASCE, 3630-3642.

Hervouet, J. M., & Bates, P. (2000). The TELEMAC modelling system special issue. *Hydrological Processes*, 14(13), 2207-2208.

Inman, D. L., & Bagnold, R. A. (1963). Littoral processes. *The sea*, 3, 529-553.

Janssen, T. T., & Battjes, J. A. (2007). A note on wave energy dissipation over steep beaches. *Coastal Engineering*, 54, 711–716. doi:10.1016/j.coastaleng.2007.05.006

Jonsson, I. G. (1966). Wave boundary layers and friction factors. *Coastal Engineering Proceedings*, 1(10).

Kamphuis, J. W. (1991). Alongshore sediment transport rate. *Journal of Waterway, Port, Coastal, and Ocean Engineering*, 117(6), 624-640.

Kamphuis, J. W., & Readshaw, J. S. (1978). A model study of alongshore sediment transport rate. *Coastal Engineering Proceedings*, 1(16).

Komar, P. D., & Inman, D. L. (1970). Longshore sand transport on beaches. *Journal of geophysical research*, 75(30), 5914-5927.

Komar, P. D., & Miller, M. C. (1975). On the comparison between the threshold of sediment motion under waves under unidirectional currents with a discussion of the practical evaluation of the threshold. *Journal of Sedimentary Research*, 362–367.

Kriebel, D. L., and Dean, R. G. (1985). Numerical simulation of time-dependent beach and dune erosion. *Coastal Engineering*, 9(3), 221-245.

Larson, M and Kraus, N. C. (1989). “*SBEACH: Numerical Model for Simulating Storm-induced Beach Change; Report 1: Empirical Foundation and Model Development*”, Technical Report CERC-89-9, U.S. Army Engineer Waterway Experiment Station, Vicksburg, MS.

Larson, M., Kraus, N.C. (2002). NMLONG: numerical model for simulating longshore current; report 2: wave–current interaction, roller modeling, and validation of model enhancements. Technical Report ERDC/CHL TR-02-22, US Army Engineer Research and Development Center, Vicksburg, MS.

Larson, M., Kraus, N.C., Byrnes, M.R., (1990a). SBEACH: Numerical Model for Simulating Storm-Induced Beach Change, Report 2: Numerical Formulation and Model Tests. Technical Report CERC-89-9, US Army Engineer Waterways Experiment Station, Coastal Engineering Research Center, Vicksburg, MS.

Larson, M., Kraus, N.C., Hanson, H. (1990b). Decoupled numerical model of three-dimensional beach change. *Proc. 22nd Coastal Engineering Conference*, ASCE, 2173–2185.

Larson, M., Wamsley, T.V. (2007). A formula for longshore sediment transport in the swash. *Proceedings Coastal Sediments '07*. In ASCE, New Orleans, pp. 1924–1937.

Le Méhauté, B., Soldate, M. (1978). Mathematical modelling of shoreline evolution. *Proc. 16th Coastal Engineering Conference*, ASCE, 1163–1179.

Lin, L., Demirbilek, Z., Mase, H., Zheng, J., and Yamada, F. (2008). "CMS-Wave: a nearshore spectral wave processes model for coastal inlets and navigation projects." Coastal Inlets Research Program, Coastal and Hydraulics Laboratory Technical Report ERDC/CHL TR-08-13. Vicksburg, MS: U.S. Army Engineer Research and Development Center.

Lin, M. C., and Wang, J. C. (1984). Numerical modeling of shoreline evolution around the river mouth. *Coastal Engineering Proceedings*, 1(19).

Longuet-Higgins, M. S. (1970). Longshore currents generated by obliquely incident sea waves: 1. *Journal of geophysical research*, 75(33), 6778-6789.

Longuet-Higgins, M. S., & Stewart, R. W. (1964). Radiation stress in water waves: a physical discussion with applications. *Deep-Sea Research*, 529–562.

Lowe, R. J., Falter, J. L., Koseff, J. R., Monismith, S. G., & Atkinson, M. J. (2007). Spectral wave flow attenuation within submerged canopies: Implications for wave energy dissipation. *Journal of Geophysical Research: Oceans*, 112, 1–14. doi:10.1029/2006JC003605.

Luo, J., Li, M., Sun, Z., & O'Connor, B. A. (2013). Numerical modelling of hydrodynamics and sand transport in the tide-dominated coastal-to-estuarine region. *Marine Geology*, 342, 14-27.

Mase, H., (2001). "Multidirectional random wave transformation model based on energy balance equation." *Coastal Eng. Journal* 43 (4), 317–337.

Mase, H., Oki, K., Hedges, T. S., & Li, H. J. (2005). Extended energy-balance-equation wave model for multidirectional random wave transformation. *Ocean Engineering*, 32(8), 961-985.

Miles, J. (2013). Wave shape effects on sediment transport. *Journal of Coastal Research*, 65(sp2), 1803-1808.

Militello, A.; Reed, C. W.; Zundel, A. K., and Kraus, N. C. (2004). Two-dimensional depth-averaged circulation model M2D: Version 2.0, Report 1: Documentation and user's guide. ERDC/CHL TR-04-02, Vicksburg, Mississippi: US Army Engineer Research and Development Center, 128p.

Nam, P. T., Larson, M., & Hanson, H. (2009). A numerical model of nearshore waves, currents, and sediment transport. *Coastal Engineering*, 56(11), 1084-1096.

Nam, P. T., Larson, M., & Hanson, H. (2010). Modeling morphological evolution in the vicinity of coastal structures. *Coastal Engineering Proceedings*, 1(32), 68.

Nardin, W., & Fagherazzi, S. (2012). The effect of wind waves on the development of river mouth bars. *Geophysical Research Letters*, 39(12), 1–6. <http://doi.org/10.1029/2012GL051788>

OCDI (2002). “Technical Standards and Commentaries for Port And Harbor Facilities in Japan.” *Overseas Coastal Area Development Institute, Japan*.

Ochi, T., Kanda, K., Miwa, H., & Nakamura, F. (2015). Research on the Dynamic State of River-Mouth Bar under Flood Conditions in The Yuragawa River. *36th IAHR World Congress 28 June – 3 July, 2015, The Hague, the Netherlands*. <http://89.31.100.18/~iahrpapers/86643.pdf>

Pelnard-Considere, R. (1956). "Essai de Theorie de l'Evolution des Forms de Rivage en Plage de Sable et de Galets." 4th Journees de l'Hydraulique, Les Energies de la Mer, Question III, Rapport No.1, pg.289-298

Raschle, N., & Ardhuin, F. (2012). A global wave parameter database for geophysical applications. Part 2: Model validation with improved source term parameterization. *Ocean Modelling*, 70, 174-188.

Reed, C. W., Brown, M. E., Sánchez, A., Wu, W., & Buttolph, A. M. (2011). The coastal modeling system flow model (CMS-Flow): Past and Present. *Journal of Coastal Research*, 1-6.

Rienecker, M. M., & Fenton, J. D. (1981). A Fourier approximation method for steady water waves. *Journal of Fluid Mechanics*, 104, 119. [doi:10.1017/S0022112081002851](https://doi.org/10.1017/S0022112081002851)

Roelvink, D., van Dongeren, A. R., McCall, R. T., Hoonhout, B., van Rooijen, A., van Geer, P., ... Quataert, E. (2015). XBeach Technical Reference: Kingsday Release.

Roelvink, J. A. (1993). Dissipation in random wave group incident on a beach. *Coastal Engineering*, 19, 127–150.

Ruessink, B. G., Miles, J. R., Feddersen, F., Guza, R. T., & Elgar, S. (2001). Modeling the alongshore current on barred beaches. *Journal of Geophysical Research*, 106(22), 451–463.

Ruessink, B. G., Ramaekers, G., & van Rijn, L. C. (2012). On the parameterization of the free-stream non-linear wave orbital motion in nearshore morphodynamic models. *Coastal Engineering*, 65, 56–63. doi:10.1016/j.coastaleng.2012.03.006

Savage, R. P. (1962). Laboratory determination of littoral-transport rates. *Journal of the Waterways and Harbors Division*, 88(2), 69-92.

Shields, A. (1936). Anwendung der Aehnlichkeitsmechanik under der Turbulenzforschung auf die Geschiebebewegung. *Preussischen Versuchsanstalt Fur Wasserbau and Schiffbau*, 26, 524–526.

Smagorinsky, J. (1963). General circulation experiments with the primitive equations I. The basic experiment. *Monthly Weather Review*, 91, 99–164. doi:10.1126/science.27.693.594

Soulsby, R. (1997). *Dynamics of marine sands: a manual for practical applications*. Thomas Telford.

SPM. (1984). "Shore Protection Manual." Department of the Army, U.S. Corps of Engineers, Washington, DC 20314.

Sutherland, J., Obhrai, C., Whitehouse, R. J. S., & Pearce, A. M. C. (2006). Laboratory tests of scour at a seawall. In *Proceedings 3rd International Conference on Scour and Erosion, CURNET, Gouda, The Netherlands*. Technical University of Denmark.

Syvitski, J. P., & Saito, Y. (2007). Morphodynamics of deltas under the influence of humans. *Global and Planetary Change*, 57(3), 261-282.

Trouw, K., Zimmermann, N., Mathys, M., Delgado, R. and Roelvink, D. (2012), “*Numerical Modelling of Hydrodynamics and Sediment Transport in the Surfzone: A Sensitivity Study with Different Types of Numerical Models*”, Coastal Engineering. U.S. Army Engineer Research and Development Center.

Van Dongeren, A., Bolle, A., Voudoukas, M. I., Plomaritis, T., Eftimova, P., Williams, J., ... & Haerens, P. (2009, December). MICORE: dune erosion and overwash model validation with data from nine European field sites. In *Proceedings of coastal dynamics* (Vol. 9, pp. 1-15).

Van Rijn, L. C. (1984). Sediment transport, part I: bed load transport. *Journal of hydraulic engineering*, 110(10), 1431-1456.

Van Rijn, L. C. (1984). Sediment transport, part III: bed forms and alluvial roughness. *Journal of Hydraulic Engineering*, 110(12), 1733–1754.

Van Rijn, L. C. (1993). *Principles of sediment transport in rivers, estuaries and coastal seas* (Vol. 1006). Amsterdam: Aqua publications.

Van Rijn, L. C. (2007a). Unified view of sediment transport by currents and waves. I: Initiation of motion, bed roughness, and bed-load transport. *Journal of Hydraulic Engineering*, 133(6), 649-667.

Van Rijn, L. C. (2007b). Unified view of sediment transport by currents and waves. III: Graded beds. *Journal of hydraulic engineering*, 133(7), 761-775.

Van Rijn, L. C. (2007c). Unified View of Sediment Transport by Currents and Waves: part I and II. *Journal of Hydraulic Engineering*, (June), 649–667.

Van Thiel de Vries, J. S. M. (2009). *Dune erosion during storm surges* (Doctoral dissertation, TU Delft, Delft University of Technology).

Walton, T. L., & Dean, R. G. (2009). Landward limit of wind setup on beaches. *Ocean Engineering*, 36(9), 763-766.

Wang, P. (2006). Measuring longshore sediment transport in a large-scale 3-dimensional laboratory facility. *Journal of Coastal Research*, 816-821.

Wang, P., Smith, E.R. and Ebersole, B.A. (2002). "Large-scale laboratory measurements of longshore sediment transport under spilling and plunging breakers." *Journal of Coastal Research* 18 (1), 118– 135.

Warner, J.C., Sherwood, C.R., Signell, R.P., Harris C.K. and Arangoc, H.G. (2008). "Development of a three-dimensional, regional, coupled wave, current, and sediment-transport model." *Computers & Geosciences* 34, 1284–1306.

Watanabe, A. (1992). "Total rate and distribution of longshore sand transport." *Proc. of the 23rd Coastal Eng. Conf.*, pp. 2528-2541.

Willis, D. H. (1978). An Alongshore Current Beach Evolution Model, Hydraulic Laboratory, Division of Mechanical Eng., National Res. Council of Canada, Rept. No. HY-92.

Wu, W., A. Sanchez, and M. Zhang. (2011). An implicit 2D shallow water flow model on unstructured quadtree rectangular mesh. *Journal of Coastal Research Special Issue* 59:12–26.

Yüce, H., & Alpar, B. (1994). Investigation of low frequency sea-level changes at the Strait of Istanbul (Bosphorus). *Turkish Journal of Engineering and Environmental Sciences*, 18, 233-238.